Crossing borders in coastal morphodynamic modelling

Luijendijk, Arjen

DOI
10.4233/uuid:75ac8d9e-293f-4bff-90b3-467010352032

Publication date
2019

Document Version
Final published version

Citation (APA)
Luijendijk, A. (2019). *Crossing borders in coastal morphodynamic modelling*. [Dissertation (TU Delft), Delft University of Technology]. https://doi.org/10.4233/uuid:75ac8d9e-293f-4bff-90b3-467010352032

CROSSING BORDERS IN COASTAL MORPHODYNAMIC MODELLING

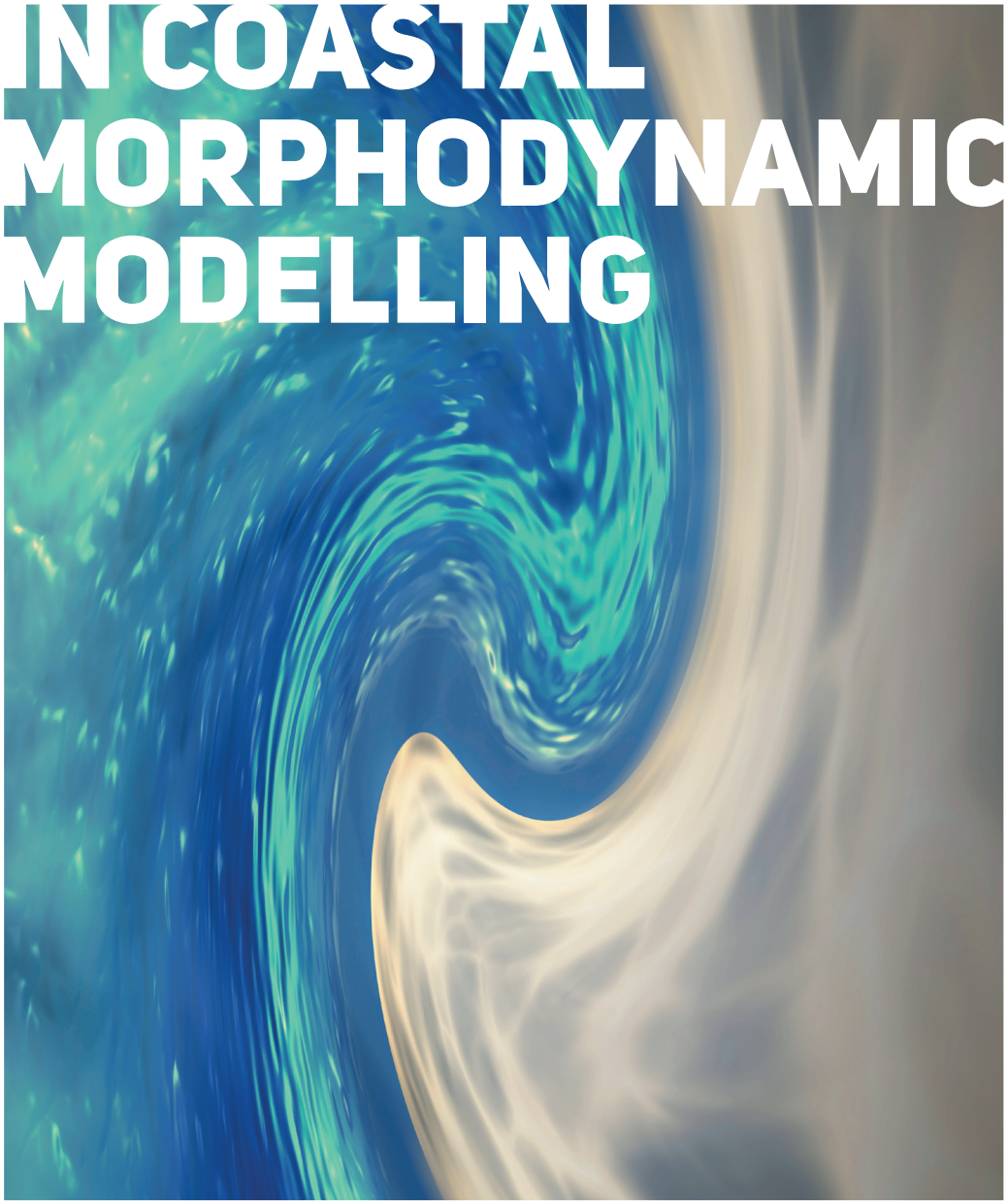

ARJEN LUIJENDIJK

CROSSING BORDERS IN COASTAL MORPHODYNAMIC MODELLING

ARJEN LUIJENDIJK

CROSSING BORDERS
IN COASTAL MORPHODYNAMIC MODELLING

Seamless Modelling of Sandy Coastal Interventions

PROEFSCHRIFT

ter verkrijging van de graad van doctor
aan de Technische Universiteit Delft,
op gezag van de Rector Magnificus, prof. dr. ir. T.H.J.J. van der Hagen,
voorzitter van het College voor Promoties,
in het openbaar te verdedigen op woensdag 4 december 2019 om 15:00 uur

door

Arjen Pieter LUIJENDIJK

civiel ingenieur
(Technische Universiteit Delft)

geboren te Rotterdam

This dissertation has been approved by the promotors prof. dr. ir. M.J.F. Stive and prof. dr. ir. S.G.J. Aarninkhof and copromotor dr. ir. M.A. de Schipper.

Composition of the doctoral committee:

Rector Magnificus	Chairman
Prof. dr. ir. M.J.F. Stive	Delft University of Technology, promotor
Prof. dr. ir. S.G.J. Aarninkhof	Delft University of Technology, promotor
Dr. ir. M.A. de Schipper	Delft University of Technology, copromotor

Independent members:

Prof. dr. ir. J.A. Roelvink	UNESCO-IHE, Delft
Prof. dr. K.M. Wijnberg	Twente University, Enschede
Prof. dr. R. Medina	University of Cantabria, Santander, Spain
Dr. S. Vitousek	USGS Santa Cruz, USA
Prof. dr. ir. A.J.H.M. Reniers	Delft University of Technology, reserve member

Nederlandse Organisatie voor Wetenschappelijk Onderzoek

Prof. Dr. R. Ranasinghe has contributed greatly to the realization of this research.

Cover design: Schinkelshoek Communicatie

ISBN 978-94-6366-219-2

An electronic version of this dissertation is available at
http://repository.tudelft.nl/.

Sand is almost like the air we breathe.
We don't think too much about it, but we can't live without it.

— Kiran Pereira

SUMMARY

In a time of societal and environmental changes there is a growing demand for actions to protect and sustainably manage coastal ecosystems. In recent years, various nature-based solutions (NBS) have been implemented that combine coastal functions of safety, recreation and nature development. Coastal NBS require a comprehensive understanding of the dynamics to better embed the solution in a natural coastal ecosystem, for they are typically designed to adapt to changing and uncertain environmental conditions. This work explores new techniques for obtaining historic information on shoreline dynamics and for predicting impact of coastal interventions along sandy beaches, both at scales from days to decades.

To determine the shoreline dynamics over the past decades a new cloud-based image analysis technology is developed. Using freely available optical satellite images captured since 1984 in conjunction with sophisticated image interrogation and analysis methods, occurrence of sandy beaches and rates of shoreline change are assessed at global scale. By applying pixel-based supervised classification, it is found that 31% of the world's ice-free shoreline are sandy. The application of an automated shoreline detection method to the identified sandy shorelines resulted in a global data set of shoreline change rates for the 33-year period 1984-2016. Analysis of the satellite derived shoreline data indicates that 24% of the world's sandy beaches are eroding at rates exceeding 0.5 m/yr, while 28% are accreting and 48% are stable. The majority of sandy shorelines in marine protected areas are eroding, raising cause for serious concern. The developed methods provide a unique opportunity to retrieve relevant historic information on ambient signals in shoreline dynamics at a decadal scale for any beach in the world, which is crucial in view of coastal NBS.

The anticipated future increase in global nourishment volumes and request for more complex nourishment shapes requires adequate predictions of the morphodynamic evolution of such sandy interventions. Yet, the primary drivers that control this evolution are not always known as well as the skill of current state-of-the-art models for such projects. A process-based Delft3D model has been used to successfully hindcast the initial response of the Sand Engine ('Zandmotor' in Dutch; hereafter referred to as ZM) mega-nourishment in The Netherlands. Analysis of the model results indicated that the erosion of the ZM has a linear dependency on the cumulative wave energy of individual high-energy wave events. The integrated erosion volume due to the 12 events with the highest cumulative wave energy events sums up

to approximately 60% of the total eroded volume of the peninsula after one year. Hence, the less energetic wave events, with a higher probability of occurrence, are almost equally important, accounting for 40% of the initial response of the ZM. Further analysis indicates that wave forcing dominated the initial morphological response, accounting for approximately 75% of the total erosion volume after the first year. Resolving the variations in wave energy, at time scales from days (storms) to months (seasons) to multi-year, is key to provide realistic answers at all desired time scales.

The design and acceptance of a coastal intervention demands information on the predicted morphodynamics, both on the short and longer term. The performance of different morphological acceleration techniques in predicting both short-medium term (1-5 yrs) and long-term (20-30 yrs) morphodynamic evolution are evaluated. The brute-force ZM model, calibrated with first year bathymetric measurements, is shown to be able to reproduce the observed morphological changes in the first five years with 'excellent' skill. Testing different acceleration techniques shows that the predicted details in alongshore and cross-shore distribution of the morphological evolution as well as the spit development have a strong dependency on the selected technique. Results show that acceleration techniques using representative (schematized) wave conditions are not capable of accurately reproducing the morphological response in the first two years. A newly proposed 'brute force merged' technique involves an attractive and flexible method providing a combination of phenomenological accuracy and computational efficiency (factor 20 faster than the benchmark brute force technique) at both the short-medium and long time scales. Decadal predictions reveal a lifetime of the ZM beyond 40 years which is much longer than the expected lifetime of 20 years.

Even though one of the main goals of the ZM is to stimulate the natural growth of the dunes, effects of windblown transports have been neglected in aforementioned predictions, because the magnitude of the annual windblown transports is typically of smaller order than the wave-driven transports. Yet, measurements after four years show a growth of the dune area by about 1 ha, necessitating inclusion of these transports; especially, when predicting the growth of nature area on the timescales of years.

As the majority of sediments deposited in the dunes originate from the low lying beach zone that is regularly reworked by waves, it is required to accurately predict the subaqueous and subaerial behavior in concert. As such a combined model for coastal interventions did not exist, a seamless coupling of three models (Delft3D Flexible Mesh, SWAN and AeoLiS) has been developed here that can resolve the interactions between aeolian, hydrodynamic and morphodynamic processes with a coupled, smooth method (i.e. seamless). Simulation with this new

modelling system reproduces the observed changes between 2011 and 2016 for both subaqueous and subaerial domain with higher skill than the (non-coupled) prediction. Specially dune growth values predicted with the coupled model show a much better correspondence to the observed dune growth between 2012 - 2015. The results show that the seamlessly coupled model can efficiently and realistically resolve the interactions between the subaqueous and dry beach morphodynamic evolution; both in magnitude and in spatial and interannual variations.

In summary, the combined results of this thesis provide new insight in the dynamics of sandy interventions and displays new methods for the prediction of these. It demonstrates the importance of seamless modelling, in which both subaqueous and subaerial beach changes are resolved with realistic forcing conditions for time scales of days to decades. These, in combination with information on the long-term historical dynamics of coastal sections, result in better informed coastal management strategies and NBS solutions in particular.

SAMENVATTING

In deze tijd van grote maatschappelijke en ecologische veranderingen is er een groeiende behoefte ontstaan aan maatregelen voor het beschermen en duurzaam beheren van ecosystemen langs de kust. In de afgelopen jaren zijn diverse natuur-gebaseerde kustwaterbouwkundige projecten (nature-based solution; NBS) uitgevoerd die de verschillende functies van de kust - veiligheid, recreatie en natuurontwikkeling - combineren. Een NBS in het kustgebied vereist een grondig inzicht in de kustdynamiek opdat de ingreep optimaal in het natuurlijk ecosysteem ingepast kan worden. Temeer omdat zulke oplossingen typisch ontworpen worden om zich natuurlijk aan te passen aan veranderende en onzekere omgevingscondities. Deze studie ontwikkelt nieuwe technieken voor het verkrijgen van historische informatie over de kustlijndynamiek en voor het voorspellen van de effecten van ingrepen in zandige kusten, zowel op tijdschalen van dagen tot decennia.

Om de historische kustlijndynamiek in kaart te brengen is een nieuwe beeldherkenningstechnologie ontwikkeld. De geavanceerde beeldanalysemethoden zijn toegepast die, met behulp van vrij beschikbare optische satellietbeelden sinds 1984, de aanwezigheid en de mate van kustlijnveranderingen van zandige stranden wereldwijd kan afleiden. Door middel van deze pixel-gebaseerde classificatie is vastgesteld dat 31% van 's werelds ijsvrije kusten zandig zijn. De toepassing van een geautomatiseerde kustlijndetectie op deze zandige kusten resulteerde in een globale dataset van kustlijnveranderingen over de 33-jarige periode 1984 – 2016. Analyse van de kustlijndata toont aan dat 24% van de kustlijnen wereldwijd eroderen met snelheden hoger dan 0.5 m per jaar, terwijl 28% aanzanden en 48% stabiel zijn. De meerderheid van de zandige kusten in beschermde natuurgebieden blijkt te eroderen, wat aanleiding geeft tot serieuze zorg. De ontwikkelde technieken bieden een unieke kans om relevante historische informatie over de kustlijndynamiek van ieder strand wereldwijd over de afgelopen decennia op te vragen. Deze informatie is van cruciaal belang met het oog op de ontwikkeling van NBS projecten die in harmonie zijn met de bestaande kustontwikkeling.

De verwachte wereldwijde toename in suppletievolumes en de meer complexe suppletie ontwerpen vereisen adequate voorspellingen van de morfologische ontwikkeling van zandige oplossingen. Echter, zowel de primair drijvende krachten die deze ontwikkeling sturen als de nauwkeurigheid van de huidige state-of-the-art modelvoorspellingen zijn niet volledig bekend. Deze beide aspecten zijn daarom verder onderzocht. Een proces-gebaseerd Delft3D model is – met succes -

gebruikt om de initiële respons van de Zandmotor (een mega-suppletie in Nederland) te simuleren. Analyse van de modelresultaten toont aan dat de erosie van de Zandmotor lineair afhankelijk is van de cumulatieve golfenergie van individuele hoogenergetische golfcondities. Het geïntegreerde erosievolume ten gevolge van de 12 gebeurtenissen met de hoogste cumulatieve golfenergie is ongeveer 60% van het totaal geërodeerde volume van de Zandmotor na 1 jaar. Dit betekent dat de minder energetische golfcondities met een veel hoger kans van voorkomen nagenoeg even belangrijk zijn en verantwoordelijk zijn voor 40% van de initiële respons van de Zandmotor. Nadere analyse toont aan dat de initiële respons grotendeels wordt bepaald door golfkrachten; deze zijn verantwoordelijk voor ongeveer 75% van het totale erosievolume in het eerste jaar. Het meenemen van de variatie in golfenergie over tijdschalen van dagen (stormen), maanden (seizoenen) en meerjarige periodes blijkt daarom cruciaal om nauwkeurige modelvoorspellingen te kunnen maken op alle tijdschalen.

Het ontwerp en de acceptatie van een kustingreep vraagt om inzicht in het verwachte morfologisch gedrag op zowel de korte als de lange termijn. Voor voorspellingen van het gedrag zijn numerieke modellen geschikt, maar deze vereisen acceleratie technieken om de rekentijd te beperken. De prestatie van verschillende morfologische acceleratie technieken op korte- tot middellange termijn (1-5 jaar) en op lange termijn (20-30 jaar) zijn hier geëvalueerd. De brute-force (real-time) aanpak, gekalibreerd aan de hand van bodemmetingen in het eerste jaar, blijkt in staat om de geobserveerde morfologische veranderingen bij de Zandmotor in de eerst 5 jaar goed te kunnen reproduceren. Door verschillende acceleratie technieken te testen blijkt dat de voorspelde morfologische details in kustlangse en kustdwarse richting en de ontwikkeling van de spit sterk afhankelijk zijn van de gekozen techniek. De resultaten tonen dat de acceleratietechniek met representatieve (geschematiseerde) golfcondities niet in staat is de ontwikkeling in de eerste 2 jaar nauwkeurig te voorspellen. Een nieuw voorgestelde 'brute force merged' techniek behelst een aantrekkelijke en flexibele methode die een combinatie van fenomenologische nauwkeurigheid en rekenkundige efficiëntie biedt (20x sneller dan de benchmark simulatie) voor zowel de korte- tot middellange termijn als op langere tijdschalen. Langjarige voorspellingen tonen tevens dat de levensduur van de Zandmotor meer dan 40 jaar is, aanzienlijk langer dan de oorspronkelijk verwachte levensduur van 20 jaar.

Hoewel één van de hoofddoelen van de Zandmotor is om de natuurlijke aangroei van de duinen te stimuleren, is het effect van windgedreven zandtransport niet meegenomen in bovengenoemde voorspellingen. De omvang van de jaarlijkse windtransporten zijn meestal een orde kleiner dan de golfgedreven transporten. Echter, metingen na vier jaar laten bij de Zandmotor een groei van het duingebied van ongeveer

1 ha zien, wat de noodzaak van het meenemen van deze transporten in de modelvoorspellingen illustreert; vooral wanneer er getracht wordt de groei van het natuurlijk duingebied te kwantificeren. De meerderheid van het zand dat afgezet wordt in het duinen blijkt afkomstig van de laaggelegen strandzone, dat regelmatig door golven omgewerkt wordt. Voor nauwkeurige voorspellingen is het daarom nodig om zowel het gebied onderwater als het droge strand simultaan uit te rekenen. Aangezien zo'n model functionaliteit nog niet bestaat, is er een naadloze koppeling van drie modellen (Delft3D Flexibel Mesh, SWAN en AeoLiS) ontwikkeld die de interacties tussen de eolische, hydrodynamische en morfologische processen kan oplossen. Een simulatie met deze nieuwe gekoppelde modelaanpak reproduceert de waargenomen veranderingen tussen 2011 en 2016 voor zowel onderwater als het droge strand met een hogere nauwkeurigheid dan de niet-gekoppelde voorspelling. De duin aangroeisnelheden op de Zandmotor, voorspelt met het gekoppelde model, laten een goede overeenkomst zien met de waargenomen duingroei tussen 2012 en 2015. De resultaten tonen aan dat de naadloos gekoppelde modelaanpak de interacties tussen de veranderingen in het onderwater en droge strand efficiënt en realistisch kan oplossen; zowel in omvang als in ruimtelijke en jaarlijkse variaties.

Samenvattend toont dit werk dat de integratie van realistische variaties in golf-randvoorwaarden gecombineerd met een gekoppelde modelaanpak voor interacties tussen processen onderwater en op het droge strand cruciaal is voor realistische morfologische voorspellingen van (NBS) ingrepen langs zandstranden op tijdschalen van dagen tot decennia.

CONTENTS

1 INTRODUCTION

1.1 CONTEXT

Our planet Earth comprises approx. 361 million km^2 of water (71% of total planet surface) and about 149 million km^2 of land area (29% of total planet surface) (Martínez et al., 2007). Coastal zones form the interface between the land and seas and have historically attracted humans due to the abundant amenities, aesthetic value and diverse ecosystem services that they provide. Nearly 2.4 billion people (41% of the world's population) live within 100 km of the coast (UN, 2017 based on 2003 data). Twenty-one of the 33 world's megacities (with more than 8 million inhabitants) are located within the coastal area (Martínez et al., 2007).

The coastal zone is subject to 'coastal squeeze' with increasing pressure due to growing population and economic value on the landward side and a foreseen sea-level rise on the seaward side. Sea-level rise and associated extreme water levels will lead to a range of impacts including temporary flooding, permanent submergence of low lying areas, increased coastal erosion, wetland change and loss, and salinity intrusion into coastal aquifers and the lower reaches of rivers (Nicholls, 2007). Coastal flooding, submergence and erosion are distinct, but related processes (Nicholls and Cazenave, 2010). Flooding and submergence relate to rising relative water levels without any change in absolute elevation, while erosion is a morphodynamic process produced by the removal of sediment, due to waves, wind, currents and other hydrodynamic processes.

The global coastline is spatially highly variable and comprises several different types of coastal landforms, some examples being barrier islands, beaches, sea cliffs, tidal flats, and river deltas. The focus of this thesis is on sandy coasts. They form a substantial part of the world's coastline and provide natural protection from storms by absorbing energy from the waves. The sandy beach itself can be highly dynamic in time and space, due to the action of tides, waves, and change in morphology. Erosion of the beach can occur at a range of timescales from storms to decades (Ranasinghe and Stive, 2009; Stive et al., 2002). Individual storms will generally lead to rapid short-term erosion, followed by rapid short-term recovery; the net change being often negligible. If sediment deficiencies persist, more chronic long-term erosion can occur (Hinkel et al., 2013). As sandy shorelines are constantly changing, human assets in the vicinity such as buildings and infrastructure

are frequently threatened. This becomes even more relevant as sandy shorelines are expected to be highly responsive to sea-level changes (Le Cozannet et al., 2019). The need for protecting these high-valued sandy shorelines will hence increase in future.

1.2 MOTIVATION

1.2.1 *Nature-based solutions*

In an era of societal and environmental changes there is a growing demand for actions to protect and sustainably manage and restore coastal ecosystems. The Building with Nature program (referred to as BwN; run by Ecoshape) has developed an interesting new approach to hydraulic engineering that harnesses the forces of nature to benefit environment, economy and society (De Vriend et al., 2015; De Vriend, 2013). Over the last years various nature-based hydraulic projects have been implemented that effectively address societal changes while providing protection, human well-being and biodiversity benefits. Fig. 1.1 shows four examples of nature-based sandy solutions in the Netherlands.

Figure 1.1: Aerial photographs of four nature-based sandy solutions in the Netherlands: a) the Sand Engine, b) the Hondsbossche Dunes, c) the Houtrib Dyke, and d) the Prins Hendrik sand dyke (artist impression).

Nature-based solutions (NBS) demand thorough insight in the natural dynamics to come to an optimal solution. More specifically for coastal flood defenses a comprehensive understanding of the environmental conditions, such as the tides, waves and wind, is required to better embed the solution in the natural coastal ecosystem. Therefore, the first design step in the BwN philosophy focuses on 'system understanding'. Often, this system understanding is limited due to lack of historical data.

NBS are often designed to adapt to changing environmental conditions. This dynamic behavior, albeit desirable, leads to uncertainty in the future performance of the solution.

Consequently, predictive numerical models are more and more applied to provide information on the future behavior. However, they lack capabilities in resolving interactions across temporal scales. For example, the effects of storms are not fully incorporated in decadal forecasts using the present-day process-based numerical models, like Delft3D or MIKE. Only a few examples of dedicated offline-coupled applications are reported in literature (Van Ormondt, 2016) even though feedback between short-term and long-term coastal evolution may be highly relevant at decadal horizons.

Projects involving coastal NBS have exposed another shortcoming of existing morphodynamic models. The existing morphodynamic models focus on either the subaqueous or the subaerial domain of a sandy beach system. They lack capabilities in predicting the wind-blown transports at the intertidal and beach area and hence the development of dunes on the dry beach in case of a changing foreshore. Not resolving the wind-blown transports can be a significant limitation in longer term predictions, as the wind can transport large volumes of sediment from the beach into the dunes, therefore being a significant contribution on longer time scales. In addition, the dune volume is a crucial component in the coastal safety assessment in the Netherlands.

1.2.2 *Motivational trends*

This thesis will discuss the advances made in utilizing global data to feed the 'system understanding' of coastal systems at planetary scale and the development of new methods and tools to allow for crossing borders in morphodynamic predictions, both in time and spatial domains. This section discusses three of the most important trends that inspired and motivated the research presented in this thesis.

Earth observation

Geospatial data play an increasing role in answering major societal questions such as those related to the environment, climate change,

and sustainable development goals. At the same time, geospatial data are becoming popular given the multiplication of digital data sources initiated by individuals and private and public organizations. An important source of geospatial data for studies from regional to planetary scale is provided by earth observation satellites generating an ever increasing flow of raster image data since the launch of Landsat-1 in 1972 by the National Aeronautics and Space Administration (NASA) of the United States (Belward and Skøien, 2015). In 2008, the United States Geological Survey (USGS) has democratized the use of Landsat data by making all imagery accessible over the Internet under a free and open data policy (Wulder et al., 2012).

An exponential increase in the availability of free geospatial data has recently emerged with the Copernicus Earth observation and monitoring program of the European Union that delivers satellite imagery complemented by in-situ observations (Malenovský et al., 2012). The Copernicus Sentinel satellites are developed by the European Space Agency (ESA). To illustrate the rapid increase, Fig. 1.2 shows the yearly volume of data available for download by Landsat, MODIS and ESA missions between 2013 and 2019 (Soille et al., 2018).

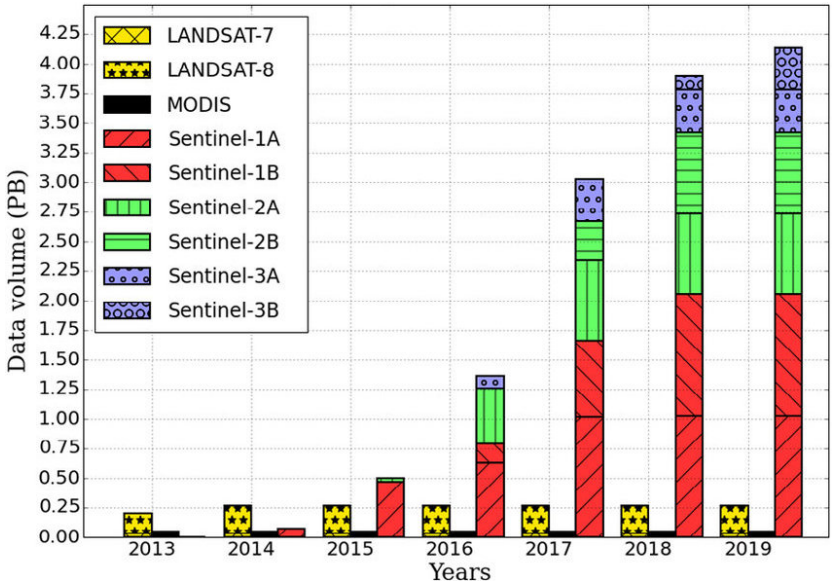

Figure 1.2: Estimates of the yearly volume (in petabyte i.e. 1000 terabyte) of open and free data for Landsat-7 and Landsat-8, MODIS (Terra and Aqua units), and the first three Sentinel missions (figure from Soille et al., 2018).

Technological developments and outreach efforts undertaken by large companies, have resulted in the development of parallel processing platforms like Google Earth Engine (GEE). GEE combines a multi-petabyte catalog of satellite imagery and geospatial data sets with planetary-scale analysis capabilities, making the data available for scientists and developers to detect changes, map trends, and quantify differences on the Earth's surface. This platform has truly revolutionized the processing of satellite imagery and has already led to a significant number of successful research efforts. This would have been unimaginable to perform otherwise because of the large volumes of data that need to be stored and processed (Donchyts, 2016; Hansen, 2013; Pekel et al., 2016). Here, we examine if the GEE platform can also be used to examine coastline dynamics at a global scale. This would provide an unprecedented view on the behavior of the world's coastline.

Seamless modelling

Different types of morphological models are available to study the behavior of sandy coasts. One-dimensional shoreline models have proven to be useful in engineering applications for providing information on the long-term (years to decades) and larger spatial scales (> 10 km to 100 km's). Process-based area models are available to study coastal behavior at time scales ranging from weeks to multi-year for coastal stretch of km's to tens of km's (see Fig. 1.3). For studying the impacts of storms, process-based storm erosion models have been developed in the past decade. Each of the three models typically have a loyal community applying the models and developing the specific software, although the interaction and exchange between these groups could be improved. After all, they study the same coastal area and hence the same processes yet on other time and spatial scales. Note that the processes at different scales are interrelated and per definition not all included in any one of the models.

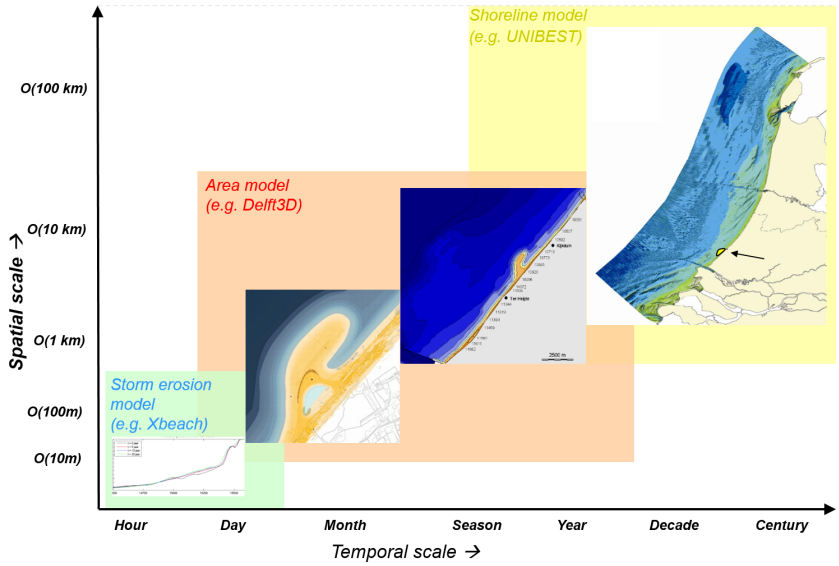

Figure 1.3: Typical application ranges in space and time of present coastal morphological models.

In this sense, the evolution of weather and climate models provided great inspiration for the development towards a seamless modelling approach for coastal morphodynamic applications. Where in the past weather and climate models were also strictly separated, the initiatives for the development of a unified model were very successful. For example, the MET office in the UK has successfully developed their seamless modelling approach (Brown et al., 2012) where the daily weather predictions are computed within the same computational system as the climate projections over many decades, feeding e.g. the IPPC (Intergovernmental Panel on Climate Change) research. These developments have inspired the testing and application of a framework for flexible and efficient coupling of different models in this thesis.

Monitoring of 'Living Labs'

The increasing number of 'living lab' experiments in the hydraulic engineering world also illustrates an important trend. Especially, the extensively monitored experiments call for the application of numerical models to understand the processes driving observed behavior. Such experiments facilitate the verification of performance of numerical models, which can then be applied to upscale the implemented knowledge (rules) to other sites in the world. Without these highly monitored field cases, the system understanding would have been less developed and the desire for new advances in morphodynamic modelling would be lower as crucial validation data are lacking.

Here, one of the first large-scale 'living labs'[1], the Sand Engine (see Fig. 1.1a; Luijendijk and Oudenhoven, 2019) was adopted as a case study to 1) gain detailed understanding of the coastal system, 2) show the limitations of present modelling tools, and 3) investigate the added-value of new model functionality.

The Sand Engine provides a unique case study due to its size, resulting in a large signal-to-noise ratio and due to the comprehensive monitoring campaign. For example, measurements now show that the models overpredicted growth of dune area by 500% after four years (Taal et al., 2016). Furthermore, the observed erosion volume in the first years after completion is significantly higher than predicted upfront. The high resolution and frequency of the measurements facilitated a unique 'numerical living lab' where the relevance of a range of environmental forcings and processes can be analyzed in detail.

1.3 RESEARCH OBJECTIVES

The previous section revealed that there is a number of shortcomings in the understanding and prediction of sandy beach systems that can be improved significantly.

The main goal of this thesis is to cross borders in coastal morphodynamic models by augmenting the forecast horizon in temporal space, by advanced morphodynamic acceleration techniques, and in spatial space, by integrating subaerial and subaqueous morphodynamic processes. This work attempts to fill some of the previously stated gaps in scientific literature guided by the following four research objectives:

Objective 1: Analyze the historical shoreline dynamics of beaches globally using satellite imagery
When designing sandy solutions in a coastal system, a sound understanding of the dynamic behavior is desired. Historical records on shoreline positions can play a vital role in generating system understanding of the coastal system. The large majority of the world's coasts are not regularly monitored hampering the development of a sound system understanding. In this thesis a global assessment on the sandy beach dynamics using satellite imagery is carried out providing information on the historical behavior of every beach around the globe.

1 A living lab is a research concept in which the user plays an important role. The idea is that new innovative ideas and concepts are developed and tested together with users in real life situations; here at a coastal field site.

Objective 2: Determine the processes governing the response of a large-scale sandy intervention
The processes driving the response of a sandy coastal intervention over multiple time scales are not sufficiently understood. Also, the capability of present-day process-based models in reproducing the observed behavior is only limitedly verified. The pilot experiment of a mega-nourishment, called the Sand Engine, is therefore adopted as a case study. Its unprecedented 'signal-to-noise' ratio provides unique opportunities to identify the contribution of different processes to the response of a sandy coastal intervention and test the model applicability. These insights are essential for upscaling the morphological evolution to decadal time scale.

Objective 3: Evaluate the performance of morphological acceleration techniques on the predicted evolution at multiple time scales
The influence of morphological acceleration techniques on the predicted coastal evolution at multiple timescales, from storms to decades, has received very little scientific attention and is still poorly understood. Morphological predictions are more and more applied to satisfy the increasing need for information by coastal managers regarding the behavior of a coastal intervention; in this case a sandy nourishment. Coastal managers demand information at various spatial and time scales, ranging from storms to decades. For example, they want to know when and how much sand is expected at a certain location downdrift of a nourishment. This thesis aims at evaluating the influence of existing and novel upscaling techniques across different time scales.

Objective 4: Develop and validate a coupled morphodynamic model which seamlessly integrates the subaqueous and subaerial domains
The morphological response of coastal interventions are commonly modeled with models covering only the topography below the water surface, i.e. the subaqueous part. However, these models lack physical processes that can be of importance at (partly emerged) sandy developments. Especially, wind-blown (aeolian) transports at the dry beach surface can significantly contribute to morphological changes at various time scales. The transport of sand from the intertidal and dry beach area into the dunes are relevant on both the short (seasons) and long term (decades). In this thesis, a coupled model system has been developed that seamlessly integrates process-based models for the subaqueous and subaerial domains.

1.4 OUTLINE

The main part of this thesis consists of four chapters following the stated objectives above. Each chapter covers one of the research objectives (see Fig. 1.4). Chapter 2 addresses the study on the behavior of sandy beaches at planetary scale. Automated shoreline detection methods have been developed and applied to more than 2 million satellite images to derive the historic changes of all sandy shorelines from 1984 to 2016. This valuable data source feeds the understanding of beaches at a global scale. At a more local scale, in-situ measurements at the Sand Engine feed the system understanding into the processes driving the response of a large-scale sandy intervention. This information is used in Chapter 3, which discusses the performance of present-day process-based models in reproducing the observed subaqueous changes at the Sand Engine during the first year. To efficiently predict the future evolution of the Sand Engine, the research in Chapter 4 focuses on evaluating morphodynamic acceleration techniques. The interaction across multi-timescales is given special attention in the evaluation and development of acceleration techniques. Chapter 5 investigates the added-value of seamlessly coupling two morphodynamic models integrating the subaqueous and subaerial domain of the sandy beach system and its impact on dune growth. Finally, Chapter 6 revisits the research questions and reflects on the research by discussing potential applications to future nature-based solutions.

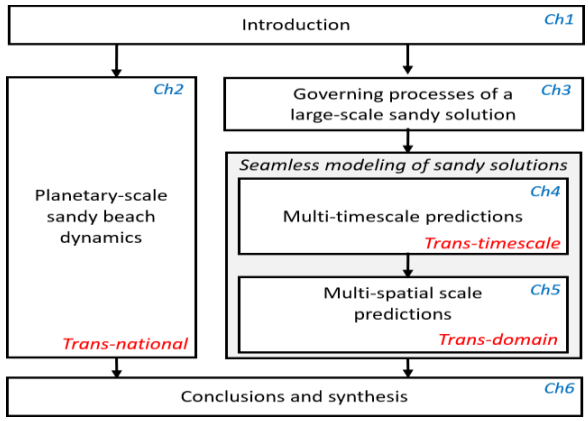

Figure 1.4: Thesis visual map.

The main part of this thesis is arranged as a compilation of research papers. In order to retain chapters that are legible individually, some parts are repeated. A brief introduction on the coherence with other chapters is made at the start of chapters, if relevant.

Part I

EARTH OBSERVATION

2 SANDY BEACHES OF THE WORLD

Large part of this chapter is based on: Arjen P. Luijendijk, Gerben Hagenaars, Roshanka Ranasinghe, Fedor Baart, Gennaddi Donchyts, Stefan G.J. Aarninkhof. "The State of the World's Beaches". Published in Nature Scientific Reports Volume 8, Article number: 6641 (2018) (Luijendijk et al., 2018).

2.1 INTRODUCTION

Coastal zones have historically attracted humans and human activities due to the abundant amenity, aesthetic value and diverse ecosystem services that they provide. As a result, the coastal zone all over the world has become heavily populated and developed (Small and Nicholls, 2003, Hallegate et al., 2013, Hinkel et al., 2013) with 15 of the 20 megacities (population > 10 million) of the world being located in the coastal zone. The global coastline is spatially highly variable and comprises several different types of coastal landforms, some examples being barrier islands, sea cliffs, tidal flats, and river deltas. Of these different coastline types, here we focus on sandy coasts, which are highly dynamic in time and space, and constitute a substantial part of world's coastline (Bird, 1996). As sandy coasts are highly developed and densely populated due to the amenity and aesthetics that they provide, erosion of these coasts over the last few decades is already resulting in coastal squeeze (Pontee, 2013).

Inevitably, climate change impacts on sandy coasts will only exacerbate this situation (Nicholls, 2007, Ranasinghe, 2016). Thus, reliable assessments of the occurrence of sandy coasts and their rates of shoreline change are basic necessities for effective spatial planning, sustainable coastal development, coastal engineering projects, and mitigation of climate change impacts along high value coastlines around the world.

Despite the utility, economic benefits, and the dynamic nature of sandy coasts, there is no reliable global-scale assessment of their occurrence or rates of shoreline change (i.e. erosion/accretion rates) therein. Presently available global scale estimates of these phenomena vary widely, and the way in which most of these estimates have been derived is unclear at best. For instance, the percentage of occurrence for sandy shorelines worldwide reported in literature varies by a factor 7 ranging from 10% (Van Rijn, 1998) to 75% (Bascom, 1980). With regard to rates of change in sandy shorelines, several reliable recent regional scale estimates exist for Europe (27% eroding (Eurosion, 2004)) and the US East coast barrier beaches (86% eroding (Galgano et al., 2004)). The

only global scale assessment available is reported by Bird (1985) that estimated 70% of sandy shorelines worldwide were eroding. However, because Bird's study, ground breaking as it was at the time, was primarily based on a survey of 200 participants from 127 countries, this estimate is rather qualitative.

Robust estimation of shoreline change rates by necessity requires continuous and long-term information on shoreline position. Historically, the acquisition of shoreline data sets has been a laborious and expensive task as it involved traditional land-based surveys or the analysis of temporally sparse data collected from aerial platforms (photographs or lidar). The increasing availability, resolution and spatial coverage of satellite imagery in recent years now provide a powerful alternative to derive reliable, global scale shoreline data as we demonstrate in this article.

The method commonly used to extract shorelines from satellite images in the past involved painstaking image by image analysis of series of overlapping images. The recent launching of the Google Earth Engine (GEE) platform, containing a continuously updated global satellite image archive, now enables efficient global scale shoreline detection. Having both a petabyte satellite image collection and parallel computation facilities combined on the server side of the platform reduces image processing time to only several minutes per image (Gorelick, 2017) and enables efficient validation of the automatically detected shorelines at multiple sites where ground-truth field data are available.

To enable global mapping of sandy shorelines it is first necessary to identify sandy beaches and then determine shoreline positions in every image in the GEE platform. The spatio-temporal scales associate with this study (i.e. global scale, 33 year analysis) and the large amount of satellite images that therefore need to be analyzed necessitates the use of robust automated image analysis techniques. Machine learning (Johansen et al., 2015) and image processing (Garcia-Rubio et al., 2015) techniques that lend themselves to such automated analyses are readily available. However, to be able to use satellite derived shoreline positions for real-world applications such as reliably estimating trends and structural damage to infrastructure, a horizontal resolution of at least 10-20 m is required. For example, shoreline change rates above 0.5 m/yr over a long period are typically employed to flag a coastal area as one experiencing chronic (=long term i.e. decades to centuries (Ranasinghe, 2016)) erosion or accretion. Over a period of 30 years that would mean a total displacement of just 15 m.

Previous studies have evaluated the positional accuracy of satellite derived shorelines (SDS) based on single images (Bayram et al., 2008, Kuleli et al., 2011, Pardo-Pascual et al., 2012, Garcia-Rubio et al., 2015, Liu et al., 2017) to range between 1.6 and 10 m. It should be noted that these studies suffered from limitations such as the number of images

used, the quality of the in-situ data used for validation or the magnitude of changes in observed shoreline position. Recently, Hagenaars et al. (2017) presented a long-term, but local scale satellite image analysis on shoreline trends, that overcomes all of the aforementioned limitations. They found the accuracy of the SDS derived from moving average composite images to be of subpixel precision (∼half a pixel size, i.e., 15 m for Landsat and 5 m for Sentinel-2). The accuracy of <15 m, reported by Hagenaars et al. (2017) for composite Landsat images, matches the required displacement of 15 m for reliable shoreline change classifications over the last 30 years. For that reason, we adopt the same approach in this study, yet at a global scale.

Here we present an up-to-date global-scale assessment of dynamics of sandy shorelines using a fully automated analysis of 33 years (1984-2016) of satellite images. First, we detect sandy beaches worldwide by applying a pixel-based supervised classification to a cloud-free high-resolution global composite image for 2016. A digital beach training data set is provided to the classification software and validated for 50 locations worldwide that include both sandy and non-sandy beaches. Next, we apply a shoreline detection algorithm to cloud free global annual composite images using more than 1.9 million historical Landsat images. After a successful quantitative validation of this technique at multiple sites located in various geographical settings and environmental conditions, we derive shoreline change rates in m/yr at transects with an alongshore spacing of 500 m along the world's shoreline. The above mentioned methods are elaborated in the Methods section below while the complete validation is presented in Appendices A and B.

The main outcomes of our analysis include: (a) the global occurrence of sandy beaches, (b) rate of erosion/accretion at all sandy beaches in the world, (c) highlights of observed natural and human induced impacts on coastal erosion/accretion at selected locations, and (d) identification of global hot spots of coastal erosion/accretion.

2.2 METHODS

The workflow applied in this study comprises three methods as discussed below and illustrated in Fig. 2.1.

2.2.1 *Global transect system*

For global analysis and visualization purposes, we defined 500 m spaced transects orthogonal to the global shoreline from the OpenStreetMap (OSM) data set of 2016 (OpenStreetMap, 2015). The length of the global shoreline, as well as per country, is calculated by multiplying the number of transects with the distances between the transects. The total length of the world's ice-free shoreline determined from this analysis is 1.11 million km, which is comparable with previously reported values of 1 million km (Hinkel et al., 2013), 1.16 million km (CIA, 2016), and 1.47 million km (Burke, 2001). In the future, we intend to merge the 500 m transect system with locally available grids and refine it where appropriate.

2.2.2 *Detection of sandy beaches*

Sandy beaches are detected by applying a pixel-based supervised classification to a global Top of Atmosphere (TOA) reflectance percentile composite image for the year 2016 using all available Sentinel-2 images. To facilitate this, the world has been divided into boxes of 20 km x 20 km. Using the 2016 OSM shoreline, we only select the boxes that intersect with the 2016 shoreline, which results in about 24,000 boxes to be analysed. To train the supervised classifier, a beach area consisting entirely of sand is selected (at the Dutch Texel island) as well as training areas on land representing different types of land use. To select the most promising classification algorithm, the validation results were quantitatively compared to the sandy beach feature in OSM. From the four considered classification algorithms, the Classification and Regression Tree (CART) classifier resulted in the lowest omission error and the highest percentage of true positives (97%) using the beach features in a 100 km long section of sandy beaches along the Dutch coast.

Next, we apply the trained supervised classification method to all boxes to detect sandy beaches at global scale as the OSM beach feature is not available for the entire globe. A search area of 500 m land- and seaward of the 2016 OSM shoreline is defined, after which the supervised classification is conducted using GEE to automatically detect sandy beaches. The result is a series of polygons encapsulating all sandy beaches worldwide, including both quartz and carbonate sands, and gravel. More than 50 sand validation locations, randomly spread

across the world, were selected independently from the training data set. Validation through visual inspection resulted in 96% accuracy (see Appendix A). Transects that intersect with a sandy polygon are classified as 'sand' and others as 'non-sand'. Transects for which no sand classification could be made due to the absence of a cloud-free Sentinel-2 image are labelled as 'undetermined sediment composition'. As this is applicable for 5.2% of all transects the percentage of sandy beaches is 31% $\pm$ 1.5%, assuming that the unknown areas behave similar to the global mean.

2.2.3 *Dynamic shoreline detection*

To remove the effects of clouds, shadows, snow, and ice, we generate yearly top-of-the atmosphere reflectance composites, which we then use to estimate an accurate surface water mask using dynamic thresholding method described in Donchyts (2016). Yearly composite images generated by the 15% reflectance percentiles per pixel were analysed to determine global shoreline positions, resulting in the removal of clouds and shadows. This approach is comparable to how Hansen (2013) generates composite images. However, the use of an exact percentile value turns out to be more suitable than the interval mean averages used in that study. Analysis of the composite images significantly decreases the influence of the tidal stage on the detected shoreline positions and averages out seasonal variability in wave and beach characteristics. Nevertheless, at sites with persistent swell conditions, hence persistent wave breaking, the wave-induced foam due to wave breaking will introduce a seaward offset in detected shorelines. Fortuitously, however, this persistency ensures that the wave-induced offset is most likely also present in annual composites and shorelines of other years. Thus, the wave effects on detected shorelines are likely to be limited, especially where long-term shoreline change rates at such sites are concerned. For validation purposes with long-term in-situ shoreline changes, an optimal averaging period of 192 days is applied; i.e. the first integer that is found when dividing the global revisiting time of the satellite sensor (16 days) by a semi-diurnal tidal period (approx. 12 hrs). In case all satellite images in this averaging interval are cloud-free the average water level corresponds to mean sea level. The potential year-to-year random deviation from 'mean sea level' due to omitted satellite images is assumed to have a limited effect on the 33-year trend of shoreline change; this assumption will be verified as part of further research. Next, the resulting composite images are used to estimate the Normalized Difference Water Index (NDWI). The Canny edge detection filter is used to roughly estimate the position of the water-land transition, followed by the use of the Otsu thresholding method (Otsu, 1979) on a buffer polygon around the water-land transi-

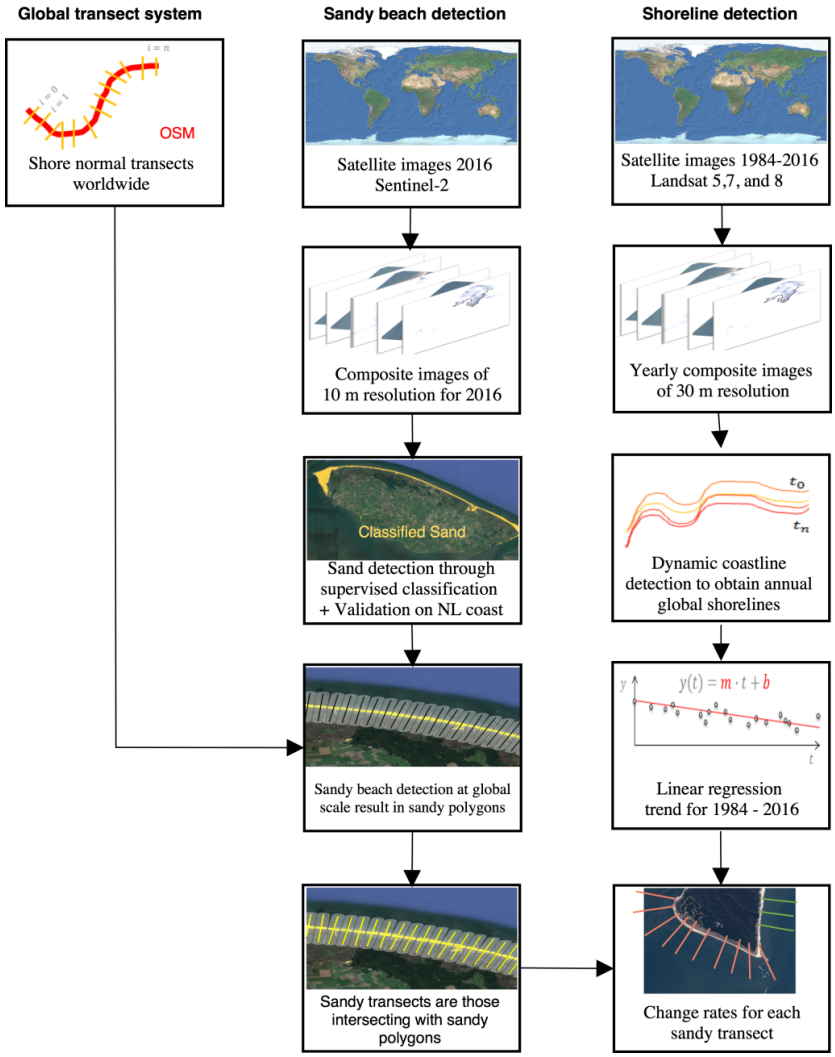

Figure 2.1: The procedure followed for deriving shoreline change trends for sandy shorelines using a global transect system.

tion to identify the most probable threshold to classify water and land on the image. The detected water lines at the edge of the water mask are smoothed using a 1D Gaussian smoothing operation to obtain a gradual shoreline avoiding the pixel-induced staircase effect. A value of three for the standard deviation (σ) gives the best results based on the four validation cases; meaning that it takes three cells on both sides during the 1D smoothing. The method may result in several shoreline vectors since lakes and small channels are detected. In this case, only the most seaward shoreline position is analysed.

Other studies have applied global surface water change and occurrence detection (Donchyts, 2016,Pekel et al., 2016), but they lack validation with in-situ measured shoreline changes. A number of studies have validated their methods with either cross-shore positions at one location (Liu et al., 2017) or over limited spatial scales (Garcia-Rubio et al., 2015). Here we evaluate the validity of the shoreline detection method for four cases representing different types of beaches, sand, tidal and wave characteristics. Given the geographical spreading, we selected the following beaches with long-term shoreline monitoring programs: the Sand Engine (The Netherlands), Long Beach, WA (West Coast, USA), Narrabeen (Australia) and Hatteras Island (East Coast, USA). The latter case is presented below while the others are presented in Appendix B.

2.2.4 *Hatteras Island validation*

Validation of the shoreline detection method with observed shoreline changes was conducted along 63 km of sandy shoreline of Hatteras Island, North Carolina, spanning 13 years (Hapke and Henderson, 2015). The measured shorelines used in the analysis were generated from georeferenced historical aerial photographs and are used to develop shoreline change rate indicators for Hatteras Island, from Oregon Inlet in the North to Cape Hatteras in the South. A total of nine aerial photographs, covering the period ranging from 1989 through 2002, were obtained by the U.S. Army Corps of Engineers Field Research Facility in Duck, North Carolina. The high water line shorelines were digitized to produce a time series of shorelines for the study area. Rates of shoreline change were calculated for 1989–2002 using linear regression. For the same time period we collated 325 cloud-free satellite images and determined the shoreline position for this coastal stretch; the analysis took only 8 hours in total due to the computational power of the GEE platform. For each transect a linear regression was performed. The linear trends calculated from the SDS show good agreement with the observed shoreline change rates (see Fig. 2.2). The mean offset for all transects between observations and SDS is 2.0 m with a RMSE of 17 m. Appendix B summarizes the error statistics for all four cases. Based on

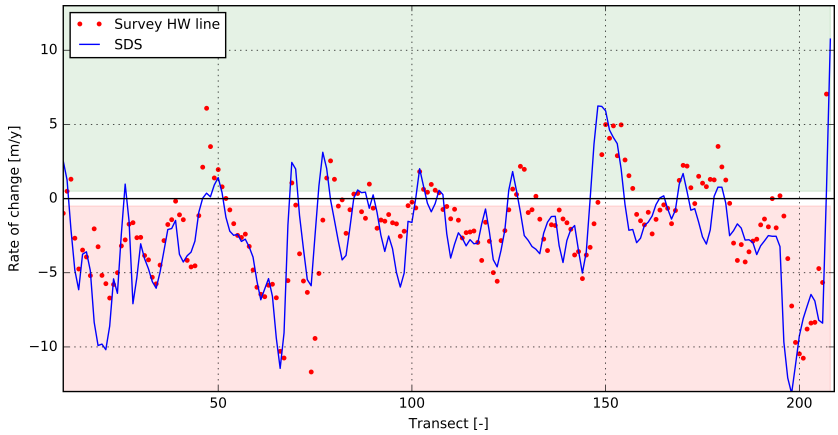

Figure 2.2: Observed trend rates (red dots) and satellite-derived trend rates of shoreline change (blue line) along Hatteras Island for the period 1989–2002.

these validations, the shoreline detection method can be concluded to be capable in deriving long-term shoreline change rates for a variety of coastal settings. The average of the offsets over three validation sites (excluding Long Beach) is 2.3 m with a RMSE of 21 m. Although the quantitative evaluation of the applied shoreline detection method with in-situ observations shows good capabilities, more verification is essential. Unfortunately, however, quantification of the influence of macro-tidal ranges, wave breaking and run up, beach slopes, etc. requires tidal, wave and beach characteristic information, which are generally not freely available.

2.2.5 *Global change rates for sandy shorelines*

For the global application presented here, we generated cloud-free annual-composites using the historical Landsat image archive. The automated shoreline detection method produces 33 annual global shorelines (1984–2016) with an alongshore resolution of 30 m. We then specified transects at a 500 m alongshore spacing, and determine the intersection point of each transect with the aforementioned annual shorelines, which provides a sequence of shoreline positions per transect. The shoreline change rate (m/yr) at each transect is then computed by applying linear regression to all shoreline positions at that location. Ideally, a SDS position is available for each transect annually. However, the availability of satellite images and cloud cover can limit the number of SDS positions. Encouragingly, however, 82% of all sandy transects consist of more than ten annual shoreline positions between

1984 and 2016. Nevertheless, to avoid unrealistic shoreline change rates we applied the following filters to all sandy transects:

- Transects containing less than 5 (out of 33) SDS data points as well as transects with a temporal coverage shorter than 7 years are omitted from the analysis (9% of all transects).
- Transects located beyond latitudes 60°N and 50°S (including Greenland and Antarctica) are omitted from the analysis due to possible ice coverage (9% of all transects).
- In the linear regression, outliers are identified as SDS points deviating more than three times the standard deviation and hence not considered in the regression. If the remaining number of data points is smaller than 5 points, then the transect is omitted from the analysis.

Application of these filters reduces the global data set to 81% of the original number of sandy transects.

The linear regression method used to quantify long-term shoreline change rates performs well in capturing trends of chronic sandy shoreline change, which is in line with Crowell et al. (1993). Shoreline changes at some transects however are characterized by unsteady changes in SDS positions for which other (fitting) methods may be more appropriate. For instance, human interventions such as the construction of ports, nourishments and dams in rivers can all lead to sudden shoreline changes, which may result in unrealistic change rates using the linear method on decadal scale.

However, for a first order quantitative comparison of change rates along a coastal section it is desirable to avoid using various fitting methods depending on the shoreline change signal. It is therefore recommended to add a second layer of information with characteristics per transect revealing the non-linear behavior; this is subject of further research.

Ultimately, more than 60% of the 2.2 million transects show an uncertainty bandwidth of less than 50% of the linear trend rate, which can be considered as a proxy for the representativeness of the linear regression method.

The shoreline change rates, presented at an alongshore resolution of 500 m along the world's shoreline, are publicly available and be accessible through the interactive website at: http://shorelinemonitor.deltares.nl.

2.2.6 *Defining Hot Spots*

In order to avoid localized hot spots, it was ensured that each eroding/accreting hot spot comprised at least 5 km of sandy shoreline where

all considered transects showed either erosive or accretive change rates larger than 0.5 m/yr over the 33 year data set. Two large-scale land reclamations appear in the top seven accretive beaches in the world. One reason is that those land reclamations consisted of bare sand in 2016, and hence are recognised as a wide sandy beach area by our methodology. The other reason is that the adjacent shorelines have advanced either due to the beach nourishment schemes or natural accumulation of sand in the shadow zones of these interventions.

2.3 RESULTS

2.3.1 *Global Occurrence of Sandy Shorelines*

Coastal classifications have been widely employed in the field of geomorphology to characterise the diversity of coastal landforms and the contexts within which they emerge, but hitherto no single system of classification has been comprehensive in scope or coverage (Finkl, 2004, French, 2016). Criteria in these classifications typically include tectonic (Inman and Nordstrom, 1971) and hydrodynamic controls, as well as the sedimentological response. Hydrodynamics controls considered include classifications of wave parameters (Davies, 1964), tidal range (Davies, 1964,Hayes, 1979) and a combination of both (Davies and Hayes, 1984). A ternary classification presented by Boyd et al., 1992, which considers the relative importance of fluvial inputs, wave energy, and tidal forcing provided a useful analysis of siliciclastic sedimentary coasts. The combination of tectonic and hydrodynamic controls led to the proposition of coastal morphogenetic classifications (Shepard, 1976), which are probably the most widely used classification schemes. Sediment texture and composition (Friedman, 1961) are additionally useful to classify and describe coastal sedimentary environments. However, previously reported values of the global occurrence of sandy shorelines vary between 10% and 75% (see Table 2.1). The methods used to arrive at these values remain, in most cases, unclear or qualitative (as also indicated in Table 2.1).

Table 2.1: Reported values of global and regional occurrences of sandy shorelines and percentages of chronic erosion and accretion.

Region	Parameter	References	Method used	Reported values		Derived values
Global	Percentage of sandy shoreline	Bird[12]	Interviews	20%		31%
		Bird[4]	Not stated	30%		
		Inman & Nordstorm[23]	Not stated	11%		
		Hardisty[54]	Not stated	34%		
		Van Rijn[8]	Not stated	10–15%		
		Bascom[9]	Not stated	75%		
		Brown[55]	Not stated	67%		
		Durgappa[56]	Not stated	20%		
		Bird[38]	Not stated	40%		
		Hinkel *et al.*[3]	Not stated	11%		
	Percentage of eroding sandy shoreline	Bird[12]	Interviews	Accretion	10%	27%
			Interviews	Stable	20%	49%
			Interviews	Erosion (<−0.5 m/yr)	70%	24%
			n.a.	Intense erosion		16%
			n.a.	Severe erosion		7%
			n.a.	Extreme erosion		4%
Europe	Percentage of sandy shoreline (sandy shoreline length)	Eurosion[10]	Aerial photos & surveys	40% (40,000 km)		23% (31,000 km)
	Percentage of eroding sandy shoreline	Eurosion[10]	Aerial photos & surveys	27% (excluding uplift of Finland and Sweden)		28%
USA	Percentage of sandy shoreline	Short[43]	Not stated	33%		30%
	Percentage of eroding sandy shoreline (Atlantic and Gulf coast only)	Heinz Center[44]	Aerial photos	80–90%		52%
Australia	Percentage of sandy shoreline	Woodroffe *et al.*[57] Short incl. Tasmania	Not stated	43–49%		52%
	Percentage of eroding sandy shoreline	No source found	n.a.	Not reported		25%

In our analysis, we applied supervised (human-guided) classification to global cloud-free satellite images (see Section 2.2) to identify sandy shorelines. One of the main reasons for our focus here on sand y beaches is that detecting shoreline dynamics for non-sandy shores like muddy coasts can be complex. Mild foreshore slopes, resulting in large horizontal tidal excursions, and high water content hampers correct shoreline detection. In the case of mangroves, seasonal growth cycles can impede correct shoreline detection. Moreover, it should be noted that as the reflectance signatures of sand and gravel beaches cannot be differentiated in the satellite imagery, as both materials originate from the same granular composites of finely divided rock, our references to sandy beaches herein also includes gravel beaches.

Our analysis showed that 31% of the ice-free world shoreline is sandy. The continent with the highest presence of sandy beaches is Africa (66%), while in Europe only 22% of the shoreline is sandy (see Fig. 2.3). The percentage of sandy shorelines obtained from this analysis for USA and Australia compare well with the more recently reported regional scale values (see Table 2.1). The larger deviation in percentage found for Europe is significantly influenced by the smaller total length of shoreline used in the Eurosion (Eurosion, 2004) data base. It should

be noted that the sandy beach classification also includes the gravel beaches in the world.

The global latitudinal distribution of sandy shorelines shows a distinct relation with latitude and hence with climate; no relation is found with longitude. The relative occurrence of sandy shorelines increases in the subtropics and lower mid-latitudes (20°–40°) with maxima around the horse latitudes (near 30°S and 25°N; see Fig. 2.3). In contrast, they are relatively less common (<20%) in the humid tropics where mud and mangroves (Giri et al., 2011) are most abundant as a result of high temperatures and rainfall. The percentage of sandy shorelines decreases beyond the 50° parallel. This latitudinal distribution of sandy shorelines is in line with the latitudinal variation of the common sediments in the inner continental shelf reported by Hayes (1967), based on ∼2000 transects from 131 coastal areas (see right subplot in Fig. 2.3).

2.3.2 *Global sandy beach erosion*

Worldwide beach erosion became apparent during the 1980s following the studies of the International Geographical Union working group on the Dynamics of Coastal Erosion (1972–1976) and the Commission on the Coastal Environment (1976–1984). In these studies, two hundred participants representing 127 countries contributed to a survey which indicated that 70% (10%) of the world's sandy beaches experienced net erosion (accretion) while 20% were stable (Bird, 1985). However, as these estimates were primarily a result of interviews, they are necessarily qualitative, at best. Furthermore, the estimates likely did not take into account changes occurring along undeveloped and uninhabited coasts due to the subjective methodology adopted.

The quantitative global distribution of sandy shorelines presented herein, for the first time, allows the derivation of objective and up to date global scale assessment of chronic shoreline changes (i.e. beach erosion/accretion). Beach erosion can occur at a range of timescales (Stive et al., 2002). Individual storms will generally result in rapid short-term erosion, followed by short-term accretion, leading to negligible net change over time scales of a few weeks-months. If sediment deficiencies persist for long periods of time (e.g. due to longshore gradients in sediment transport, reduction of fluvial sediment supply to the coast), chronic erosion can result. The analysis presented here focuses on such chronic erosion and accretion. However, there are no common standards for the classification of rates of chronic beach change (Moore, 2000) which is generally quantified through some statistical treatment of erosion rates and/or volumetric losses (e.g. Leatherman, 1983).

The accuracy of the SDS data of ∼0.5 pixel (see Section 2.1) and the study period of ∼30 years allows for a classification of beach change rates with class boundaries of 0.5 m/yr. Hence, we adopted the

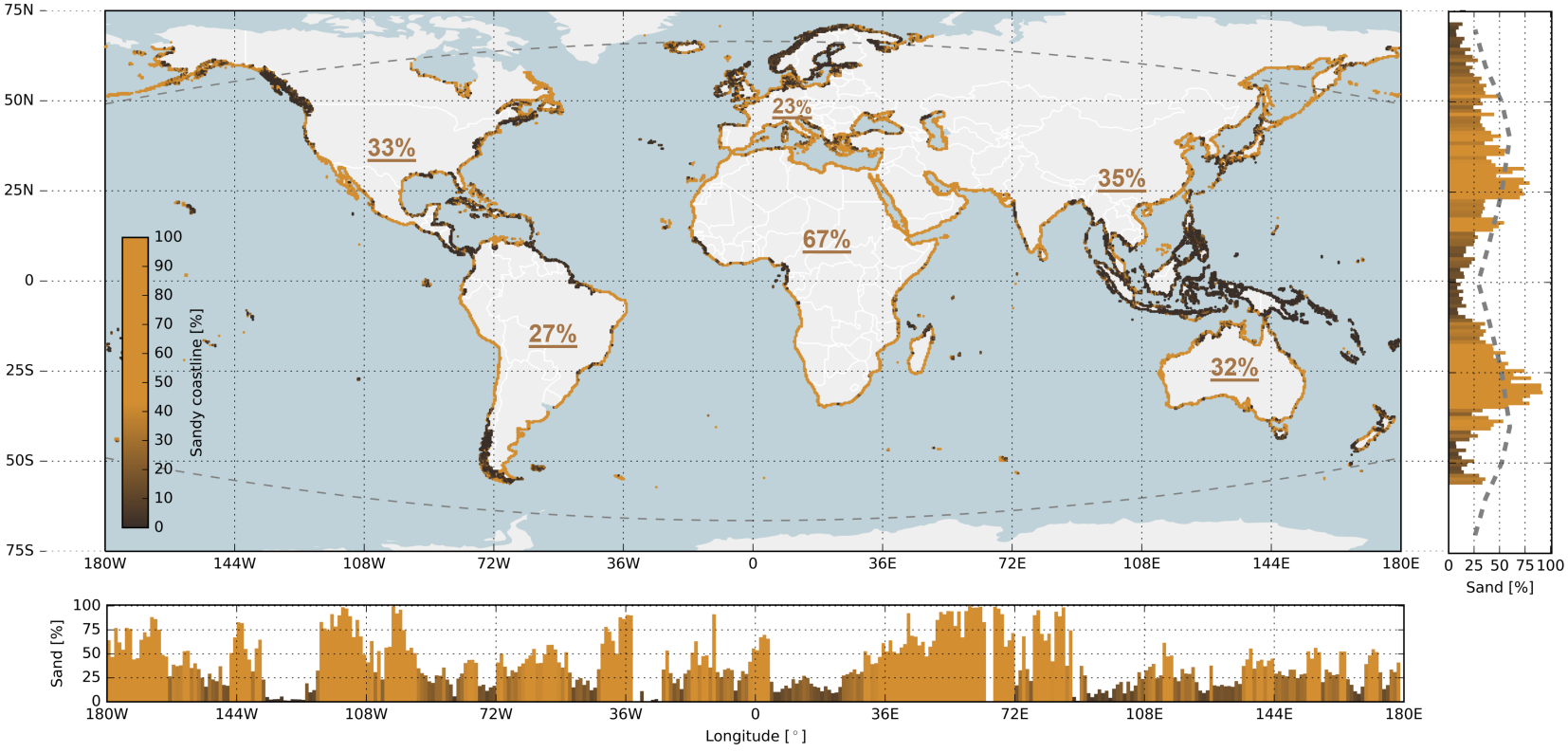

Figure 2.3: Global distribution of sandy shorelines; the coloured dots along the world's shoreline represent the local percentage of sandy shorelines (yellow is sand, dark brown is non-sand). The subplot to the right presents the relative occurrence of sandy shorelines per degree latitude, where the dashed line shows the latitudinal distribution of sandy shorelines reported by Hayes (1967). The lower subplot presents the relative occurrence of sandy shorelines per degree longitude. The curved, dashed grey lines in the main plot represent the boundaries of the ice-free shorelines considered in our analysis. The underlined percentages indicate the percentages of sandy shorelines averaged per continent.

chronic beach erosion classification scheme proposed by Esteves and Finkl (1998) and extended it with a classification for extreme erosion resulting in the below scheme:

- Accretion >0.5 m/yr
- Stable -0.5 to 0.5 m/yr
- Erosion -1 to -0.5 m/yr
- Intense erosion -3 to -1 m/yr
- Severe erosion -5 to -3 m/yr
- Extreme erosion <-5 m/yr

Our assessment shows that 24% of the world's sandy beaches are persistently eroding at a rate exceeding 0.5 m/yr over the study period (1984–2016), while 27% are accreting (see Table 2.1). About 16% (18%) of sandy beaches are experiencing erosion (accretion) rates exceeding 1 m/yr. Chronic erosion of beaches (smaller than -0.5 m/yr) is shown across the globe with relatively low latitudinal variation (see Fig. 2.4). Generally, between 30% and 40% of sandy beaches per degree latitude are eroding with relatively high eroding values up to 50% just south of the equator associated with large-scale land losses adjacent to the Amazon River mouth. More severe erosion rates are found at various locations across the globe. About 7% of the world's sandy beaches experience erosion rates classified as severe. Erosion rates exceed 5 m/yr along 4% of the sandy shoreline and are greater than 10 m/yr for 2% of the global sandy shoreline. On the other hand, about 8% of the world's sandy beaches experience significant accretion (larger than 3 m/yr), while 6% (3%) are accreting more than 5 m/yr (10 m/yr).

Taking a continental perspective, Australia and Africa are the only continents for which net erosion (-0.20 m/yr and -0.07 m/yr respectively) is found, with all other continents showing net accretion. The continent with the largest accretion rate (1.27 m/yr; see Fig. 2.4) is Asia, likely due to the artificial development of the Chinese coast and large land reclamations in, for example, Singapore, Hong Kong, Bahrain and UAE. On a global scale, the world's beaches have accreted on average 0.33 m/yr over the past three decades, i.e. a total gain of 3,663 km^2 over this period.

Using the SDS data we then focused on coastlines that are internationally recognised as nature protected areas by the World Database on Protected Areas (WDPA), which is the most comprehensive global database on terrestrial and marine protected areas, produced by UNEP-WCMC and IUCN (IUCN, 2016). Compared to the global average, a relatively high percentage of sandy shorelines in the WDPA-identified

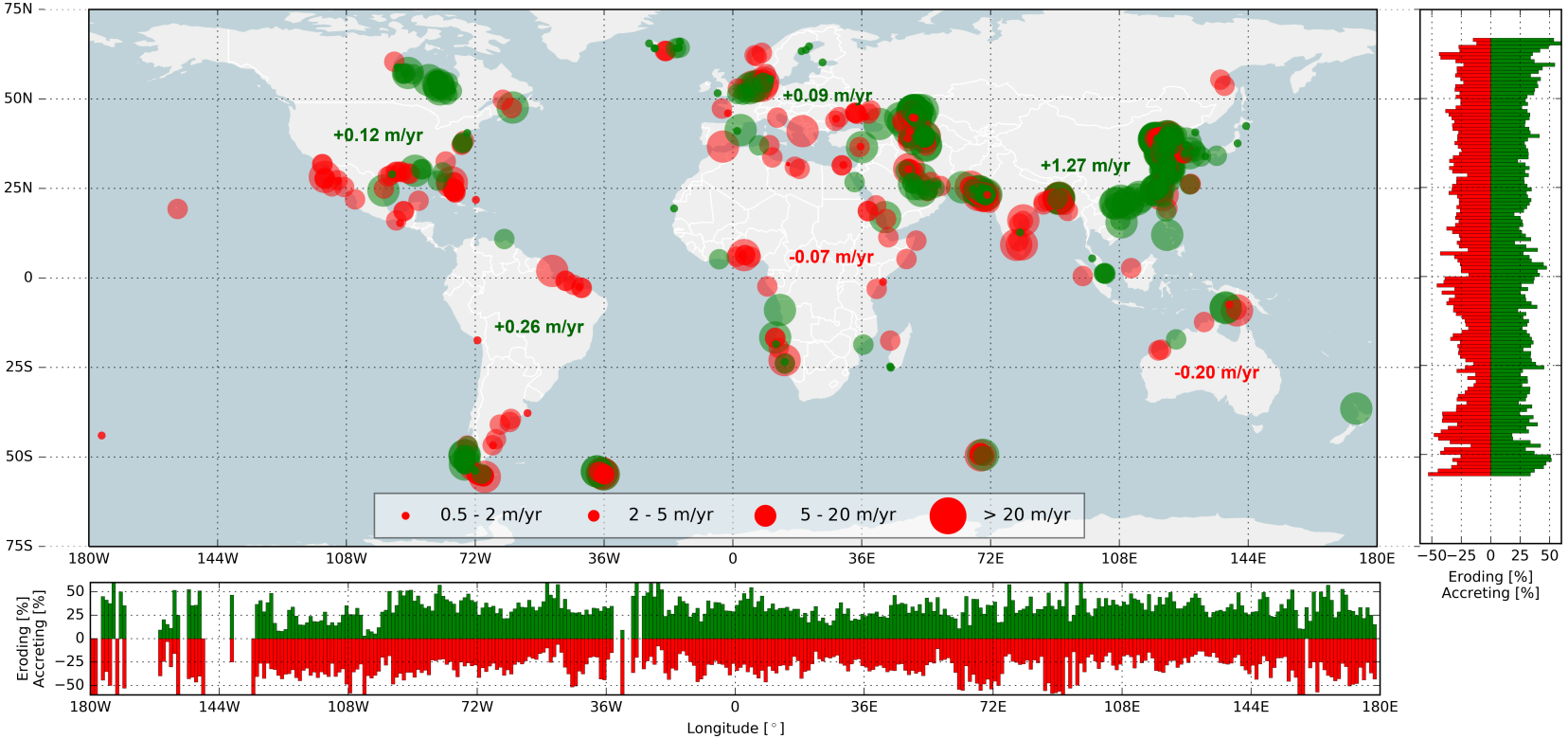

Figure 2.4: Global hotspots of beach erosion and accretion; the red (green) circles indicate erosion (accretion) for the four relevant shoreline dynamic classifications (see legend). The bar plots to the right and at the bottom present the relative occurrence of eroding (accreting) sandy shorelines per degree latitude and longitude, respectively. The numbers presented in the main plot represent the average change rate for all sandy shorelines per continent.

areas are experiencing erosion. Our analysis indicates that 32% of all marine protected shorelines are sandy of which 37% are eroding at a rate larger than 0.5 m/yr, while 32% are accreting.

2.3.3 *Quantifying local scale erosion/accretion due to human interventions*

No single explanation can easily account for the observed erosion/accretion trends along the global sandy shoreline, or for the acceleration of erosion/accretion on any particular beach (Bird, 2008). However, analysis of local trends derived from the global scale shoreline assessment presented herein can help identify natural and human drivers of shoreline change. To illustrate this, we present four highlights of erosive behaviour and four of accretive behaviour.

a) Sand mining and subsidence

The Mekong Delta in Vietnam, the third largest delta in the world, is increasingly affected by human activities and exposed to subsidence and coastal erosion. The large-scale shoreline erosion is attributed to excessive sand mining in the river and delta channels, and subsidence due to unregulated groundwater extraction (Anthony, 2015). Analysis of the SDS data (Fig. 2.5a) reveals slight erosion between 1984 and 1990, after which higher, but steady erosion rates are found. Erosion rates in the considered area typically range between 25–30 m/yr over the last three decades. Based on the strong linear trend, the SDS data may be used for projections of land loss and displacement strategies, as it is not expected that erosion rates will decrease in the near future unless mitigating measures are implemented.

b) Coastal structures

The harbour structures at Nouakchott, Mauritania, blocked the large unidirectional north-south longshore transport of sand since 1986, causing areas of beach erosion that has impacted the local social and urban developments. The shoreline evolution rates observed after the harbour construction are 10 times larger than the values that would have been observed in the natural state (Elmoustapha et al., 2007). The harbour breakwaters induced severe erosion over a distance of more than 10 km in the downdrift zone where accretion was likely to occur in the absence of the harbour. The SDS data (Fig. 2.5b) shows erosion rates of 20 m/yr.

c) Sand nourishments

A large-scale bypass system became operational in 2001 at the Tweed River, New South Wales, Australia, to mitigate erosion of the beaches to the north of jetties constructed at the river entrance (Dyson et al., 2001). The bypass system pumps sand from south of the river mouth

to three beach compartments located north of the river through buried pipelines. The SDS data (Fig. 2.5c) depicts a beach widening of ~250 m at Coolangatta Bay in the four years after the bypass system was commissioned.

d) Interception of longshore drift by coastal structures

The construction of two training breakwaters at Praia da Barra near the Aveiro Lagoon, Portugal interrupted the high southward ambient alongshore transport estimated at about 1 million $m^3/m/yr$ (Pranzini, 2013). This resulted in erosion at the south of the trained inlet affecting the shoreline over about 30 km downdrift, but also strong accretion updrift. The SDS data reveals the continuous and ongoing accretion of the northern beach at a rate of about 10 m/yr (Fig. 2.5d).

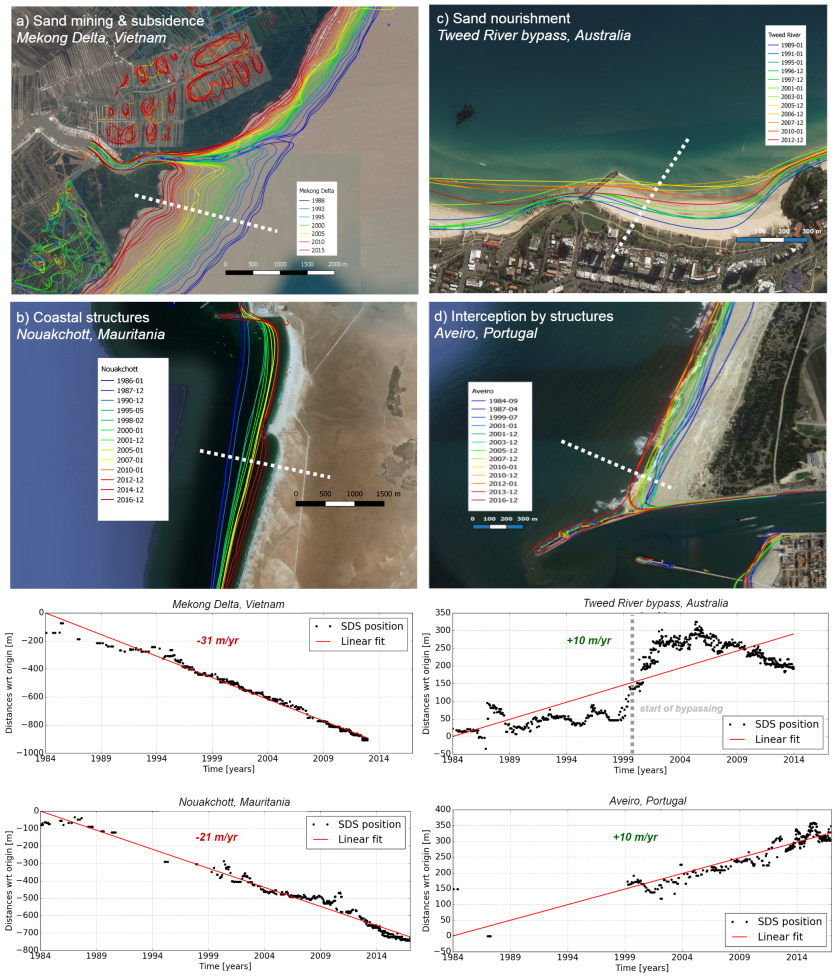

Figure 2.5: Examples of the satellite derived shorelines for four selected cases of beach erosion and accretion due to human interventions. The left column presents two erosive cases while the right column shows two accretive cases. In each figure, the blue line indicates the oldest SDS shoreline while the red line is the most recent SDS shoreline. The graphs below indicate the shoreline positions over time at the white dashed transect for each case; the upper graphs correspond to the images on the upper row. The indicated change rates (m/yr) are obtained from fitting a line-of-best fit to the shoreline position data for each transect.

e) Erosion due to river damming

Since the construction of Aswan High Dam in 1964 the Nile Delta in Egypt has been seriously impacted due to the change in water and sediment flow regimes. Based on shoreline observations of 1990 and

2013, extreme erosion at the mouth of the Rosetta branch were found, with erosion rates up to ∼25 m/yr (Ali and El-Magd, 2016). Analysis of the SDS data suggests that the erosional process increased around the 2000s, with a shoreline erosion of approx. 200 m in ∼12 years (see Fig. 2.6a). This example shows that SDS data can reveal fingerprints of human interventions on the coastal dynamics in time and space.

f) Erosion due to extreme events

Hurricane Sandy made landfall at the East coast of the US in 2012, resulting in a breach of the barrier island at Fire Island, New York (Hapke et al., 2013). The storm, with offshore wave heights up to 10 m, raised the local water level by more than 4.5 m. Surveys revealed that exposed parts of the dunes that are usually not impacted by waves, experienced significant dune erosion . This caused sediment deposition in the foreshore resulting in local shoreline advancement after the storm. The SDS data (see Fig. 2.6b) shows the hurricane-induced beach accretion at this location, but also the local post-hurricane beach recovery in the years after. Interestingly, the SDS data of this transect indicate that the beach width at this location became wider after the hurricane than it had been in the preceding three decades.

g) Accretion due to sudden changes in fluvial sediment supply

The phased removal of two large dams in 2012 in the Elwha River, Washington, as part of the river-restoration project aimed at stimulating habitat restoration, resulted in sudden availability (for fluvial transport) of about 21 million m^3 of sediment that had been impounded in the reservoirs (Warrick et al., 2015). This has resulted in large volumes of fluvial sediment being deposited at the river mouth (Warrick et al., 2015). The SDS data (see Fig. 2.6c) shows the development of an ebb tidal delta since 2014. Beach growth rates of ∼15 m/yr are found in the first years after removal.

g) Accretion due to ebb delta dynamics

Due to a closure of an estuary in the southwest of the Netherlands the relics of the corresponding ebb-tidal delta are migrating landward. The adjacent beaches are fed by the erosion of the delta front of ebb-tidal delta, which in 2005 resulted in the merger of a nearshore sand bank with the beach near Ouddorp (Elias et al., 2012). The SDS data (see Fig. 2.6d) shows the spatio-temporal characteristics of the beach accretion which led to significant beach widening of up to 500 m in a time span of just five years.

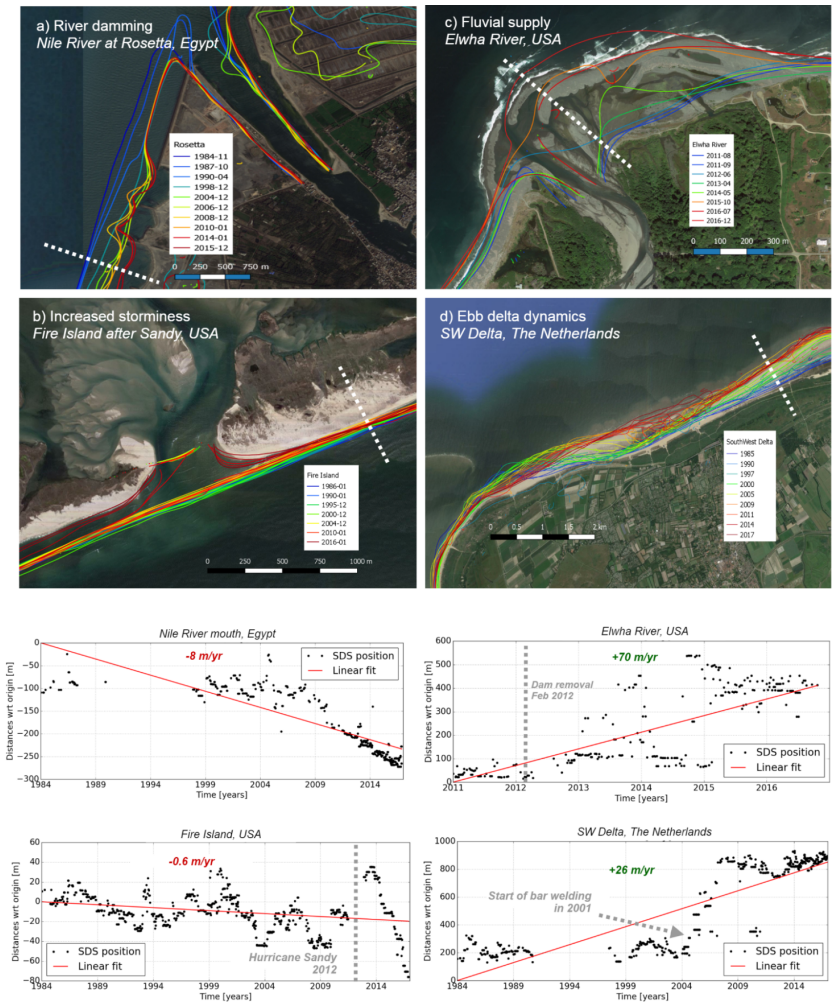

Figure 2.6: Examples of the satellite derived shorelines for four selected cases of beach erosion/accretion. The left column presents two erosive cases while the right column shows two accretive cases. In each figure, the blue line indicates the oldest SDS shoreline while the red line is the most recent SDS shoreline. The graphs below indicate the shoreline positions over time at the white dashed transect for each case; the upper graphs correspond to the images on the upper row. The indicated change rates (m/yr) are obtained from fitting a line-of-best fit to the shoreline position data for each transect.

2.3.4 *Global hot spots of erosive and accretive beaches*

Here we present the top eroding and accreting coastal stretches (i.e. hot spots) in the world (Table 2.2). The largest erosive hot spot is just south of Freeport in Texas where a 17 km stretch the beach has eroded on average more than 15 m/yr over the last three decades. The world's longest coastal stretch suffering severe erosion is located farther to the east in Texas where we observed a 29 km stretch of sandy beach with a mean erosion rate of 5.3 m/yr. Interestingly, four of the seven largest hot spots are located in the USA, consistent with the widespread concern and reports of erosion in the USA (Center, 2000; Galgano et al., 2004; Leatherman, 1983; Short, 1999).

The largest accretive hot spot is in Namibia at a location where a mining company has built unprotected sandy bunds in the sea to facilitate the diamond prospecting. The area landward of the bunds is dried out to enable more convenient diamond prospecting. Naturally accreting beaches of lengths exceeding 20 km and change rates larger than 7 m/yr are found at a migrating barrier island (Schiermonnikoog, The Netherlands) and at locations where sand dunes migrate into the sea (Madagascar and Mauritania). It is noteworthy that four of the seven largest accretive hot spots are in fact human-induced.

Table 2.2: World's largest erosive and accretive sandy beach hot spots. Areal change rate is calculated by multiplying the length of the section with the mean of the shoreline change trends of all transects in the relevant coastal stretch. The human-induced accretive hot spots are indicated by an asterisk.

	Areal change Rate (m^2/yr)	Mean change rate (m/yr)	Length of section (km)
Erosive Hot Spot Beaches			
Freeport, Texas, USA	−258,678	−15.2	17
San Rafael National Park, Chile	−243,459	−8.4	29
Rockefeller reserve, Louisiana, USA	−192,758	−16.0	12
Nebel island, Germany	−175,716	−12.1	15
Esbjerg, Denmark	−162,695	−8.1	20
High Island, Texas, USA	−155,287	−5.3	29
Hog Island, Virginia, USA	−154,848	−13.5	12
Accretive Hot Spot Beaches			
Diamond mines, Oranjemund, Namibia*	219,748	8.8	25
Around Karachi Port, Pakistan*	203,752	13.1	16
Schiermonnikoog Island, Netherlands	194,752	9.7	20
Rijnland Coast, Netherlands*	190,105	12.3	16
South Coast of Madagascar	153,573	7.0	22
Port Said, Egypt*	149,133	13.0	12
Mauritania	140,239	6.9	22

2.4 A CLOSER VIEW AT THE DUTCH COAST

The satellite derived shorelines can equally contribute on a more local scale in the coastal protection strategy. This is illustrated using the Dutch coast, a shoreline which has been nourished considerable in the last decades. Periodic sand nourishments have been carried out to maintain the coastline at its 1990 position, as prescribed by the 'Dynamic Preservation' policy. Between 1984 and late 2016 about 361 million m^3 of sand has been placed along the entire Dutch coast.

To have a closer view on the historic shoreline dynamics of the Dutch coast, the shoreline change rates are shown for the seaward facing beaches north of Hook of Holland (see Fig. 2.7). Interesting spatial variations in shoreline changes over a period of three decades can be observed. The beaches along the Holland coast (between Hook of Holland and Den Helder) have grown significantly between 1984 and late 2016. Shoreline accretion is largest in the south, only partly affected by the Sand Engine, and gradually reduces towards Den Helder. At the barrier islands a typical response is observed showing chronic erosion

of island heads while the center parts of the seaward facing beaches show accretion.

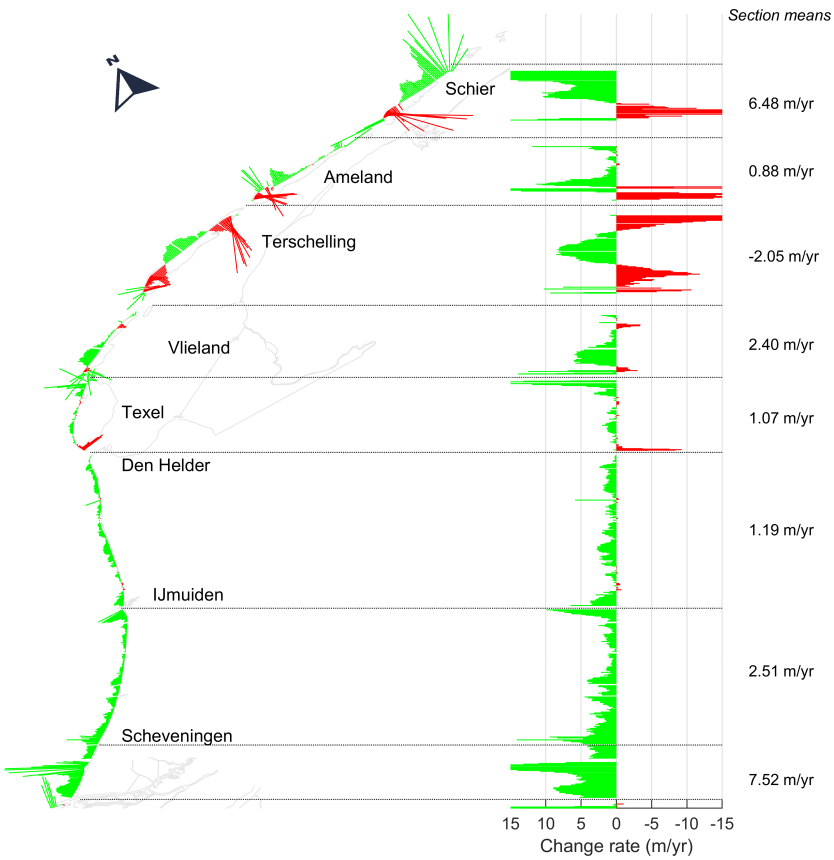

Figure 2.7: Shoreline change rates in m/yr based on satellite-derived positions between 1984 and 2016 for the Dutch coast. Rates in the right column represent the average of all transects in each alongshore section.

The average shoreline change rate for the Holland coast is 2.6 m/yr resulting in a seaward advancement of 86 m, averaged over the alongshore, since 1984.

Shoreline dynamics can be used to make a first-order estimate of the sediment budget for this coastline, e.g. for coastal zone management purposes. Integrating the shoreline advancement (2.6 m/yr) over the full length of the Holland coast (117 km) and assuming an active profile height of 12 m (from -8 to +4 m MSL), gives an estimated total sand volume of $\sim$120 million m^3 that has been added to the Holland coast in the period 1984 - 2016.

Records in the Dutch nourishment database of Rijkswaterstaat[1] unfold that approx. 206 million m^3 has been placed in this coastal stretch between 1984 and 2016, including two large-scale nourishments after 2011 accounting for 52.5 million m^3. This leaves a difference of approx. 86 million m^3 with the estimated volume.

A major explanation for the deviation between placed and derived volumes is expected to be the windblown transport redistributing sand from the intertidal area into the dunes above +4 m MSL. For the Holland coast the annual windblown transports typically range between 10 - 20 $m^3/m/yr$ (De Vries et al., 2012). Assuming an average rate of 15 $m^3/m/yr$, this adds up to a total volume of 58 million m^3 for the Holland coast in the period 1984 - 2016. Other possible reasons are related to the sand losses to offshore (beyond the -8 m MSL) and into the Marsdiep inlet between Den Helder and Texel.

Although the derived volumes are lower than the actual placed volumes, it demonstrates that the trend in shoreline position can act as an interesting proxy to assess changes in coastal sand volumes.

2.5 APPLICATION TO THE DELFLAND COAST

The historic shoreline dynamics of the Delfland coast are shown at the location of the Sand Engine near The Hague. Fig. 2.8a shows the shoreline positions at Ter Heijde between 1984 and 2010; so, prior to construction of the Sand Engine in 2011. A distinct prograding trend can be observed over time, which is the result of frequently nourishing this part of the coast since 1988.

Extending the analysis period until January 2019 clearly shows the impact of the Sand Engine in the shoreline position (see Fig. 2.8b). An advancement of $\sim$1 km occurred in 2011 followed by a gradual retreat of the shoreline ever since.

This example application illustrates that efficient automated processing of historic satellite imagery, which typically takes a couple of hours, can provide a unique view back in time on the dynamics of the coastal system at hand.

1 http://kml.deltares.nl/kml/rijkswaterstaat/suppleties/

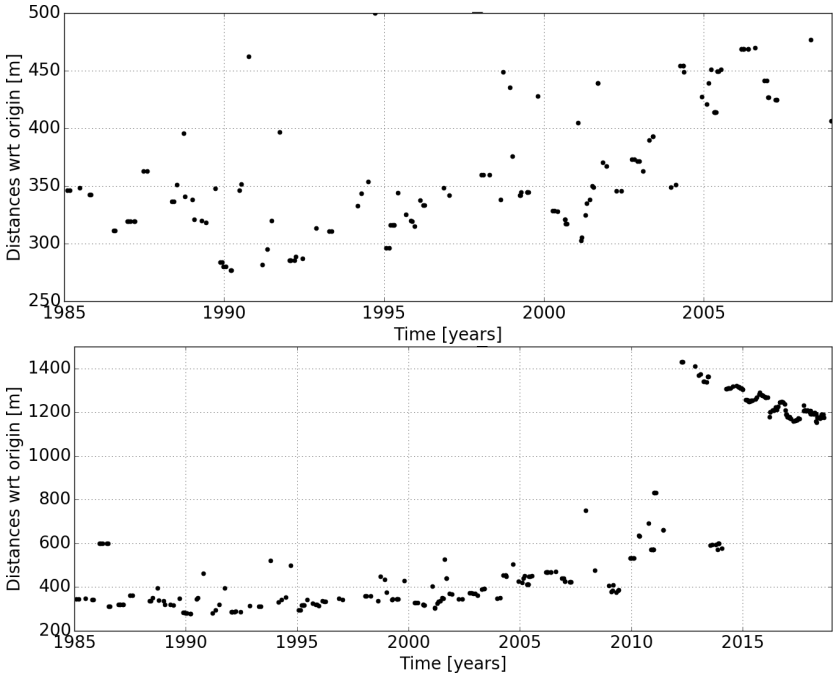

Figure 2.8: Satellite-derived shoreline positions at Ter Heijde for the period a) 1985 - 2010 and b) 1985 - 2019.

2.6 CONCLUSIONS

Coastal zones constitute one of the most heavily populated and developed land zones in the world. Despite the utility and economic benefits that coasts provide, there is no reliable global-scale assessment of historical shoreline change trends. Here, via the use of freely available optical satellite images captured since 1984, in conjunction with sophisticated image interrogation and analysis methods, we present a global-scale assessment of the occurrence of sandy beaches and rates of shoreline change therein. Applying pixel-based supervised classification, we found that 31% of the world's ice-free shoreline are sandy. The application of an automated shoreline detection method to the sandy shorelines thus identified resulted in a global dataset of shoreline change rates for the 33 year period 1984–2016. Analysis of the satellite derived shoreline data indicates that 24% of the world's sandy beaches are eroding at rates exceeding 0.5 m/yr, while 28% are accreting and 48% are stable. The majority of the sandy shorelines in marine protected areas are eroding, raising cause for serious concern.

Part II

NUMERICAL MODELLING

3

PROCESSES DRIVING THE INITIAL RESPONSE OF A MEGA-NOURISHMENT

Large part of this chapter is based on: Arjen P. Luijendijk, Roshanka Ranasinghe, Matthieu A. de Schipper, Bas A. Huisman, Cilia M. Swinkels, Dirk J.R. Walstra, and Marcel J.F. Stive. "The initial morphological response of the Sand Engine: a process-based modelling study". Published in Coastal Engineering, Volume 119 (2017) (Luijendijk et al., 2017).

3.1 INTRODUCTION

Around 75% of the Dutch coast consists of dune areas that provide protection from flooding for the low-lying hinterland (Ronde et al., 2003; Southgate, 2011). Besides that, the sandy coast is also important for ecological and recreational functions and fresh water extraction. Large sections of the Dutch coast have been eroding for centuries (Van Vessem and Stolk, 1990; Van Rijn, 1995; Van Rijn, 1997; Wijnberg, 2002) which has traditionally been negated with measures such as groynes and/or managed retreat, and since the 1990s, beach/shoreface nourishments. Over the years, the total annual sand nourishment volume along the Dutch coast has steadily increased (Elias et al., 2012; De Sonneville and Spek, 2012) to its present value of approximately 12 million m^3/yr.

In 2008, a Dutch State Committee (the 2^{nd} Delta Committee, Stive et al., 2011) provided critical advice for protecting the Dutch coast and the low-lying hinterland from the consequences of foreshadowed climate change in the 21^{st} century. In line with a key recommendation of the Delta Committee, an innovative pilot project was developed to achieve a more efficient and sustainable nourishment approach; the Sand Engine ('Zandmotor' in Dutch; hereafter referred to as ZM). This 'mega-nourishment', built in 2011 along the Delfland coast (see Fig. 3.1a) consists of a total dredged sediment volume of 21 million m^3. The ZM is a combined beach/shoreface nourishment and consists of a man-made peninsula of about 128 ha (Stive et al., 2013). It is expected that over the next 20 years, natural coastal processes will redistribute the sand in the peninsula along the coast between Hook of Holland and Scheveningen (see Fig. 3.1b and c), leading to an increase of the footprint of the dunes of 33 ha (Mulder and Tonnon, 2010).

The scale of the ZM is unprecedented for a sand nourishment. A comprehensive multidisciplinary ten-year monitoring program was launched in 2011 to monitor and investigate multiple aspects of the initial ZM evolution and coastal response to the ZM. The monitor-

ing campaign provides valuable data on both the forcing conditions and the behavior of the ZM. However, the observed morphological behavior cannot be directly related to specific forcing conditions due to the relatively low temporal resolution (∽monthly) of the bathymetric surveys of the ZM. A numerical model that can reproduce the observed behavior to a high degree of detail is therefore the only means of understanding the physical processes that govern the initial evolution of the ZM and the adjacent coast. Therefore, this study uses data acquired in the first 12 months following the completion of the ZM (August 2011 - August 2012) in conjunction with state-of-the-art process based morphodynamic modelling to gain insights into the initial response of the nourishment and the adjacent coastline as well as the dominant physical processes. The study period of the first 12 months is selected here to focus on the initial development from a man-made shape to a more smooth shape, a transition which is poorly produced in one line models and vital to the overall development (Elko and Wang, 2007). These insights are anticipated to provide a guide for other large-scale sandy strategies such as artificial islands, land reclamations, (mega-) nourishments worldwide.

Specifically, this study attempts to answer the following:

1) Can a state-of-the-art 2DH process-based morphodynamic model reproduce the initial morphological evolution of the ZM and the adjacent coast with sufficient accuracy?

2) What are the forcing conditions that govern the initial morphological evolution of the ZM?

Figure 3.1: a) overview of the Dutch Coast, b) the Delfland coast showing the location of the Sand Engine (harbour structures in yellow), and c) aerial photograph of the Sand Engine in July 2011 just after construction (courtesy: Rijkswaterstaat/Joop van Houdt)

This chapter is arranged as follows. Section 3.2 introduces the ZM project and the available monitoring data used in this study. In Section 3.3 the morphodynamic modelling approach, verification, and the evaluation of the model performance are described. Section 3.4 investigates the relationships between environmental forcing and the initial morphological evolution of the ZM and the adjacent coast as

well as the relative contribution of the different forcing mechanisms. Finally, Section 3.5 presents the conclusions of this work.

3.2 THE SAND ENGINE PROJECT

3.2.1 *Coastal setting*

The Delfland coast is the southern section (16.5 km) of the Holland coast between Hook of Holland and Scheveningen (see Fig. 3.1a and b). The nearshore zone is characterized by a rather uniform, gradually sloping beach profile with occasionally a nearshore bar (Wijnberg and Terwindt, 1995). The width of the dune area from the dune foot varies from narrow (i.e. 150 to 250 m width) in the central section of the Delfland coast to very wide (500 m width) at Hook of Holland and just north of the ZM. The dune height is generally between NAP +10 m to NAP +15 m, but locally, dunes can reach over NAP +20 m.

The tide at Scheveningen is semi-diurnal with a spring/neap tidal amplitude of 1.98/1.48 m. The tide is asymmetric with on average a rising period of 4 hours and 21 minutes, while the falling period lasts for about 8 hours. This causes asymmetric alongshore velocities with maximum flood tidal currents of $\sim$0.7 m/s (northeast directed) and maximum ebb tidal currents of $\sim$0.5 m/s (southwest directed). The 1-year return period surge level at Hook of Holland is 2.35 m.

The wave climate along the Dutch coast shows little spatial variation but is characterized by a distinct seasonal signal with average winter (Nov-Jan)/summer (Apr-Aug) offshore wave heights (H_s) of 1.7/1 m. Small waves ($H_s < 1$ m) originate predominantly from the northwest, average waves (1.5 m $< H_s <$ 3.5 m) predominantly from both the southwest and northwest while the highest waves ($H_s > 4.5$ m) originate predominantly from the west and northwest (see Fig. 3.2a). The 1-year return period offshore wave height H_s is 4 m.

The Delfland coast consists of sandy beaches with an average median grain size (D_{50}) of 242 μm with a standard deviation of about 50 μm (Wijsman and Verduin, 2011). Previous studies on the sediment transport along the Dutch coast indicate a northward longshore transport between 50.000 to 170.000 m^3/year at the location of the ZM (Van Rijn, 1995; Rest, 2004). Near Hook of Holland the alongshore sediment transport is completely blocked due to the presence of a large groin called the *Noorderdam* protruding 4.2 km into sea (see Fig. 3.1b). In contrast, the relatively small harbour moles of Scheveningen harbour allow sediment bypassing. The Delfland coast is subject to chronic erosion due to the sediment demand by neighboring tidal inlet systems, relative sea level rise and reduced sediment supply from the rivers (Van Rijn, 1995; Stive et al., 2013). A dominant factor in the long-term erosive process at the Delfland coast is the presence of the nearby Rhine-Meuse estuary,

which acts as a sink for the marine sediments as the fluvial sediment supply has diminished substantially over the last centuries. Based on reconstructions of the coastline using old charts (since 1600s), Van Rijn, 1995 estimated that the coastline at the location of the ZM has retreated about 1 km between 1600 and 1990; roughly ∼2.5 m per year.

After a successful test with three groynes in 1791, twelve additional rock groynes were built in the years thereafter, which locally reduced coastline recession to $0.5 - 1$ m/year (Van Rijn, 1995). In the period 1807 to 1827 the groin field was extended northwards with nine more groynes. Thereafter, another 47 groynes were placed until 1930, resulting in a total of 68 groynes along the Delfland coast (Hendriks, 2011). Despite these efforts, this coastal stretch remained erosive.

A sea change in the Dutch thinking related to coastal protection led to the introduction of sand nourishments from the 1970s along this part of the coast. Since then, the frequency of nourishments has increased to once every 3 - 4 years. In total, approximately 55 million m^3 of sand has been nourished at the Delfland coast for erosion mitigation and land reclamation (e.g. nature-compensation for the extension of the Port of Rotterdam, Maasvlakte II). In the decade prior to construction of the ZM, nourishment volumes in this stretch had increased to ∼1.7 million m^3 per year, which is about 100 m^3 of nourished sand per alongshore meter of coast per year (De Schipper et al., 2016).

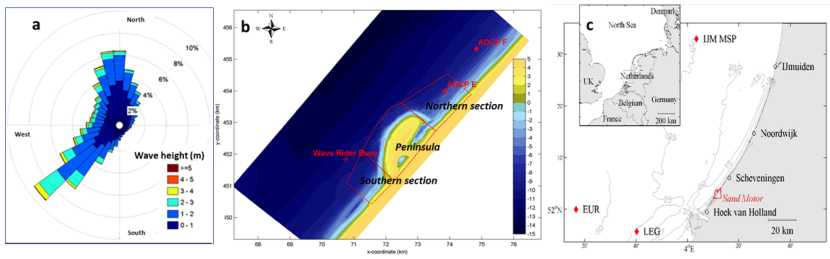

Figure 3.2: a) wave rose for Europlatform based on 25 years of wave records, b) the observed ZM bed elevation (in meters) of August 2011 and the locations of two ADCPs, a wave rider buoy, and the three control sections and c) locations of ZM and relevant measuring stations in the Netherlands (IJM MSP = IJmuiden MunitieStortplaats, EUR = Europlatform, LEG = Licht Eiland Goeree).

3.2.2 *The Sand Engine design*

The ZM project consists of a large peninsula (see Fig. 3.2b) with two flanking shoreface nourishments. The main peninsula part is hook shaped with the outer tip curved towards the north. This design and location best fulfilled the multidisciplinary and multi-stakeholders requirements of safety in combination with recreation, nature develop-

ment and scientific innovation (Stive et al., 2013). The most seaward position of the ZM coastline (NAP 0 m contour) protrudes ∽1000 m from the original coastline. The cross-shore slope of the peninsula is 1:50, such that the toe of the nourishment is positioned at NAP -8 m and 1500 m from the original coastline. The alongshore base length of the ZM peninsula was ∽2000 m just after construction. The northern tip of the peninsula creates a sheltered area that is anticipated to form a nurturing area for different biotic species. Furthermore, the ZM contains a small (∽8 ha) lake at the base of the peninsula (see Fig. 3.1c). This lake is intended to prevent the freshwater lens in the dunes from migrating seaward, which could endanger groundwater extraction from the more landward existing dune area (De Schipper et al., 2016). Sediment for the nourishment was required to be similar to the surrounding coast and regular grain size analysis during construction (after each 0.5 million m^3 of nourished sediment) showed an average D_{50} of 278 μm (Huisman et al., 2014). The total cost for construction of the peninsula was about 50 million euro.

3.2.3 *Data and observations*

The post-construction monitoring program included regular bathymetrical, topographical, current, and wave measurements. Table 3.1 provides an overview of the type of measurements that were undertaken as well as the instruments, frequency and the area that was covered as relevant for this study.

Table 3.1: Overview of monitoring at the Sand Engine during the first 12 months (as relevant for this study)

Measured parameter	Means	Frequency	Coverage (locations in Figure 2b and c)
In-situ bathymetry and topography	Jetski and quad bike	Monthly for the first year; Every two months thereafter	The ZM and adjacent coastal areas (longshore stretch of ∽4.7 km)
Wave data	Wave Rider buoy	Continuous from December 2011	Located at 10 m water depth just south of the ZM
	Two platforms	Continuous (part of standard monitoring)	Europlatform 3 (EUR; water depth h = 30 m) and Ijmuiden Munitiestortplaats (IJM MSP; h = 24 m)
Hydrodynamic data	Two ADCP's	Continuous from April 2012	Located at h =6 and 8 m north of ZM
	Tide gauge	Continuous	Located in Scheveningen Harbour
Sediment samples	Grab samples	Annual	Several cross-shore transects at the ZM
Wind data	Weather station	Continuous	Lichteiland Goeree (LEG) and Hook of Holland

A detailed analysis of the morphological evolution of the ZM in the first 12 months (see Fig. 3.3) undertaken by De Schipper et al., 2016 has revealed the following main behavioral characteristics.

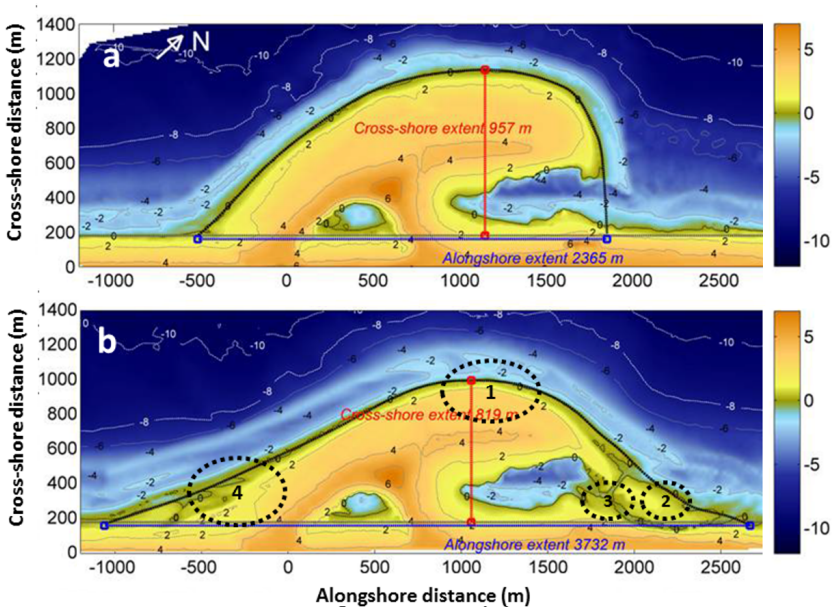

Figure 3.3: Observed bed elevations (in meters) in August 2011 (a) and August 2012 (b) after De Schipper et al., 2016.

The most seaward point (at the water line) of the ZM retreated from 960 m to 820 m, indicating a large initial erosion of the tip of the peninsula (see ① in Fig. 3.3b). The cross-shore profile on the seaward side of ZM became gentler and more similar to the natural slope of the coast. Simultaneously the alongshore extent of the nourishment increased from 2370 to 3730 m. Considerable accretion was observed on the adjacent coast to the northeast and southwest of the ZM; the nourishment disperses approximately symmetrically from the center of the peninsula. On the northern side of the peninsula, the morphological behavior is dominated by the dynamics of the lagoon entrance. Soon after construction of the peninsula, a spit developed, squeezing the lagoon entrance. In the first months, the spit mostly elongated along the adjacent coast and widened to about 300 - 400 m (②). The crest level of the spit is approximately similar to the high water level (NAP +1.2 m), such that it is flooded during high tide and storms. The tidal channel into the lagoon migrated to the northeast and extended considerably over time (③). Strong velocities of over 1 m/s were observed here during rising and falling tide. The accretion on the southern side of the ZM is attributed to the local reduction in net sediment transport capacity (④). Changes on the dry beach were small; i.e. order of 0.2 - 0.3 m lowering after one year.

The observed cumulative volume changes during the study period (August 2011 - August 2012) and concurrent wave heights and surge levels are shown in Fig. 3.4. To facilitate a detailed analysis, the study area has been divided into three control sections as illustrated in Fig. 3.2a: Peninsula (i.e. the main central part of the ZM), and Northern and Southern sections (i.e. adjacent coast to the northeast and southwest of the ZM). The control areas cover the area from approximately NAP -10 m to NAP +3 m. By August 2012, approximately 1.7 million m^3 had eroded from the peninsula area while about 1.2 million m^3 had accreted along the adjacent coastal sections (see Fig. 3.4a). Consequently, it appears that about 0.5 million m^3 has been transported out of the overall survey domain; this volume may be constituted of cross-shore (both offshore and landward, into the dunes) and/or alongshore losses.

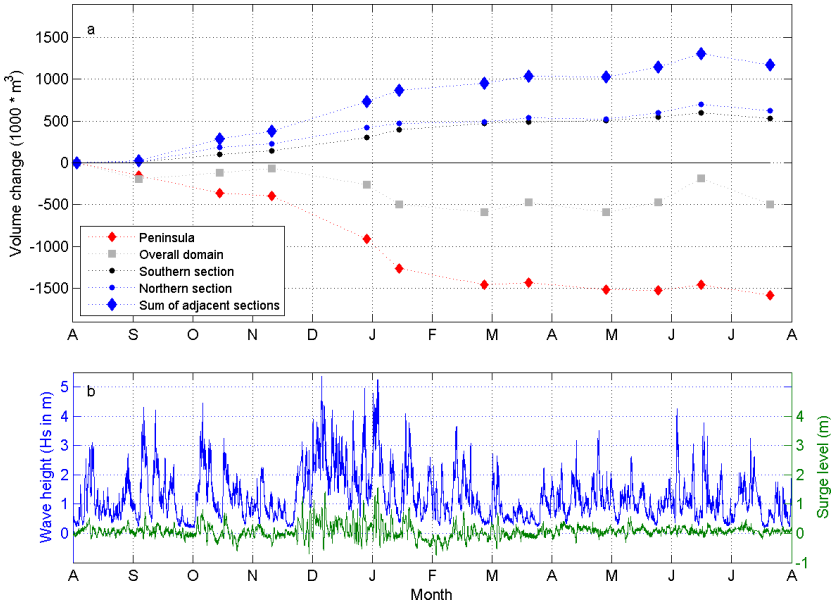

Figure 3.4: a) cumulative volume change in the three different control sections (see Fig. 3.2b) from August 2011 till August 2012 (in million m^3; negative values indicate erosion) and b) time series of the observed concurrent significant wave heights at Europlatform and observed surge levels at Hook of Holland.

3.3 MODELLING THE INITIAL MORPHOLOGICAL RESPONSE

3.3.1 *Model description*

To understand the physical process governing the initial response of the ZM and the adjacent coast, first a morphodynamic model that can accurately reproduce the observed morphological changes in the study area (under concurrent forcing) needs to be established. To achieve this goal, the process-based numerical model Delft3D (Lesser et al., 2004) is used here to compute hydrodynamics, waves, sediment transport and morphology under influence of tidal, wind, and wave-driven currents. The basic model structure (see Fig. 3.5) and Delft3D are fully described in Lesser et al. (2004) and is therefore not further described here.

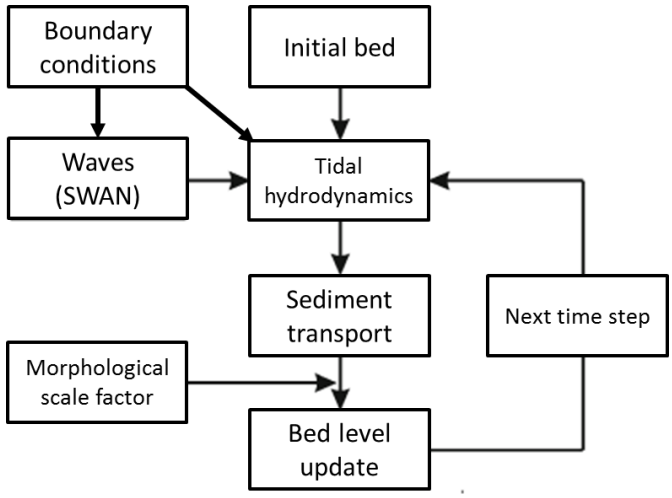

Figure 3.5: Overview of the morphodynamic feedback loop applied in Delft3D.

The target of the modelling exercise is to obtain a model hindcast (August 2011 - August 2012) that accurately reproduces 1) the magnitude of volume changes and 2) the observed erosion and sedimentation patterns in the entire study area. It is envisaged that the model can then also compute the individual impacts of separate wave conditions, which is relevant for further analysis in this research. While Delft3D includes an option to employ a morphological acceleration factor to speed up morphodynamic simulations (Roelvink, 2006; Ranasinghe et al., 2011), no such acceleration was implemented here as model accuracy is of paramount importance in this application.

3.3.2 *Model implementation*

The domain around the ZM was schematized with a curvilinear computational grid (indicated by the red box in Fig. 3.6b). The grid covers an area of 9.5 km in longshore direction and 4 km in cross-shore direction. The water depth at the offshore boundary is approximately 15 m. The grid resolution varies from 35 m to 135 m and the grid consists of 154 by 130 cells. The cell size increases with distance from the ZM. The bathymetry and the subaerial topography used in the model are based on the first survey conducted after completion of the ZM on 3 August 2011. Echo-sounding surveys conducted by Rijkswaterstaat in the last two decades are used for the remainder of the model domain (required for far-field tidal and wave models; see below).

The tidal boundary conditions for the model domain were retrieved via a series of nested hydrodynamic models to accurately incorporate the tidal characteristics along the Delfland coast and the generation of horizontal tidal currents. The simulations were conducted in depth-averaged (2DH) and hydrostatic mode. The large-scale Dutch Continental Shelf Model (Zijl et al., 2013; Slobbe et al., 2013) was simulated for three months to provide tidal boundary conditions for the medium-scale Coastal Strip (i.e. *'kustfijn'* in Dutch) model (see Fig. 3.6a) which, in turn, provided tidal information for the detailed Delft3D model covering the ZM. The tidal information was converted into astronomical components for the offshore boundary, while zero-gradient alongshore water level conditions (following the method described in Roelvink and Walstra, 2004) were invoked on the lateral boundaries. Observed surge levels at Hook of Holland (see Fig. 3.4b) were added to the tidal water level forcing. Wind effects on the hydrodynamics were included by applying the measured 10-minute averaged wind time series from Hook of Holland. All presented simulations were conducted in depth-averaged (2DH) and hydrostatic mode.

For the wave propagation modelling, three nested computational grids were applied. The large-scale wave grid with lowest resolution (see Fig. 3.6b) was forced with measured time series of wave heights, periods and directions of the two offshore platforms Europlatform (EUR; see Fig. 3.2c) and IJmuiden Munitiestortplaats (IJM MSP). A uniform wind was applied based on the measured time series of wind conditions at Lichteiland Goeree (LEG). The large-scale wave grid which extends up to the location of the offshore wave buoys covers an area of about 79 km in longshore direction and 42 km in cross-shore direction, with varying grid resolution from about 170 m to more than 2000 m. The medium-scale wave domain (25 km by 13 km) was nested in the large-scale wave grid while the ZM wave domain (10.5 km by 4.5 km) was nested in the medium-scale domain. This degree of nesting, while

computationally expensive, was required to ensure that the effect of refraction on the irregular bathymetry just north of the Port of Rotterdam was accurately represented in the ZM computations. The ZM wave domain is similar to the hydrodynamic model but has been extended by ∽500 m in southern, western and northern direction.
Although the offshore wave observations shows large angles of incidence, the angle of incidence of the waves refracted towards the seaward edge of the surf zone (5 m) is not larger than 45 degrees to shore-normal for significant wave heights up to 1.5 m; higher waves refract even more.

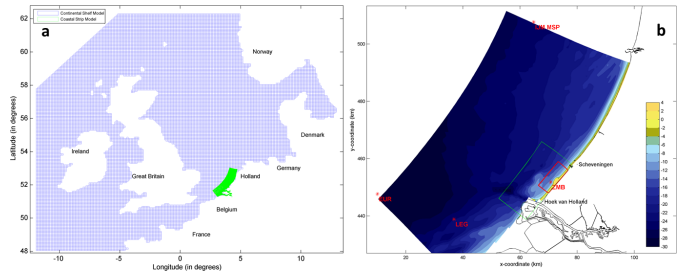

Figure 3.6: a) cascade of hydrodynamic models: Continental Shelf Model (in blue) and Coastal Strip model domains in green, and b) overall wave model domain and outlines of medium-scale (in green) and ZM wave model domains (in red; bed elevations in meters w.r.t. NAP). Note that the hydrodynamic model is equal to the ZM wave model, but slightly smaller.

3.3.3 *Model verification*

All standard hydrodynamic parameters in Delft3D were kept at default settings for the 1-year long verification simulation. Modeled water levels, velocities and wave height were subjected to quantitative comparisons with field observations. The comparison statistics obtained are summarized in Table 3.2.

Table 3.2: Model verification and comparison statistics.

Goal variable	Observation period of verification			Signal	Statistics		
	Start date	End date	Length		Corr	R^2	RMSE
Water levels	1-Jun-2012	1-Aug-2012	61 d	Time series	0.98	0.95	0.14
				Tidal amplitude	Amplitude differences; see Table 3		
				Tidal phases	Phase differences; see Table 3		
Flow velocity	1-Jul-2012	4-Aug-2012	34 d	Current amplitude	Amplitude differences; see Table 3		
				Current phases	Phase differences; see Table 3		
Wave height	17-Dec-2011	25-Jan-2012	39 d	Time series	0.94	0.82	0.40

3.3.3.1 *Water levels and currents*

As the domain of the ZM model does not cover a permanent water level station, the water level verification was conducted with the Coastal Strip model for the station of Scheveningen. Besides a time series comparison between computed and observed water levels including wind and pressure effects (statistics are presented in Table 3.2), a period of two months was used for a detailed tidal analysis using T−tide (Pawlowicz et al., 2002). Such an analysis omits all non-tidal effects. Modeled and measured water levels were compared and the differences for six dominant tidal constituents were marginal with deviations in amplitudes up to 0.02 m and less than 12 min in phase (see Table 3.2).

The model performance for depth-averaged currents was evaluated against observations from ADCP location F (see Fig. 3.2b) for a period of 34 days (see 3.7a). Time series of the computed currents show the typical characteristics of the observed current magnitudes, but regularly underestimate the peak flood velocities during neap tides and overestimate ebb currents. The good correspondence of the measured (0.29 m/s) and modeled (0.30 m/s) main tidal constituent (M2) suggests that the increase in velocity is likely due to non-tidal effects, which in this case is probably the fresh water plume from the Rhine River which would enhance (retard) the tidal flow during the flood (ebb) phase.

3.3.3.2 *Waves*

Wave measurement data were available since the deployment of a nearshore wave buoy in mid-December 2011. The modeled and measured wave heights at the location of the nearshore wave buoy (water depth of 10 m) are shown in 3.7b for the first six weeks after installation. As this period captures sufficient wave events (with wave heights H_s up to 5.5 m), it was judged that this period was sufficiently long to verify the wave model performance. The model provides a very good representation of the nearshore waves during storms (both wave heights and time of occurrence), although the peak of the storm on the 5^{th} of January 2012 is slightly underestimated. Overall, the correlation coefficient is 0.94 and the R^2 is 0.82. Model/data differences are larger when wave heights are lower than $\backsim$1.5 m. From a morphological point of view these mild wave conditions are expected to be of less importance; this will be further discussed in Section 3.4.

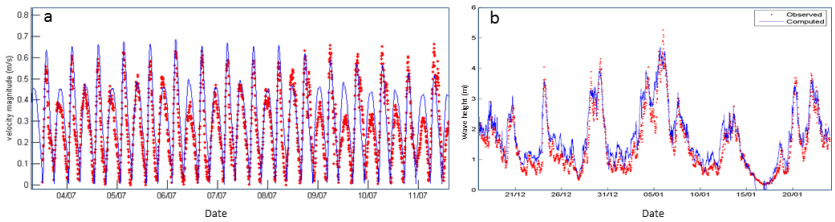

Figure 3.7: a) shows the comparison between computed and observed currents at location F for July 2012 (blue represents the computed currents) and b) presents computed and observed wave heights at the nearshore wave rider buoy for the period 17 December 2011 – 25 January 2012. For locations of the observations see Fig. 3.2b.

Table 3.3: Results of the statistical tidal analyses of water levels and currents.

	Water levels at Scheveningen					Currents at ADCP F			
	Amplitudes (m/s)		Phases (min)			Amplitudes (m/s)		Phases (min)	
Constituents	obs	mod	obs	mod	Constituents	obs	mod	obs	mod
O1	0.10	0.11	176	177	MU2	0.03	0.03	119	140
K1	0.09	0.11	338	335	N2	0.04	0.04	325	349
M2	0.78	0.76	68	73	M2	0.29	0.30	40	32
S2	0.17	0.18	136	137	L2	0.05	0.06	113	97
M4	0.22	0.22	103	114	S2	0.08	0.03	115	51
MS4	0.10	0.11	168	174	M4	0.01	0.04	2	81

3.3.3.3 *Morphology*

A brute-force (MORFAC = 1) simulation forced with tides, winds, surge and waves was undertaken for the 12 month study period (August 2011-August 2012). Analysis of the first model results after one year showed that significant bed level changes (of more than 0.1 m) only occurred for wave heights higher than 1.5 m. As the focus of this study is on erosional / accretional behavior the bed level changes were used as a diagnostic to eliminate certain wave conditions from the computation. Wave conditions with a wave height below 1.5 m and those with waves directed away from the coast (between nautical angles 30◦ and 180◦, which resulted in a combined total of 55% of the year, were omitted from the simulation, resulting in a 40% reduction of the computational effort. Applying the morphological model with its default formulations and (user manual suggested) parameter settings results in a morphological evolution that is quite far from observed (see Fig. 3.8).

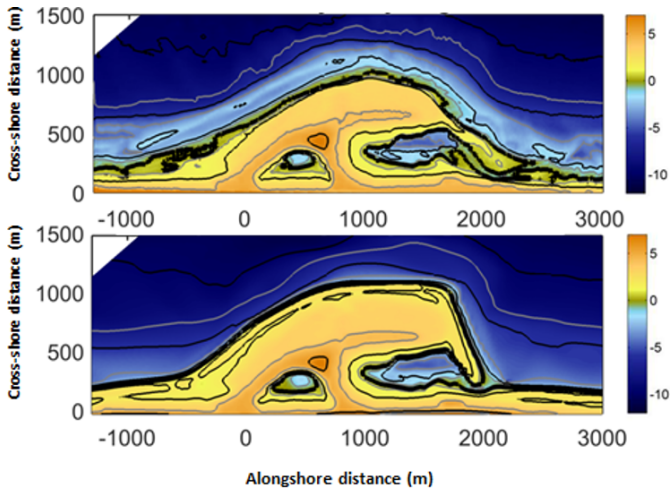

Figure 3.8: a) Observed bathymetry in August 2011; b) model predicted bathymetry for August 2012 with default processes and parameter settings. The black depth contour lines represent the isobaths of -10 m, -6 m, -2 m, 0 m and +2 m. The 0 m contour is highlighted in both panels.

Applying more advanced model features improved the results significantly. The best model/data comparison (see Fig. 3.9) was achieved with the settings shown in Table 3.4. Three key model features were found to be crucial to achieve a good model/data comparison: dry cell erosion, sediment transport formulation, and the formulation for nearshore wave energy distribution (i.e. wave and roller energy), which are discussed below.

The transition zone from wet to dry area is a dynamic area from a hydrodynamic point of view with interplay between tidal water level variations, tidal currents, wave- and wind-driven currents, swash and sometimes long waves. In present-day morphodynamic area models these processes are not fully resolved, but parameterisations have been made to enable dry areas to erode. In Delft3D, this is facilitated via a 'dry cell erosion' feature which distributes the erosion of the most landward wet cell amongst it's the adjacent dry cells. In this way computational cells that were originally above the maximum water level (i.e. dry cells) can be gradually eroded and become active wet cells when the bed level is lower than the water level at a given moment. The distribution of the total amount of erosion over the two cells is predefined by the user with, for example, a setting of 1(0.5) transferring 100% (50%) of the erosion in the wet cell to the adjacent dry cell. Based on a number of sensitivity tests a dry cell erosion factor of 1 gave the best model/data comparison for the hindcast presented in this study.

Of the several sediment transport formulations available in Delft3D, the best comparison between modelled and measured morphological change was obtained with the Van Rijn (2007) formulation. Especially, this formulation performs best in the deposition area where more sand is deposited higher up in the cross-shore profile (between NAP -1 m and NAP +2 m) which is in agreement with the observations. This is relevant for reproducing the spit development in the first year.

Two different nearshore wave models (the output of which is used by Delft3D-FLOW module to compute wave driven currents) that are dynamically linked with Delft3D-FLOW were tested: SWAN (Booij et al., 1999) and the so-called Roller model (Reniers et al., 2004). Of these two options, the Roller model was found to give the best model/data comparison. The surface roller is a phenomenon that occurs when waves break in the nearshore. When irregular waves break, (part of) the organised wave energy is converted into a surface roller. In a numerical modelling sense, the presence of the roller results in a non-zero fraction of broken waves (Battjes and Janssen, 1978) farther into the surf zone than without the roller.

The improvement in prediction skill when using the roller model is likely to originate from two incorporated breaker delay concepts: 1) delayed response of the wave-induced mass flux (Reniers et al., 2004) due to the presence of the surface roller (Dean and Dalrymple, 1991), and 2) the modification of the local maximum wave height (Roelvink et al., 1995). This, in essence, enhances onshore sediment transport and shifts the peak of the cross-shore distribution of the longshore current. In the roller formulations in Delft3D, the variable gamma scheme (Ruessink et al., 2003) results in a better agreement of the modeled and observed morphodynamics similar to the findings by Hsu (2006).

Selecting and applying these more advanced options comes at a cost: these simulations are a factor 2 more computationally expensive than the 'default' simulation, mainly due to the Van Rijn (2007) transport formulation which has several iterative approximations built in. The simulation with the best model performance required a computational effort of 20 days on a Core i7-2600 CPU machine (at 3.40GHz). The results of this simulation have been compared to the observed initial morphological evolution of the ZM and the adjacent coast both via visual comparison and an objective skill score test (Brier Skill score) discussed in the next sections.

3.3.3.4 *Visual comparison*

Modeled and measured bed level change over the 12 month study period generally compare rather well (see Fig. 3.9). The model correctly reproduces the development of a spit and a channel. The model predicted spit is however slightly less elongated compared to that observed

while the channel is slightly shallower than the measurements indicate (see ① in Fig. 3.9c). The observed erosion of the most seaward part of the peninsula is generally well reproduced by the model (②). The observed shoreline retreat of about 100 m and the extent of the erosional area are accurately reproduced by the model. The most seaward depth contour above which significant erosion occurs (NAP -6 m) is very similar in the model and observations. The observed bar around NAP -3 m is smoothed out in the model which is unavoidable given the 2DH approach. The transition zone between erosion and sedimentation in the northern part of the ZM is generally well reproduced by the model (see ③ in Fig. 3.9e). The cross-shore dominated bar behavior to the north of the ZM is not reproduced by the model, again due to the 2DH modelling approach adopted (see ④ in Fig. 3.9c). Sedimentation to the south of the ZM is also well reproduced by the model.

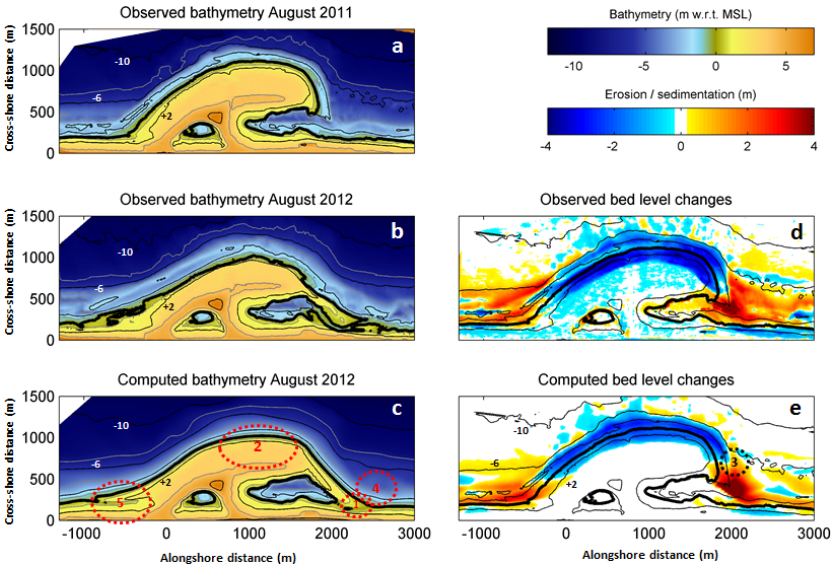

Figure 3.9: a) Observed bathymetry in August 2011; b) observed bathymetry in August 2012; c) model predicted bathymetry for August 2012; d) and e) observed and modelled bed level changes between August 2011 and August 2012, respectively. The black depth contour lines in d) and e) are based on the observed bathymetry of August 2011 for isobaths -10 m, -6 m, -2 m, 0 m and +2 m. The 0 m contour is highlighted in all panels.

The modeled plan shape evolution of the ZM is sensitive to the method adopted to affect erosion of the dry areas and the applied sediment transport formulation. The updrift part (section south of the ZM) experiences large accretion due to the blockage of the longshore transports from the south. This results in the shoreline rotating to

be perpendicular to the dominant south-westerly wave direction. The middle section (②) is also sensitive to the applied dry cell erosion method, also influencing the orientation of the downdrift part of the shape.

Table 3.4: Model features and parameter settings applied in the Delft3D Sand Engine model

Module	Parameter	Value	Description
Hydrodynamics	Roughness	Temporal and space-varying	Roughness predictor Van Rijn (2004)
	D_H	0.1 (m^2/s)	Horizontal eddy diffusivity
	V_H	1.0 (m^2/s)	Horizontal eddy viscosity (space-varying due to wave breaking)
Waves Roller model	γ	Variable	Wave breaking with variable gamma scheme (Ruessink et al.,2003)
	Gammax	0.7	Limiter to ensure wave breaking on time step level in Delft3D
Transport	D_{50}	300 mμ	Median grain size
	Formulation	Van Rijn (2004)	Sediment transport formulation
Morphology	*ThetSD*	1.0	Factor for erosion of adjacent dry cells
	MORFAC	1.0	Morphological acceleration factor

3.3.3.5 *Brier Skill score*

The Brier Skill Score (BSS) is commonly used as a measure of morphodynamic model predictions (Rijn et al., 2003; Sutherland et al., 2004a; Ruggiero et al., 2009; Ranasinghe et al., 2011; Bosboom et al., 2014). The BSS approach defined by Sutherland et al. (2004a) is adopted to evaluate the model skill:

$$BSS = 1 - \frac{MSE}{MSE_{ini}} \tag{3.1}$$

where MSE is the mean-squared error and MSE_{ini} the MSE of the reference prediction for which the initial bed is taken (zero change reference model). Therefore, the BSS can be interpreted as the model added skill relative to a prediction that nothing changes. A prediction that is as good as the zero change reference prediction receives a score of 0 and a perfect prediction a score of 1. A value between 0 and 1 can be interpreted as the proportion of improvement over the reference prediction. For a balanced appreciation of model performance Bosboom et al. (2014) recommend that multiple accuracy and/or skill metrics are considered in concert; e.g. decomposition of the BSS would give relevant information on the phase, amplitude and bias. Given the focus of this paper, the analysis is restricted to the BSS in combination with the MSE and details on a decomposition analysis are not yet discussed.

The monthly modeled and measured bathymetries, within the survey domain (three control areas) between NAP -10 m and +3 m, were used to calculate the temporal evolution of model skill for the ZM model (see Fig. 3.10a). As the BSS does not reflect an absolute accuracy the mean-squared errors are presented in Fig. 3.10b. The BSS can be

seen to increase in time, whereas the accuracy of the modeled bed levels decreases with time due to some deviations between modeled and observed bed elevations until it becomes more or less constant after February. Negative values of BSS are computed for the month of September and October (value of -2 and -0.03 resp.) as the bed changes in the first months are relatively small compared to the MSE, the latter partly being governed by interpolation errors of the initial bathymetry (see Fig. 3.10b), leading to a negative value for BSS. In the following months, with higher wave energy and hence larger bed level changes, the BSS improves rapidly to 0.4 in January after which the score steadily increases to a value of 0.59 by August 2012 which is judged as 'Excellent' according to the classification proposed by Sutherland et al. (2004a).

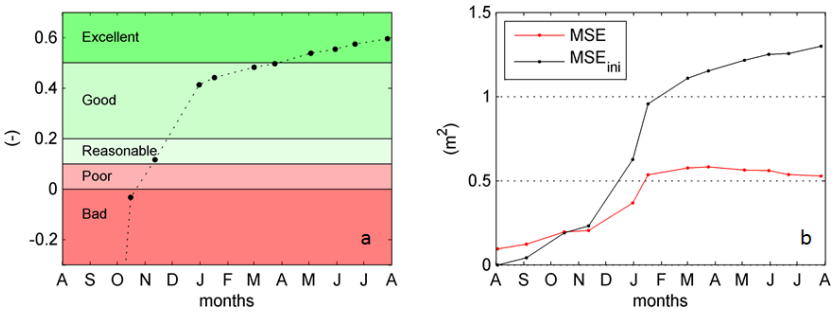

Figure 3.10: a) model performance per month from August 2011 to August 2012; the colours represent the BSS classification following Sutherland et al., 2004a; and b) monthly mean square errors.

After February, when the MSE becomes more or less constant, the increase of the BSS is governed by the MSE_{ini} which continues to increase as a result of the natural development away from the initial situation. The increase of the BSS over time may be explained as the emerging of longer, more skillful scales (Bosboom et al., 2014) and could illustrate that the processes governing the erosion of the ZM over time are well reflected by the model and have a larger relative contribution to the skill further in the simulation than in the first months. In all, the model/data comparison demonstrates that the model can predict the redistribution well, such that the model can be used to examine the processes driving the morphological evolution.

3.3.4 *Morphological verification 2012 - 2014*

Following the successful model hindcast of the first year ZM evolution, a verification simulation was also conducted for the period August 2012 till August 2014; so, year 2 and 3 after completion of the ZM. The observed August 2012 bathymetry is used as initial model bathymetry

of this verification simulation. The measured forcing conditions, such as waves, wind and surges, for this 2-year period were compiled and applied to the model in an exact same way as the first year (calibrated) run. Figure 3.11 shows the bed levels and erosion/sedimentation pattern computed after two years. A BSS score of 0.43 was achieved, which is classified as a 'good' comparison by Sutherland et al. (2004a). This provides reasonable confidence in the predictive capability of the calibrated model.

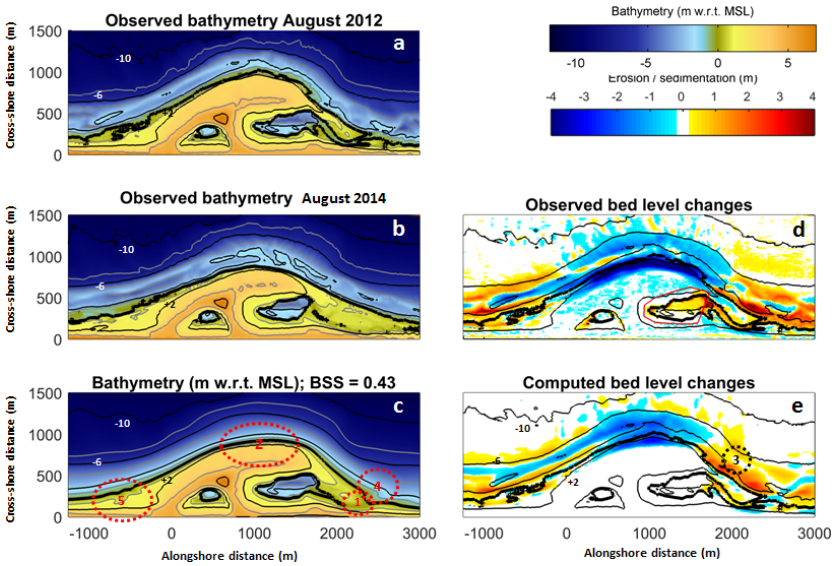

Figure 3.11: a) Observed bathymetry in August 2012; b) observed bathymetry in August 2014; c) model predicted bathymetry for August 2014; d) and e) observed and modeled bed level changes between August 2012 and August 2014, respectively. The black depth contour lines in d) and e) are based on the observed bathymetry of August 2012 for isobaths -10 m, -6 m, -2 m, 0 m and +2 m. The 0 m contour is highlighted in all panels.

Despite the good overall data/model comparison, computed shoreline positions show some deviations from the observations. This could be attributed to the lack of two processes in the present modelling: aeolian transports and sediment sorting. De Vries et al., 2014 highlighted the relation between the width of the wet intertidal area to the aeolian transports. Observations of sedimentation volumes in the dune lake and lagoon for year 2 and 3 indicate that the majority of this volume is transported from the intertidal area as the crest of the Sand Engine stabilized after the first year mainly due to armoring. Preliminary estimates indicate that the aeolian transports can be as high as 30 $m^3/m/yr$ or even more, which is in line with De Vries et al., 2012. Translating this

transport into a bed level change would mean an absolute lowering of more than 0.5 m across the intertidal area assuming an averaged width of the intertidal area of 100 m. Observations have shown that the D_{50} at the most seaward part of the ZM is coarsening over time while some patches of finer sand have been found north and south of the ZM. In the present simulation the sand fraction is represented by only one D_{50} (and a standard D_{10}/D_{90} relation). Coarsening of the seaward part of the Peninsula will reduce its erodibility over time.

3.4 GOVERNING PROCESSES

3.4.1 *First year erosional behavior*

To enable a detailed investigation of physical processes that govern the observed morphological evolution during the study period, the ZM simulation results for the first year were analysed by extracting hourly bed levels and integrating the changes in the three control areas; viz. the Peninsula, the Northern adjacent section and the Southern adjacent section (see Fig. 3.2b). In general, the temporal evolution of the computed sediment volumes match well with the observed volume changes (see Fig. 3.12).

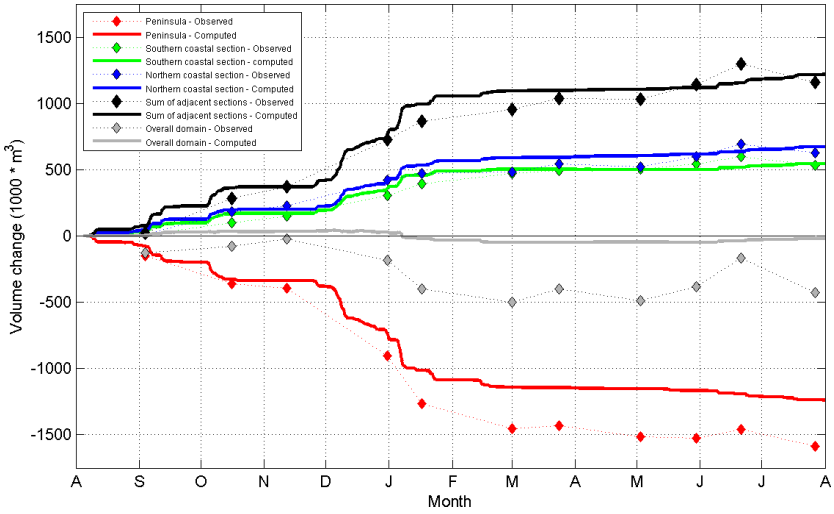

Figure 3.12: Observed (symbols) and computed (solid lines) volume changes for the ZM peninsula and two adjacent coastal sections (north and south). Note that the red diamonds represent the area up to NAP +3 m.

The model computes a total erosion volume on the Peninsula of about 1.24 million m^3 by August 2012, while the sum of the accretion

volumes in the adjacent coastal sections is 1.22 million m^3. Thus about 20,000 m^3 of sand ($\backsim$1.5% of the total eroded volume) appears to have moved out of the control areas, which is expected to have moved further alongshore or in cross-shore direction. The measured accretion volumes in both the northern and southern coastal sections are well reproduced by the model. Hence, the model results show that the redistribution of the ZM sand in the first year has largely been limited within the boundaries of the control areas. In contrast, the observations indicate that a net volume of about 450,000 m^3 was moved out of the control areas after the first year. This difference is likely due to the redistribution in alongshore direction (beyond the control areas) and the landward movement of sand from the intertidal and subaerial beach to the dunes due to aeolian transport, which is not included in the model. Possibly, although limited, a part of the deficit may be attributed to consolidation. Bathymetric surveys have shown a lowering of the bed level of about 0.2 - 0.3 m at the emerged part of the peninsula (above MSL) after the first storm months, which remains rather constant thereafter (see Fig. 3.9d). When neglecting the erosion of the (permanent) dry beach area of the ZM in the first year, the remaining observed loss is very comparable to the long-term natural background loss found at this coastal stretch of $\backsim$5 km; i.e. 300,000 m^3/yr.

The spatial distribution of the cumulative sediment transport volumes over the 12 month study period (see Fig. 3.11) shows a northward net transport of about 170,000 m^3 along the undisturbed coast (at x =-1500 m) which is in general agreement with the reported annual net sediment transport rate for the Delfland coast (Van Rijn, 1995). Upon encountering the ZM (from the southern end, or the left hand side of Fig. 3.13), the longshore transports immediately (at about x=-750 m) reverse direction to the south. Further along the ZM, the longshore transport gradually increases to a peak southward transport of $\sim$160,000 m^3 at about x=-600 m and then decreases and changes direction back to northward around x=200 m. The northward transport reaches values of about 450,000 m^3 near the tip of the ZM (at x=1400 m), where the shoreline orientation is similar to the undisturbed coast. At this location, the higher transport rate compared to the undisturbed shoreline is likely due to the steeper profile of the seaward slopes of the ZM (Kamphuis, 1991;Mil-Homens et al., 2013; De Schipper et al., 2016). Just north of the tip (at x=2200 m), the transports increase up to approx. 550,000 m^3. Further north the northerly transport decreases to a minimum of $\sim$150,000 m^3 (x=3000 m) and thereafter increases again to the ambient longshore transport rate of $\sim$170,000 m^3/yr.

Sediment from the peninsula is transported to the south at a rate of 160,000 m^3/yr (at x=-600 m) while a volume of $\sim$550,000 m^3 is transported per year to the north (at x=2000 m), resulting in a sediment

loss of approximately 710,000 m^3 from the peninsula. Converting the sediment transports (excluding pore volumes) to volume changes, assuming a porosity of 40%, leads to a calculated eroded volume of 1.18 million m^3 which is comparable to the 1.24 million m^3 presented in Fig. 3.12.

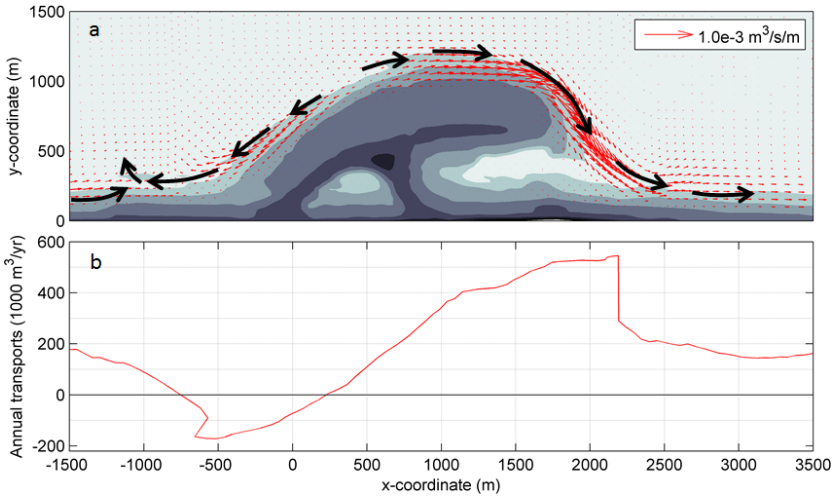

Figure 3.13: a) computed yearly-averaged sediment transports (represented by the red arrows), while the thick black arrows (drawn to a qualitative scale only) indicate the main cumulative transport pathways over the study period, and b) yearly-averaged longshore transport curve along the ZM.

To illustrate the spatio-temporal bed level changes in the study area, the cross-shore integrated daily volume changes are presented as a time-stack in Fig. 3.14. The figure presents the daily volume changes integrated over each cross-shore transect along the ZM. The central area of the ZM is subject to almost continuous erosion during the first year, intensified during the higher wave events. In summer, lower waves from the NW cause slight sedimentation in this area. It is evident that the spit development starts at approx. x=1700 m; sedimentation (red colors) is indicated almost from day 1. Just downdrift of the spit, consistent erosion takes place followed by a less pronounced second band of sedimentation. The sedimentation pattern in the south (around x=-800 m) is more stable. The results show that during the largest wave events, the ZM impacts the bed levels over a relatively large area of about 6 km alongshore (from x=$\backsim$ -2000 m to x=$\backsim$4000 m).

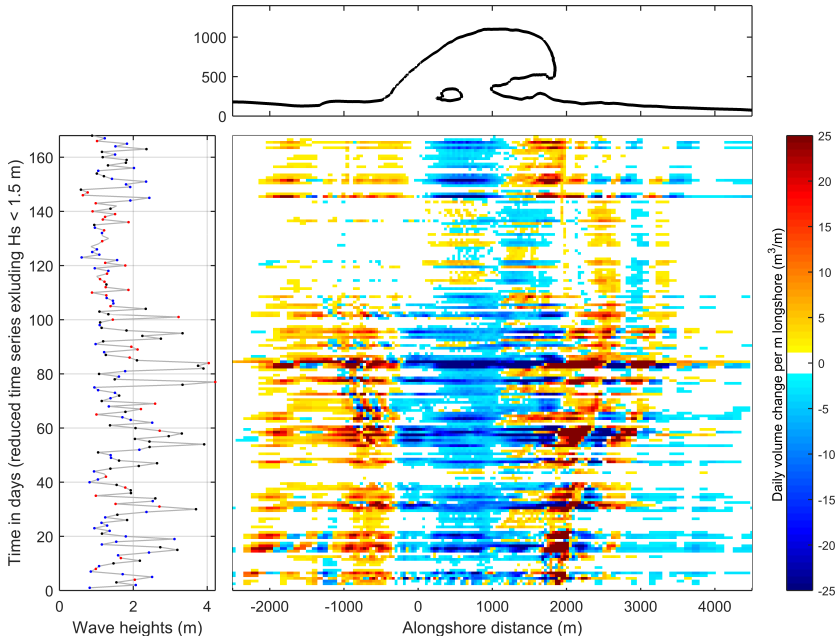

Figure 3.14: Time-stack of daily volume changes integrated per cross-shore transect (from NAP -5 m to NAP +2 m). Blue patches indicate erosion; yellow / red indicate sedimentation. The left panel shows concurrent daily-averaged wave heights. Black/red/blue dots represent south-westerly/north-westerly/westerly waves.

3.4.2 *Erosion due to wave events*

Figures 3.12 and 3.14 both indicate that the most dominant morphodynamic process occurring at the study site is erosion of the ZM during high energy wave events and the deposition of the eroded sand along the adjacent coast (both to the north and south of the ZM). Therefore, to investigate the dependencies between the morphological behavior and environmental forcing conditions, high energy wave events were determined on the basis of the integrated wave energy over individual events (i.e. meteorologically independent events). Here, a high energy wave event is defined as a consecutive period (duration) over which the offshore significant wave height is higher than 2 m. The 12 largest high energy wave events during the study period thus determined were extracted for further analysis. Assuming a Rayleigh distribution of waves, the integrated wave energy density $\sum E$ was determined for each event as follows (Splinter et al., 2014):

$$\sum E = \int_0^N \frac{1}{16} \rho g H_s^2 \triangle t \tag{3.2}$$

where ρ is the density of sea water (kg/m^3), g is gravitational acceleration (m/s^2), H_s is the significant wave height (m), $\triangle$t is the time interval of measurements (s), and N is the total duration of the storm. The integrated volume changes of the peninsula for the 12 events with the highest wave energy density are presented in Fig. 3.15. For reference, the events are chronologically numbered (see Fig. 3.15c). The largest total net sediment loss (185,000 m^3) from the peninsula occurs during storm event #9 (2nd of January 2012, southwesterly waves, mean H_s of 3.7 m, duration approx. 90 hours).

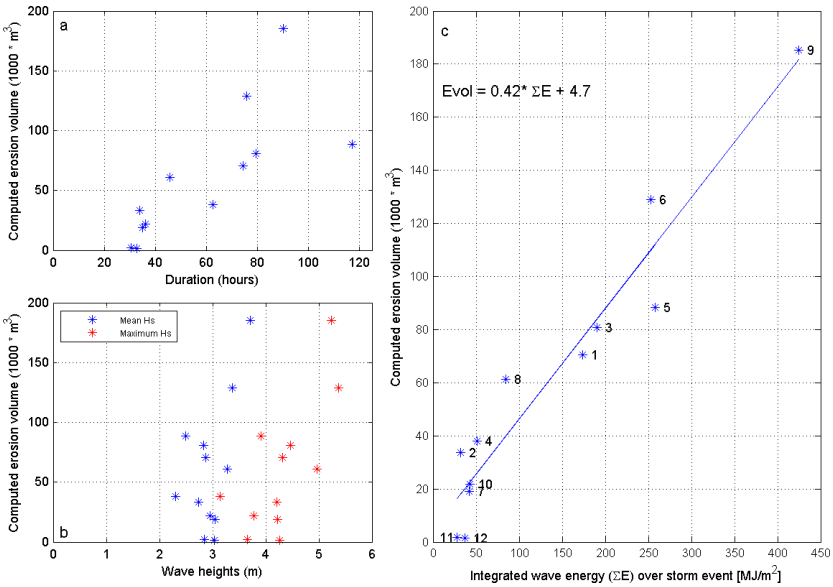

Figure 3.15: Computed ZM erosion volume for the 12 identified high energy wave events versus a) the storm duration, b) the averaged and maximum wave height per event and c) the integrated wave energy during the event. The numbers in c) indicate the sequence of the event during the year.

Figure 3.15b shows the averaged and maximum wave height for each considered wave event. Generally, with increasing wave heights more erosion is computed, but there is too much variation to define a strong relation. The duration of a storm event shows an increasing relation with eroded volume for events with durations exceeding 72 hours (see Fig. 3.15a). Analysis of the 12 different storm events shows that the computed erosion volume for a given storm is proportional to the integrated wave energy density of an individual storm (see Fig. 3.15c). Wave directions during the considered wave events do not seem to play an important role as the e.g. six largest storms are close to a linear dependency while these storms had different predominant wave

directions (see Fig. 3.15c). Model results indicate that due to the shape of the ZM waves higher than about 2 m cause a divergence point in the wave-driven currents, whereby the angle of the incoming waves determines the location of the divergence point. In the divergence zone erosion will occur due to the opposite sediment transports directions. So the wave direction does influence where along the ZM most erosion takes place during a given wave event. But the erosion volumes in Fig. 3.15 are aggregated over the entire ZM which is why they are more correlated with wave height than with wave direction."

Although, individual events with high wave energy densities result in large erosion volumes, the sum of the erosion volumes of the 12 largest events account only for about 60% of the measured erosion volume on the Peninsula (Luijendijk et al., 2015). The stormy months of December 2011 and January 2012 are responsible for approximately 60% of the total erosion volume. Events with high wave energy densities accelerate the erosion of the peninsula, while a gentle trend of erosion is observed during the rest of the year when milder conditions occur.

3.4.3 *Relative contributions of environmental forcings*

To gain insights into the relative contributions of the various environmental forcings to the initial morphological response of the ZM, a series of simulations where the different forcing processes were sequentially eliminated was undertaken using the verified model. The forcing types thus investigated were: horizontal and vertical tide, storm surge, wind and waves. This investigation comprised six separate simulations (see Table 3.5), wherein the reference case (Run A) is the above described brute-force simulation with all available processes activated.

Table 3.5: Overview of simulations with different types of forcing

Simulation	**Forcing types applied**
Run A: Ref. run	Wave effects, vertical tide, wind-driven currents, surge, hor. tide
Run B	Wave effects, vertical tide, wind-driven currents, surge
Run C	Wave effects, vertical tide, wind-driven currents
Run D	Wave effects, vertical tide
Run E	Wave effects only
Run F	Run E, but without wave effects

The evolution of the computed erosion volume of the ZM Peninsula through the study period is shown for each simulation in Fig. 3.16. Note that several sets of simulations were undertaken to assess whether the order of elimination of the different forcing (except for the wave forcing,

which was always present) would affect the results. All such sets of simulations showed similar results and therefore only one selected set is discussed below.

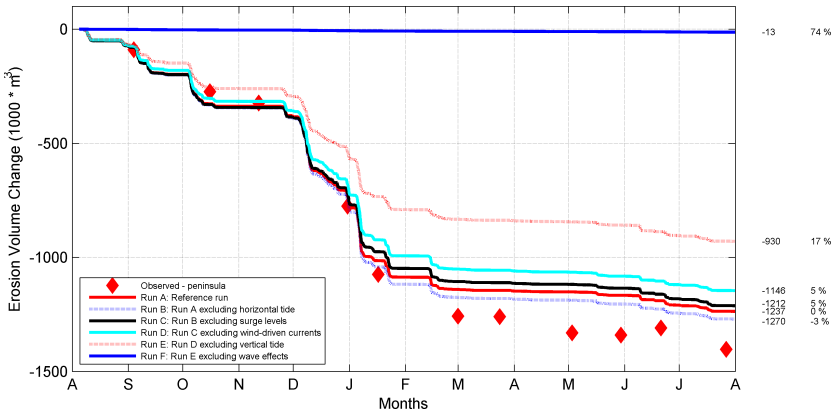

Figure 3.16: Volume changes of the ZM over the study period showing the relative contribution of the different environmental forcings. The columns on the right give the final computed volume change per simulation and the difference with respect to the reference run.

Neglecting the horizontal tide from the reference run has a very limited effect on the erosional behavior; a difference of only 3% in the total reference erosion volume. Similarly, eliminating the surge levels and wind-driven currents has minor effects; both contribute less than 5% of the total erosion volume. However, the vertical tidal variations result in a significant contribution of 17% of the cumulative erosion volume. The vertical tide is expected to influence the active part of the cross-shore profile and as such affect the erosion volumes (i.e. a larger part of the coastal profile will be mobilized when water levels vary over time). The model predictions indicate that waves are by far the dominant forcing mechanism. Wave effects, leading to wave-driven currents and enhanced bed shear stresses, contribute to approximately 75% of the total erosion volume.

The above is in line with the findings from Grunnet et al. (2004). After investigating the relative contribution of forcings on a shoreface nourishment at a barrier island, Grunnet et al., 2004 concluded that the horizontal tide had a negligible effect on the transports, but that the vertical tide played a significant role. Results presented above support the suggestion of Grunnet et al., 2004 that a more simplified approach where the horizontal tide is omitted may be justifiable in some situations. Such an omission would save significant efforts in deriving the tidal currents and schematizing it for longer-term predictions, increasing the potential of process-based modelling for the design and evaluation of coastal engineering projects.

3.5 CONCLUSIONS

The anticipated increase in global nourishment volumes and size and the request for more complex nourishment shapes demands adequate predictions of the morphodynamic evolution of such sandy interventions. Yet, the skill of current state-of-the-art models for such projects are not known as well as the primary drivers that control this behavior. A process-based model has been used to successfully hindcast the initial response of the Sand Engine mega-nourishment in The Netherlands. The Delft3D model reproduces measured water levels, velocities and nearshore waves well. Applying the morphological model with its default formulations and parameter settings results in a morphological evolution that is quite far from observed. Three key model features were found to be crucial to achieve a good model/data comparison: the erosion of dry cells, sediment transport formulation, and the formulation for nearshore wave energy distribution. Applying these features results in a computed morphological evolution which is consistent with the measured evolution during the study period, with Brier Skill Scores in the 'Excellent' range following the classification of Sutherland et al. (2004a). Model results clearly showed that the sand eroded from the main peninsular section of the Sand Engine is deposited along adjacent north and south coastlines, accreting up to 6 km of coastline in total during just the first year of the Sand Engine.

Analysis of the model results indicated that the erosional behavior of the Sand Engine has a linear dependency on the cumulative wave energy of individual high energy wave events, with the duration of a storm event being more dominant than the maximum wave height occurring during the storm. The wave directions during the events appear to be irrelevant for the erosional behavior of the nourishment. The integrated erosion volume due to the 12 events with the highest cumulative wave energy events sums up to approximately 60% of the total eroded volume at the peninsula after one year. The less energetic storm events, with a higher probability of occurrence, are hence equally important for the initial response of the Sand Engine.

Further analysis of the relative contributions of the different environmental forcings to the total erosional behavior of the nourishment using the verified model indicated that wave forcing dominated the initial morphological response of the Sand Engine, accounting for approximately 75% of the total erosion volume after the first year. The vertical tide is the second most contributing factor accounting for nearly 17% of the total erosion volume, with horizontal tide, surge and wind playing only a very minor role (all accounting for less than 5% of the total erosion volume).

4

MORPHODYNAMIC ACCELERATION TECHNIQUES FOR DECADAL PREDICTIONS

Large part of this chapter is based on: Arjen P. Luijendijk, Matthieu A. de Schipper, and Roshanka Ranasinghe. "Morphodynamic Acceleration Techniques for Multi-Timescale Predictions of Complex Sandy Interventions". Published in Journal of Marine Science and Engineering 2019, Volume 7, Issue 3, 78 (Luijendijk et al., 2019).

The previous chapter showed the relevance of wave forcing conditions at various time scales, e.g. days (storms) and months (seasonality) in wave energy, on the initial response of the Sand Engine. Hence, for decadal predictions, it is necessary to include variations in forcing conditions over multiple time scales. This motivates the need to look for efficient yet accurate acceleration techniques. This chapter builds on the morphodynamic model presented in Chapter 3. Comparisons with hydrodynamic and wave measurements have shown that the Delft3D model is able to simulate the most important processes at and around the Sand Engine well. Regarding the morphodynamics, the model is also capable of reproducing the dispersive subaqueous behavior observed during the first year after construction at the Sand Engine. In this chapter the model, extended to cover the 20-km long Delfland coast, is applied to investigate the impact of morphodynamic acceleration techniques on morphological changes at multiple time scales.

4.1 INTRODUCTION

Thirty one percent (31%) of the world's coastline consists of sandy beaches and dunes that form a natural defense protecting the hinterland from flooding (Luijendijk et al., 2018), at the same time providing valuable space for recreational activities and nature development. Due to alongshore variation in hydraulic loads, sandy shorelines can experience persistent sand losses. In the longer term this may result in a retreat of the shoreline, negatively impacting the functions and values of these areas. To mitigate these effects, coastal managers implement mitigating measures, which can either be hard constructions (e.g., sea wall, revetment) or soft (sandy) strategies comprising sand nourishments.

The design and acceptance of a sandy strategy as a mitigating measure requires sound information on the expected dynamics, both in the short and longer term. Coastal managers base their decisions mostly on medium- to long-term trends (annual to decadal scale) of coastal

change. However, extreme episodic events (short-term) can, at times, erode the beach to such an extent that it affects long-term trends of coastal change. Over the event of a storm sudden and large morphological changes may occur (Karunarathna et al., 2018). Furthermore, a rapid sequence of storms ('clusters') may have a different net impact compared to that if the same storms were to occur in the same sequence but with larger gaps in between the individual storms (Dissanayake et al., 2015; Splinter et al., 2014). Apart from the event time scale, understanding the interannual and inneranual (seasonal) variability in beach dynamics is also important for coastal management decisions. Especially when it concerns anticipating the possible coastal impacts of a new coastal intervention. This is because the temporal scale of an impact is often interrelated to the spatial scale. While the impacts of larger-scale coastal interventions at sandy coasts might be limited to the local scale in the short-term, these impacts may potentially affect a larger area over time.

For example, the proper design of a port or a mega sand nourishment requires reliable predictions of how the coastal area in the immediate vicinity ($\sim$1 km) of the intervention would respond to it over the first couple of years, as well as how the coastal area farther away from the intervention ($\sim$10 km) might change over a decade or longer. With increasing spatial scales, the potential of inter-dependencies with other (existing) coastal interventions also increases. Thus, impacts manifesting themselves at different spatio-temporal scales, may have profound inter-dependencies as well. Figure 4.1 illustrates the relevance of different processes over various time and space scales for a mega nourishment and a port development highlighting that for increasing forecast horizons, the number of physical processes that need to be taken into account necessarily increases. Therefore, to robustly predict coastal response to larger scale interventions, a multi spatio-temporal numerical modelling approach is required.

For providing information on the expected long term (i.e., greater than 10 years) coastal behavior, analytical models predicting the sandy shoreline change have proven to be useful in engineering applications for sandy and gravel beaches (Arriaga et al., 2017; Brown et al., 2016; Komar, 1987; Larson et al., 1997; Pelnard-Considère, 1956). The inherent simplifications and assumptions result in fast computations, but are limited in predicted output information; e.g., only the shoreline position over time.

Process-based coastal area models have the potential to provide comprehensive information at multiple spatio-temporal scales allowing more detailed evaluation. To date such coastal morphodynamic models are generally able to adequately simulate morphological change due to concurrent tides, waves and currents for short to medium-term time scales; events of 3–4 years (Elias, 2006; Hopkins et al., 2018; Lesser,

2009; Roelvink, 2006). Prediction of the long-term dynamics of sandy interventions have however remained a major challenge for process-based models (Miller et al., 2008).

At the same time, reducing the computational costs of morphodynamic simulations for coastal areas is a critical issue for engineers (Roelvink, 2006; Walstra et al., 2013). To reduce computational costs, for example, mixed method approaches have been studied that combine analytical and process-based models (Vitousek et al., 2017). Even though process-based models of physical systems have greatly benefited from the increasing computational power over the last decades, the use of morphodynamic acceleration techniques is still the only way to perform medium- to long-term morphodynamic predictions (Carraro et al., 2018; Li et al., 2018).

In this article, we investigate the performance of multiple acceleration methods applied to multi-timescale morphodynamic forecasts for a sandy coast with respect to accuracy and computational effort. Section 4.2 summarizes the different morphodynamic acceleration techniques used in this study. The case study, general model setup and validation is presented in Section 4.3. The details of the acceleration techniques, as applied to the case study, are presented in Section 4.4. Section 4.5 presents a verification of the techniques for short and medium-term morphodynamic evolution and discusses phenomenological accuracy and computational effort associated with the different acceleration techniques. Section 4.6 addresses the results for the different acceleration techniques at decadal time scales, while the conclusions are presented in Section 4.7.

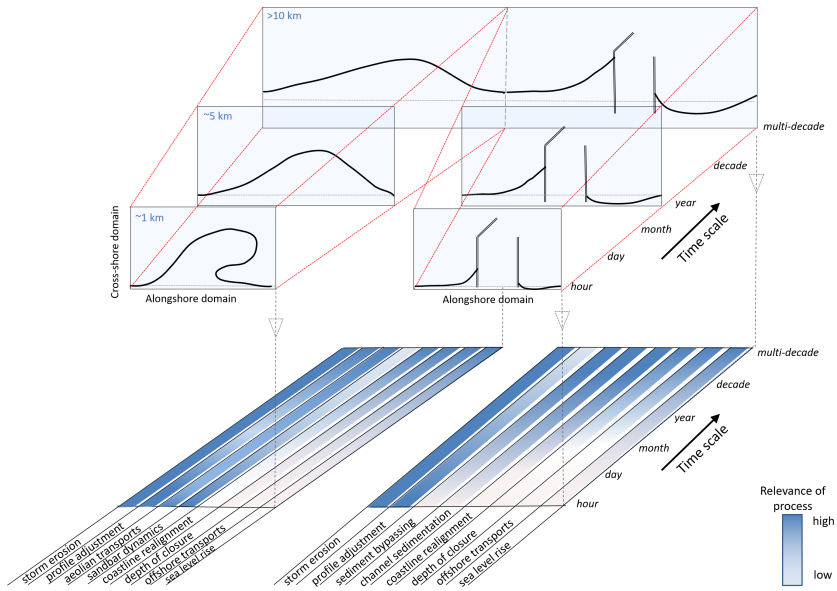

Figure 4.1: Schematic diagram of the spatio-temporal impacts of two coastal interventions; a large-scale nourishment (left) and a port (right). The bottom panels show the relative importance of processes across the different time scales.

4.2 MORPHODYNAMIC ACCELERATION TECHNIQUES

The most basic approach to morphodynamic modelling uses unfiltered real-time (hereafter referred to as brute force) time series of forcing conditions (see Fig. 4.2a), which is referred to as the brute force technique (BF). Typically, measured time series of water levels (tide and surge), waves, wind and possibly currents are applied to the morphodynamic model Elias, 2006. In this technique, no upscaling of the bed level changes takes place.

One of the major issues in long-term modelling is bridging the gap between small-scale hydrodynamic and transport processes and large-scale morphological changes Ranasinghe et al., 2011; Roelvink, 2006. Elegant acceleration methods have been developed for this purpose, such as the morphological acceleration factor introduced by Lesser et al. (2004), hereafter referred to as the *morfac*. With the *morfac* method, the simulated morphology is accelerated by multiplying the calculated bed changes with a factor equal to the *morfac*. For example, a simulation over one tidal cycle (12 h) with a *morfac* of 10 represents 120 h of morphological change. This method is presently one of the most commonly

applied acceleration methods Geleynse et al., 2011; Nahon et al., 2012; Tran-Thanh et al., 2011; Vegt et al., 2016; Wegen and Roelvink, 2008. With the use of the *morfac*, in combination with model input reduction techniques discussed in this paper, the time required to perform simulations of morphological changes over time periods of years to decades can be reduced drastically.

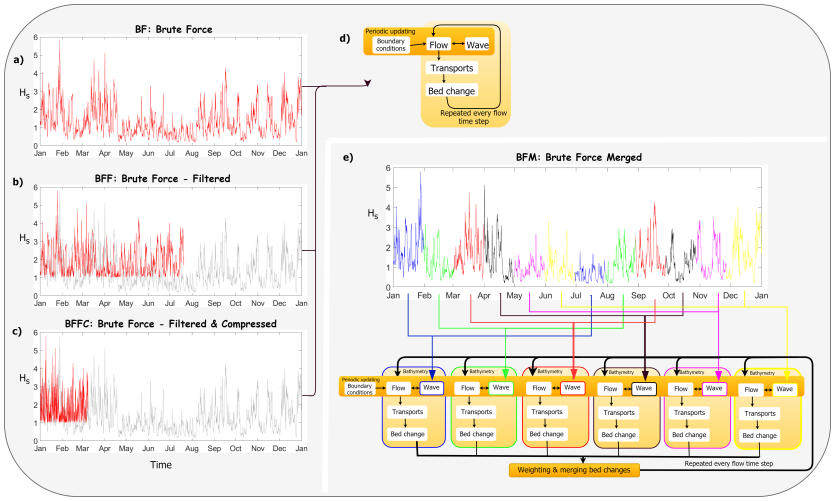

Figure 4.2: Graphical overview of (**a**) the non-scaled brute force approach (BF) and the three considered morphodynamic acceleration techniques using brute-force time series: (**b**) brute force filtered (BFF), (**c**) brute force-filtered and compressed (BFFC), and (**e**) brute force merged technique (BFM). (**d**) shows the basic morphodynamic feedback loop used in BF, BFF, and BFFC. The red wave time series in (**a–c**) indicate the selected wave time series.

Besides the *morfac*, the reduction of model input is another commonly used acceleration method on the hydrodynamic timescale. Input reduction aims to reduce the computational effort through applying a reduced set of forcing conditions representing a longer-term signal. This can be achieved by ignoring conditions in the brute-force time series that do not contribute to the bed level changes (brute force filtering), or by schematizing the forcing conditions resulting in a set of representative conditions (schematized input reduction). The latter method is commonly applied with *morfac* larger than one while the former can also be applied with a *morfac* equal to one (non-scaled).

This study focuses on the evaluation of six morphodynamic acceleration techniques: three using brute force time series and three using representative (schematized) wave conditions. The aforementioned brute force simulation (BF with *morfac* = 1) is used as the benchmark simulation.

4.2.1 *Techniques Using Brute Force Time Series*

4.2.1.1 *Existing Brute Force Techniques*

This section discusses the considered techniques to accelerate model results from a hydrodynamic time scale to morphological time scales ranging from days to decades for a wave-dominated coastal domain. The techniques are illustrated in Fig. 4.2 and characteristics are given in Fig. 4.3.

The first acceleration technique involves input reduction by filtering forcing conditions that are relevant to the morphodynamics; referred to as the filtered brute force technique (BFF; Brute Force Filtered); see Fig. 4.2b. Analysis of the brute force simulation can reveal which forcing conditions contribute to the morphological evolution. For example, Luijendijk et al. (2017) demonstrated that only waves with $H_s > 1$ m contribute to the evolution of a large-scale nourishment, and omitting the small waves results in a 40% reduction of computational time (compared to the corresponding BF simulation).

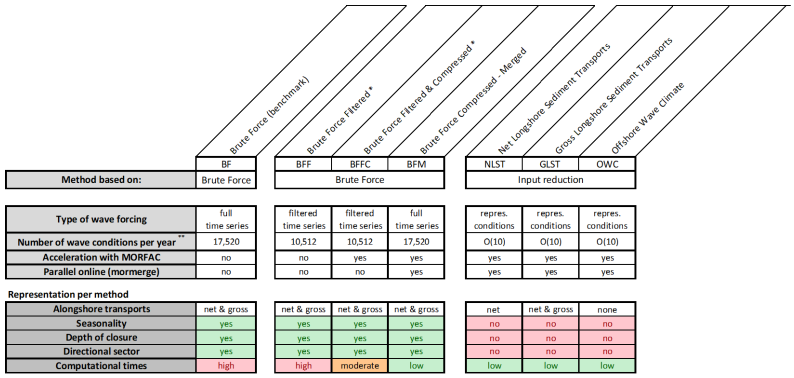

Figure 4.3: Characteristics of the considered morphodynamic acceleration techniques.

A variant to the filtered brute force technique combines the input reduction and morphological acceleration factor and is referred to as the compressed, filtered brute force technique (BFFC; Brute Force Filtered Compressed); see Figure 4.2c. In this technique the time series of the forcing conditions are compressed with a factor equal to the *morfac* (> 1) Li et al., 2018. Time series of the waves, surge and wind can be compressed in this way while this is often not appropriate for the tidal forcing. This is because compressing tidal water level variations and accompanying horizontal tidal currents may result in unrealistic behavior of tidal velocities and/or emptying or filling of basins or lagoons. Thus, the compressed wave time series is applied

over a non-compressed tidal time series assuming that the time scale of the tides can be decoupled from the time scale of the waves and morphology. The time scale of variations in waves, wind and surge are typically O(hours), which allows the compression of these time series with *morfac* typically ranging between 1 and 5. Note that frequent coupling is required between the hydrodynamic and wave model (e.g., every 10 min) to ensure physically realistic and smooth morphological development. The computational time for this technique is reduced with a factor approximately equal to the *morfac*. For example, applying a compression factor (i.e., the *morfac*) of 3, the simulation period for one year is reduced from 365 days to 122 days. This makes it a very effective acceleration technique.

4.2.1.2 *New Technique: Brute Force Merged*

Here, we present a new acceleration technique in which the brute force wave time series is split up into multiple time series by applying a phase shift in the (compressed) wave time series. The different brute force time series are then distributed over multiple processors similar to the 'mormerge' approach (Roelvink, 2006) (see Fig. 4.2e). As stated by Roelvink (2006), this approach divides the simulation into several parallel processes, which represent different wave conditions. At a prescribed frequency (i.e., the hydrodynamic time step) the bed level changes of all processes are provided to the merging process. This process calculates a weighted average bed level change and returns this to all processes, after which each process continues the simulation. An important assumption is that hydrodynamic conditions vary much faster than the morphology can develop. In case the period during which different conditions (ebb, flood, spring tide, neap tide, NW storm, SW wind, etc.) may take place is short compared to the morphological time scale, these conditions may as well occur at the same time (Roelvink, 2006).

This novel technique combines the compressed brute force technique (i.e., *morfac* > 1) with the parallel online method; referred to as 'brute force merged' (BFM; Brute Force Merged). The technique, using the standard version of Delft3D (version 6.02.13.7545, developed by Deltares, Delft (Lesser et al., 2004)), allows for seasonal variations and inherently includes the gross transport components as the brute force time series are applied. This also means that the full wave climate is resolved both in wave directions and wave heights; this is, for example, important for a correct representation of the depth of closure which is determined by the highest waves.

4.2.2 *Techniques Using Representative Wave Conditions*

In contrast to the above-mentioned brute force approaches, another set of techniques apply a set of representative wave forcing conditions (i.e., wave input reduction) to forecast morphological evolution (Benedet et al., 2016; Grunnet and Ruessink, 2005; Walstra et al., 2013). Such techniques focus on reducing the number of wave input conditions resulting in a set of limited yet representative wave conditions. The input reduction focuses on optimizing the set of representative conditions to best reflect the prevailing wave climate.

Multiple techniques are available to reduce the full range of wave conditions to a set of representative conditions. Not only can the number of representative conditions vary greatly, but so can the total weight applied to each wave condition and the chronology of wave events. All of these variables have direct implications on the quality of model results.

Generally, the resulting set of representative conditions is subsequently applied to the morphodynamic model in two manners. Either the conditions are applied sequentially, referred to as the 'sequential' schematized technique, or parallel, using the 'mormerge' approach (Roelvink, 2006; Tonnon et al., 2009). In the former, a condition-dependent *morfac* can be prescribed resulting in a time-dependent *morfac* (Dhastgheib, 2012). As the latter is equivalent to a constant averaging of the forcing parameters, it yields a much smoother bed evolution than a single time series, which allows a higher *morfac*, thus accelerating the simulation even further.

4.2.2.1 *Input Reduction Based on Longshore Sediment Transports*

Generally, the objective for schematizing the wave climate is to reproduce the net longshore sediment transports (LST) in case of wave-dominated open sandy coasts. The most common practice is to use the alongshore variation of the net LST as the target (Tonnon et al., 2009); this is referred to as the net LST technique (NLST; Net LST); see Fig. 4.4a.

For this purpose, first the LST is computed for the entire wave climate (schematized into $O(200)$ wave conditions) for the situation prior to a coastal intervention. Subsequently, a set of $O(10)$ representative wave conditions that reproduce similar LST values is determined. Optimizing methods and tools like OPTI (Benedet et al., 2016; Mol, 2007) can be used to obtain this set efficiently.

Another target using the LST is the alongshore variation of the gross components of the LST; referred to as the gross LST technique (GLST; Gross LST); see Fig. 4.4b. This variant is less used, while this may be relevant when irreversible morphological response is likely. For

example, when introducing an intervention along a coast that is in a (dynamic) equilibrium, a proper representation of the full directional wave spectrum may be important. Waves with a large-incident wave angle can have a particular (irreversible) impact on the morphology of the intervention and its surroundings (Berg, 2012), potentially captured better by the GLST technique than the NLST technique.

Furthermore, decadal predictions demand that the active profile (active cross-shore zone subject to discernible bed level changes) is well represented. In other words, the depth of closure for the considered time period should somehow be embedded in the representative wave conditions. This demands that the selected representative wave conditions cover the full (outer) range of the wave height distribution. This is a major limitation as this results in a large set of conditions, while the user goal is to limit the number of conditions.

4.2.2.2 *Input Reduction Based on Offshore Wave Climate*

Another common method is to use the wave data at an offshore location to select a set of representative conditions and probability of occurrence (Benedet et al., 2016); referred to as offshore wave climate technique (OWC; Offshore Wave Climate); see Fig. 4.4c. The offshore wave heights are converted into wave energies or energy fluxes. Next, wave classes based on wave height and direction bins are prescribed by the user and the wave energies (or fluxes) are averaged per wave class. By modifying the probability of occurrence of each wave class an optimal reproduction of the benchmark (reference wave climate) is obtained.

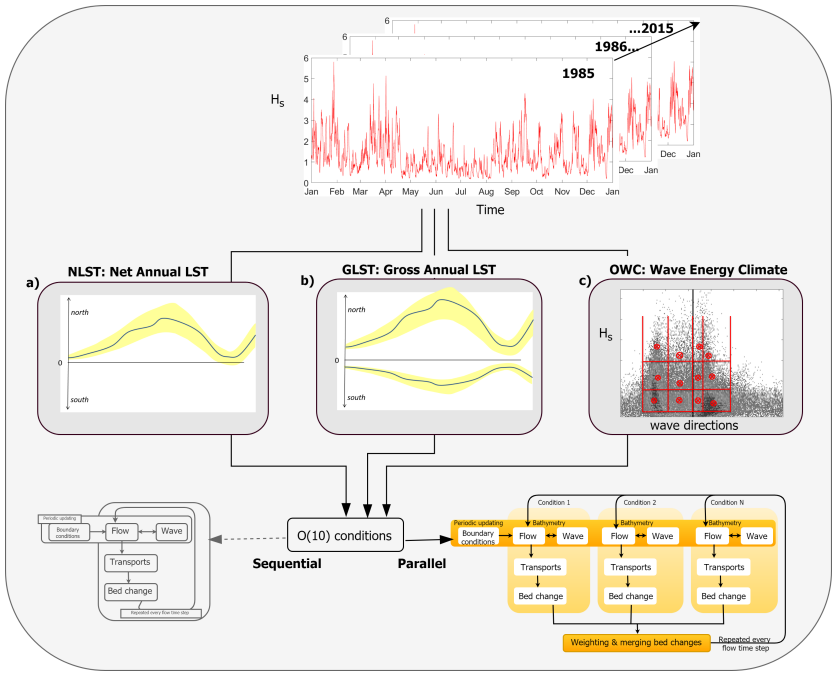

Figure 4.4: Graphical overview of the three considered morphodynamic acceleration techniques using representative (schematized) conditions: (**a**) NLST, (**b**) GLST and (**c**) OWC.

4.2.3 *Strengths and Limitations of the Morphodynamic Acceleration Techniques Considered*

All of the above discussed techniques have inherent pros and cons, which are listed in Fig. 4.3. As an example, the number of wave conditions per year are included assuming a 30-min wave time series for one year. The lower part of the table indicates whether key characteristics are resolved. Figure 4.3 shows whether a technique may potentially resolve the alongshore distribution of the southerly and northerly directed LST or just the yearly-averaged LST, and which techniques can potentially account for seasonal variations. The table also shows whether the depth of closure and the full window of the wave climate are included in the model forcing.

As computational power is often a limitation for morphodynamic simulations in engineering practice, this evaluation also provides a qualitative assessment of the computational costs associated with each acceleration technique (last row in Fig. 4.3).

4.3 CASE STUDY: THE SAND ENGINE

4.3.1 *Case Description*

The Sand Engine ('Zandmotor' in Dutch; hereafter referred to as ZM) is a large-scale, beach nourishment of 21.5 million m^3. The ZM is located at the Delfland coast, a 16.5 km stretch between the harbour of Scheveningen and Port of Rotterdam (see Fig. 4.5). This southern part of the Dutch coast is subject to persistent erosion (Stive et al., 2013). To mitigate erosion and reclaim land, a total volume of approximately 55 million m^3 of sand was added to the Delfland coast in the period 1986 and 2011, with a new nourishment on average every 3–5 years. In the years prior to the ZM the nourishment volumes in this stretch of coastline reached approximately 1.7 million m^3 per year.

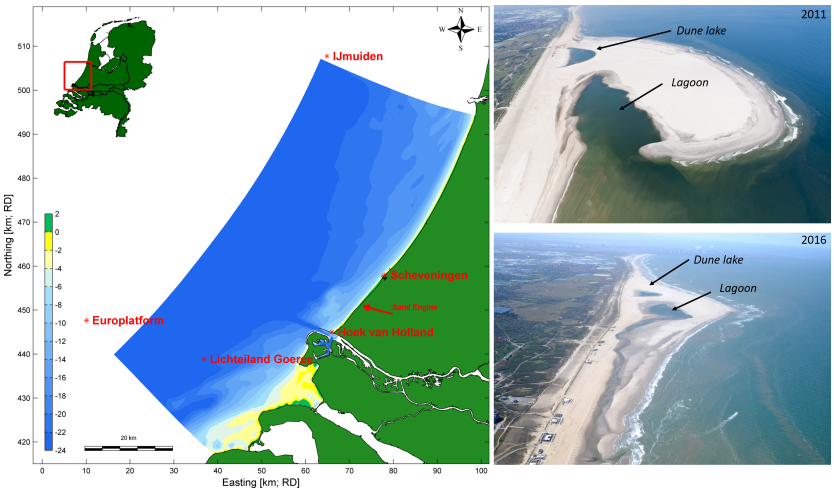

Figure 4.5: Geographical setting of the Delfland coast and the location of the Sand Motor (left). Aerial photographs from the Sand Motor in 2011 and 2016 (right).

The ZM was constructed between March and July 2011 and consists of a large peninsula of 2 km alongshore, with the most seaward part protruding 1 km into the sea. Monthly bathymetric surveys showed a rapid, predominantly alongshore redistribution of sediment in the first year after construction. The most seaward part of the peninsula eroded rapidly, leading to accretion both to the north and south. In the first half year after implementation, a spit developed from the northern tip of the peninsula, pinching the lagoon entrance (De Schipper et al., 2016). The maximum elevation of the spit and shoal were just below the high water level, making these areas prone to flooding during high tide (and storms). The channel landward of the spit formed an open connection between the lagoon and the open sea. After the rapid

initial deformation, the coastline gradually developed into a Gaussian bell-shaped curve over three years (De Schipper et al., 2016) followed by a widening of the bell curve. Since 2016, the observed shoreline shows a slight asymmetrical shape.

To predict the evolution over various time scales, it is important to reproduce the above-mentioned phenomena: specifically, the initial rapid erosion, spit and channel development, widening of the bell shape, breaching of the lagoon and the asymmetric development since 2016. Resolving the cross-shore distribution of the erosion at the most seaward part is also relevant for long-term forecasts, as this primarily determines the alongshore feeder behavior.

The driving forces for the dispersion of the ZM are the tide, wind and waves. The semi-diurnal tide at Scheveningen has a spring/neap tidal amplitude of 1.98/1.48 m (Wijnberg, 2002). The flood tidal currents peak at 0.7 m/s (northeast directed) while the ebb tidal currents peak at 0.5 m/s (southwest directed). The 1-year return period surge level at Hook of Holland is 2.35 m (Luijendijk et al., 2017), while the 1-year return period offshore significant wave height (H_s) is 4 m.

The spatial variation in the offshore wave climate along the Holland coast is small and can be characterized by a clear seasonal signal with average winter (November–January)/summer (April–August) offshore wave heights (H_s) of 1.7/1 m (Wijnberg, 2002). The highest waves ($H_s >$ 4.5 m) originate predominantly from the west and northwest, average waves (1.5 m$< H_s <$ 3.5 m) from both the southwest and northwest, while the small waves ($H_s <$ 1 m) originate mostly from the northwest.

By 2018, about 3.5 million m^3 had been eroded from the initial peninsula area. This is predominantly caused by wave action. Analysis showed that the 12 largest wave events of the first year resulted in about 60% of the total erosion observed in that year (Luijendijk et al., 2015). The intermediate wave conditions (H_s between 2–3 m), which occur more often, are thus almost as important to the erosion of the ZM as storm conditions. By 2018, the most seaward part of the ZM had retreated about 300 m since its placement in 2011. During the same period of time, the ZM extended up to 6 km alongshore.

4.3.2 *Numerical Model Setup for Delfland Coast*

The process-based numerical model Delft3D (Lesser et al., 2004) is used here to compute hydrodynamics, waves, sediment transport and morphology under influence of tidal, wind, and wave-driven currents. Delft3D is fully described in Lesser et al. (2004) and is therefore not elaborated upon here.

The domain of the Delfland coast was schematized with a curvilinear computational grid (see Fig. 4.5a). The grid covers an area of 26 km in longshore direction and 15 km in cross-shore direction. The water depth

at the offshore boundary is approximately 21 m. The grid resolution varies from 35 m to 500 m and the grid consists of 220 by 82 cells. The cell size increases with distance from the ZM. The bathymetry and the subaerial topography used in the model are based on the first survey conducted after completion of the ZM on 3 August 2011. Echo-sounding surveys conducted by Rijkswaterstaat are used for the remaining of the model domain beyond the 10 m depth contour. The tidal boundary conditions for the model domain were retrieved via nesting in a large-scale model for Dutch Continental Shelf (Zijl et al., 2013). The tidal information was converted into astronomical components for the offshore boundary, and use to derive zero-gradient water level conditions at the lateral boundaries. Observed surge levels at Hoek of Holland were prescribed to the tidal water level forcing as a concurrent time series. The measured 10-min averaged wind time series from Hoek of Holland were applied to include the wind effects on the water levels and currents.

For the wave propagation modelling, two nested computational grids were applied in a similar manner as Luijendijk et al. (2017). The large-scale wave grid (see Fig. 4.5a) was forced with measured time series of wave heights, periods and directions of the two offshore platforms Europlatform (EUR; location in Fig. 4.5a) and IJmuiden (IJM MSP). A uniform wind was applied based on the measured wind time series at Lichteiland Goeree (LEG) to ensure a sea-based wind speed. Although the offshore wave observations show large angles of incidence, the angle of incidence of the refracted waves at the 5 m depth contour is not larger than 45 degrees with respect to shorenormal for significant wave heights up to 1.5 m; higher waves with longer periods refract even more (Luijendijk et al., 2017).

As the tide, wave and morphodynamic model are similar in set up and parameter settings to the models presented in Luijendijk et al. (2017), we refer to the validation presented therein. The only difference is that the hydrodynamic model now covers a larger domain, but this was already part of an intermediate model step in obtaining the ZM models in Luijendijk et al. (2017). The sediment transport settings and morphological features are similar to Luijendijk et al. (2017) and based on the calibration of the first 12 months after the ZM implementation. The next paragraph verifies the performance of this so-named Delfland model for the time period August 2011–August 2016.

4.3.3 *Validation of the Benchmark Simulation without Upscaling (Brute Force)*

To evaluate the different acceleration techniques, first a morphodynamic model that can accurately reproduce the observed morphological changes in the study area (under observed forcing) needs to be

established (i.e., benchmark simulation). Therefore, a brute force morphodynamic simulation was conducted for the first five years (August 2011–August 2016) in which no upscaling was implemented (i.e., the BF method).

4.3.3.1 *Morphodynamic Evolution*

The computed bed level changes after five years correspond well with the observations (see Fig. 4.6). A Brier Skill Score (BSS) of 0.52 was achieved, which is classified as an excellent comparison by Sutherland et al. (2004b). This provides confidence in the predictive capability of the morphodynamic model. Phenomenologically, the predicted spit has merged with the adjacent beach and the elevation of the spit compares well with the observed elevation, i.e., around high water; the predicted behavior of the channel lags slightly compared to the observed channel configuration in September 2016 whereby the channel only floods during HW; the simulated (change in) shoreline orientation of both the southern and northern section is similar to the measured orientation; and, the observed asymmetry in the shoreline is also reproduced well by the model. With respect to the subaqueous morphology, the realignment of the -4 m depth contour is in good agreement with the observations. In addition, the depth at which significant erosion starts to take place is in line with the observed value; i.e., around the -6 m MSL.

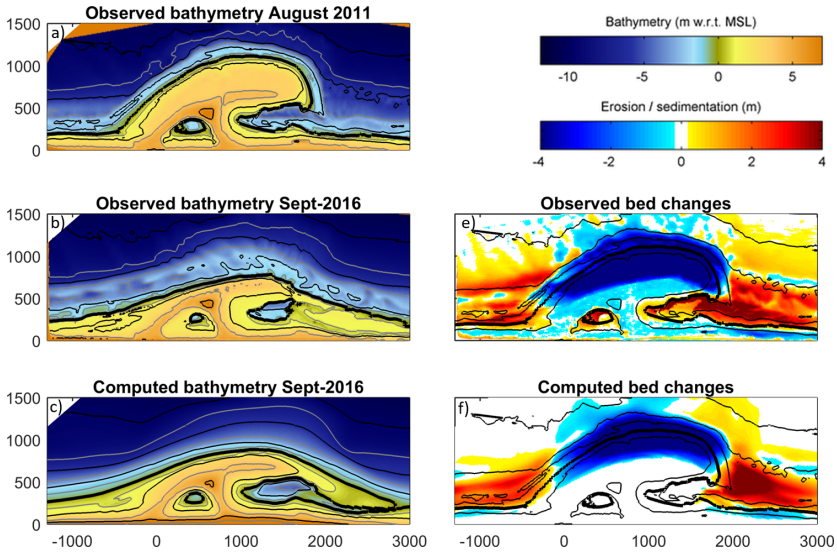

Figure 4.6: Overview of observed and computed bed levels and changes for 2016. (**a**) presents the observed bed levels in August 2011, (**b**) shows the observed bed levels in September 2016, (**c**) presents the computed bed levels in September 2016, while the observed and computed bed changes are presented in (**e**) and (**f**), resp.

As aeolian processes are not included in Delft3D, the associated windblown erosion and accretion are not reproduced by the model. Measurements show that aeolian transport caused a lowering of the dry beach area of 0.3–0.5 m in the first storm season and deposition of windblown sand in the lake and lagoon (see Fig. 4.6e) (Hoonhout and Vries, 2017). On longer time scales aeolian transports are an important driver for erosion of the subaqueous area and dune development. At present, coastal morphodynamic models lack the capabilities to realistically incorporate aeolian processes making this a limitation to the work presented.

4.3.3.2 *Volume Changes 2011–2016*

One of the key aspects in the evolution of the ZM is its feeder function, which is governed by its erosive behavior that provides new sand to be dispersed over time. The computed temporal behavior of the volume changes in three different control areas of the ZM generally agrees well with the observed volume changes (see Fig. 4.7). The observed initial erosion of the peninsula section (red outlined control area) in the first winter season (October 2011–February 2012) is reproduced well with 7% difference (1.5 vs. 1.4 million m^3). In the years thereafter, the relative effect of the storm seasons (November–February) is much smaller. After the first year, the model predicts a gradually increase of sediment leaving the overall control area indicating that the sand is transported beyond the boundaries of the three control areas (grey diamonds and line in Fig. 4.7). The computed trend is in line with the observed losses, although the observations show more variability in the first three years. The observed accretive behavior in the adjacent sections (blue and green lines) is also reproduced well by the model, although the accretion is slightly underpredicted at the southern section. The measurements show that the sand volume eroded from the peninsula area after five years is approximately 4 million m^3, while the model results indicate an eroded volume of 3.5 million m^3 over the same period (red line in Fig. 4.7).

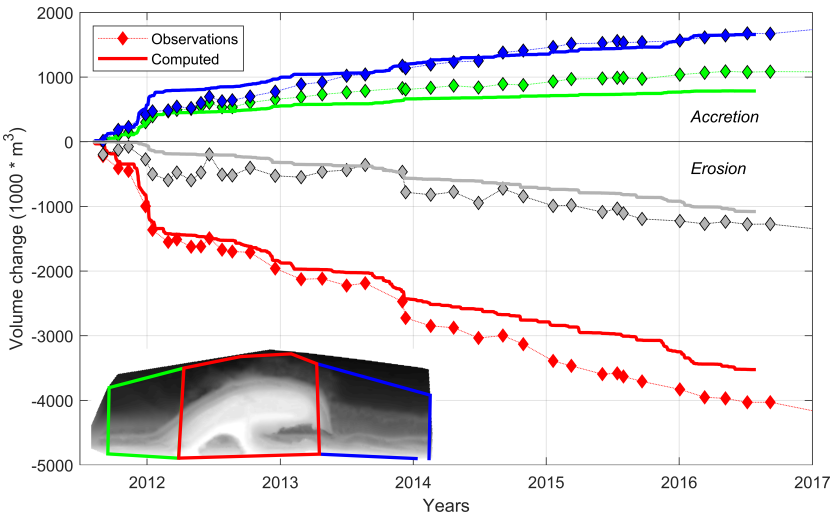

Figure 4.7: Computed and observed behavior of volume changes in the three control areas for the period August 2011–August 2016. Red dots and line represent the volume change in the peninsula area, while the blue (green) dots and lines show the volume changes in the northern (southern) section. The grey dots and lines show the sum of the volume changes in all three control areas.

The increasing deviation in the erosion curve could be attributed to the missing aeolian transports which are assessed to transport approximately 30 $m^3/m/year$ to the dunes (Hoonhout and Vries, 2017; Vries et al., 2012). This means approximately 60,000 $m^3/year$ for the 2-km long peninsula shoreline, adding up to a loss of about 300,000 m^3 for this 5-year period.

4.4 APPLICATION OF ACCELERATION TECHNIQUES TO THE SAND ENGINE CASE

To reproduce the observed behavior we applied the six morphodynamic acceleration techniques described in Section 4.2 to the ZM; i.e., three acceleration techniques that use the (filtered) real-time wave time series (filtered brute force (BFF) method, compressed, filtered brute force (BFFC) method, and brute force merged (BFM) method), and three techniques using representative (or schematized) wave conditions that adopt three different schematization targets (net LST (NLST), gross LST (GLST), and offshore wave climate (OWC)).

4.4.1 *Methodology for Brute Force Methods*

The first year analysis of the brute force simulation showed that only wave heights larger than 1.5 m contribute to the evolution of the ZM on the short timescale (Luijendijk et al., 2017). As this study focuses on multi-year evolution a threshold of 1 m was applied to be more conservative when omitting wave conditions. In addition, offshore-directed wave conditions with directions between 60 °N and 170 °N were omitted as they do not propagate into the ZM area. Omitting these input conditions from the wave time series resulted in a 40% gain in computational time without morphodynamic acceleration (*morfac* equals 1). For the decadal predictions the measured wave, wind and surge time series over the period August 2011–August 2016 were repeated every five years.

Compressing the (filtered) wave, wind and surge time series with a factor equal to the *morfac* value allows an acceleration of the simulation while still applying the brute force time series. Here, the time points of the (filtered) brute force time series are simply divided by the *morfac* value. This is based on the assumption that the tidal forcing can be disjointed from the wave and surge forcing; i.e., it is assumed that the tidal phasing does not influence the multi-year morphological response dominated by wave forcing, as confirmed by Luijendijk et al. (2017).

Simulations with *morfac* 3, 5 and 10 were compared with the reference BF simulation (*morfac* = 1). Simulations with a *morfac* of 5 and 10 showed instabilities in the computed bed levels. The main cause for this limitation is the rapid filling and emptying of the lagoon due to the compressed surge time series. The simulation with a *morfac* of 3 however showed morphological behavior that was similar to the benchmark run. This also confirms that the tidal phase in relation to the surge events is of less importance. This can be explained by the small spring to neap ratio in tidal range (factor $\sim$1.4) in the study area and the relatively long duration of surge events (multiple tidal cycles).

4.4.2 *Methodology for Representative Wave Forcing Techniques*

Three techniques with a set of representative (schematized) forcing conditions were considered in this study. Two focused on representing the alongshore distribution the LST (NLST and GLST; see Fig. 4.4) while the other concentrated on preserving the wave energy fluxes in the offshore wave field (OWC).

4.4.2.1 *Techniques Based on longshore transports*

Net longshore transports

Common way of schematizing the wave climate is to derive a limited set of wave conditions that represent the alongshore distribution of LST. For instance, Tonnon et al. (2009) derived 12 wave conditions that reproduced the alongshore distribution of the net annual LST at the Delfland coast. This approach requires a benchmark distribution of the LST computed with the full wave climate to compare with the LST simulated with a limited set of wave conditions.

Here we made separate morphostatic (no bed level updating) sediment transport simulations with the Delfland model for 214 wave conditions which cover the full extent of the wave climate (matrix consisting of wave height bins of 0.5 m and directional bins of 30 degrees). These transport computations for a single tide are very time efficient simulations (∼10 min computational time per run). Based on 30 years of offshore wave measurements (1985–2015), a probability of occurrence was calculated per wave condition, per year. In this way we could reconstruct 30 annual net LST curves for the Delfland coast (see Fig. 4.8a). The LST is zero at the Hoek of Holland boundary of the domain, due to the presence of the 1 km long harbour mole. The simulations show a bypass rates of ∼150,000 m^3/year at Scheveningen Harbour, which is in line with the measured values (Scheveningen Harbour Authority, 2018). The simulated interannual fluctuations in LST at the ZM location ranges from 100,000–300,000 m^3/year.

The input reduction tool OPTI (Mol, 2007; Roelvink and Reniers, 2012) was applied to obtain a reduced set of 10 wave conditions which are able to mimic the alongshore distribution of the net annual LST. OPTI first calculates the overall transports due to the complete wave climate (214 conditions) and their 30-year averaged probability of occurrence. Then, at each iteration step, the wave condition which has the lowest contribution to the overall transport is eliminated. The weight factors of the remaining wave conditions are modified to obtain a near-perfect solution. The iteration continues until one wave condition remains. For each iteration step OPTI shows how well the transports are represented by the reduced number of conditions in terms of statistical parameters (i.e., bias, RMS, R^2, and standard deviation). In this way, an optimal set of wave conditions can be determined based on statistical parameters. Typically, a set of 10–15 wave conditions can represent the LST distribution quite well. Here, OPTI was applied for the alongshore distribution of both the net and gross transports.

Gross longshore transports

A less common way to reduce wave input conditions is to use the alongshore distribution of the gross LST as the schematization target; i.e., to consider the southerly and northerly transports separately. Espe-

cially in case of a larger scale coastal intervention such gross transports can become relevant in both the erosive and dispersive behavior. As the morphostatic transport computations contain this information as well, the same approach as above is applied to arrive at a reduced set of 10 wave conditions that are able to adequately mimic both the southerly and northerly transport distribution (see Fig. 4.8b).

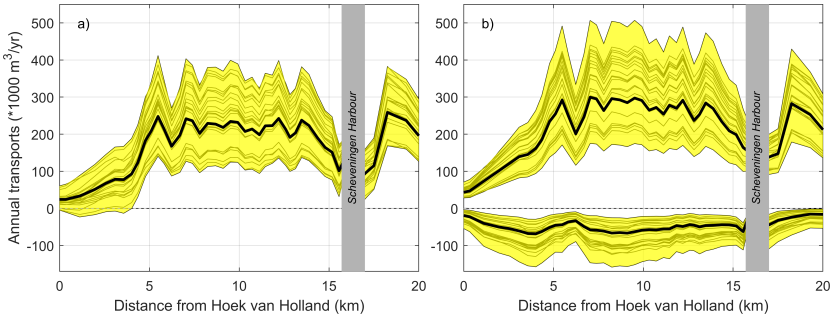

Figure 4.8: Envelope of the alongshore distribution of the annual (**a**) net and (**b**) gross longshore transports for the years 1985–2015. The grey lines are the annual longshore transport rates calculated using the 214 wave conditions and the measured probability of occurrence of the waves for each year. The black curves indicate the (**a**) net and (**b**) northerly and southerly longshore transports based on 10 wave conditions derived with OPTI to be used in the NLST and GLST computations.

Note that the generic derivation of the representative set of wave conditions should ideally be based on the coastal geometry prior to the intervention to avoid the schematization being dependent on layout and time.

4.4.2.2 *Technique Based on Offshore Wave Climate*

Another wave input reduction approach is to schematize the offshore wave climate into a limited number of wave conditions that represent the characteristics of the offshore wave climate. Long-term wave measurements at two wave buoys are available for this purpose: Europlatform and IJmuiden (for locations see Fig. 4.5a). The wave roses and density distribution show slight differences in wave characteristics at the two locations (see Fig. 4.9) with somewhat larger NW waves at IJmuiden.

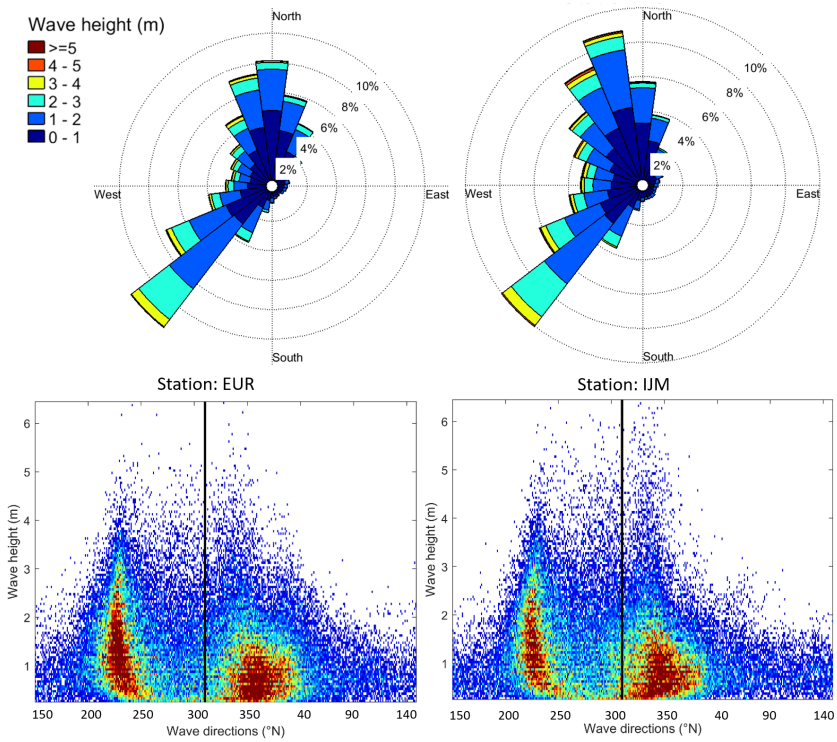

Figure 4.9: Wave rose and density distribution of wave height vs. direction for Europlatform (left) and IJmuiden (right). The black line at 311 °N represents the angle of the shore normal at the ZM location prior to implementation.

Several variants of input reduction based on wave energy have been reported in literature (Benedet et al., 2016; Lesser, 2009; Walstra et al., 2013). Here we have applied the FBM (Fixed Bins Method) approach (Benedet et al., 2016), in which a limited number of representative wave conditions are derived based on the wave energy per wave bin.

For this application, wave conditions were derived from a four by three matrix: directional cells between [200–260, 260–310, 310–330, 330–40 °N] and wave height cells between [0.5–1.75, 1.75–3.0, and $>$ 3.0 m] (see green dotted lines in Fig. 4.10). A representative wave condition was selected using the averaged wave energy per H_s-dir bin. This resulted in 10 wave conditions when omitting conditions with a probability of occurrence below 1%.

However, this schematization method has two potential limitations:

(1) the shoreline orientation varies significantly along the Delfland shoreline. The angle of the shore normals at Hoek of Holland and that near Scheveningen harbour differ by about 17 degrees. As we expect that sand from the ZM will disperse over the majority of this coastal

stretch over the next 20–30 years this could become important over time.

(2) the EUR and IJM wave buoys are located at comparable distances from the ZM (19 km and 25 km resp.). The wave heights and directions differ between the two locations and induce an alongshore gradient in wave energy and directions. Deriving a single representative set of wave conditions based on two locations using a wave energy approach is therefore not straightforward, but the effects are yet to be quantified. Here, the wave climate at EUR has been used for this schematization method.

The wave conditions thus identified in the three schematization techniques (NLST, GLST, and OWC) for this application are shown in Fig. 4.10.

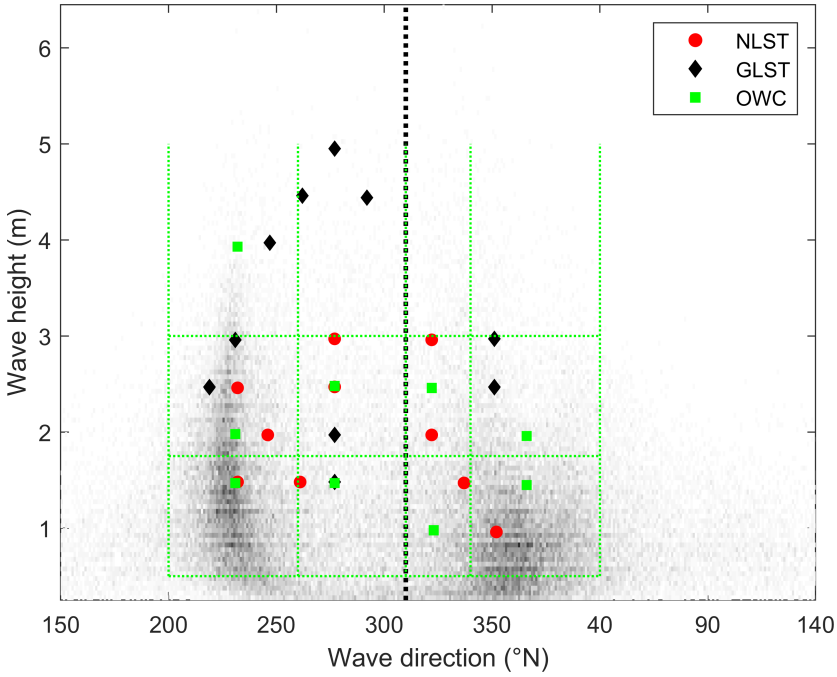

Figure 4.10: Resulting wave conditions for the three considered wave input reduction techniques. The black dashed line represents the angle of the shore normal at the ZM location prior to implementation, while the green dotted lines indicate the selected H_s-direction bins for the OWC technique.

4.5 VERIFICATION OF ACCELERATION TECHNIQUES FOR SHORT TO MEDIUM TERM MORPHODYNAMIC EVOLUTION

To investigate the performance of the different acceleration techniques described above, we first focus on the short to medium term (here, taken as the first five years after ZM construction) followed by the decadal time scale in Section 6. Hence, this section discusses the performance of the acceleration techniques with respect to the observations in the period 2011–2016.

4.5.1 *Morphological Response*

In general, the first year bed levels computed by the four selected acceleration techniques all show the spreading of sand from the peninsula to the adjacent coastal sections, and a spit develops to the north in each simulation. However, the shape of the spit differs significantly between the different acceleration techniques. The results of the BF and BFM techniques are very similar, while those of the wave schematization techniques deviate from both brute force techniques. The observed retreat of the most seaward section is best reproduced by the BF and BFM simulations (see Fig. 4.11). More specifically, the cross-shore distribution of erosion is reproduced well with erosion starting at -6 m MSL and reaching up to +3 m MSL, which is in good agreement with the measurements. Due to the lack of high wave events and high surge levels in the wave schematization techniques, the erosion in the upper profile is not reproduced well by the wave schematization techniques. Differences between the acceleration techniques are even more distinct with respect to the accretive behavior. The spit development simulated by the brute force techniques is much more prominent and follows the observed orientation. The spit orientation reproduced by the wave schematization techniques is more diffused than the observed one.

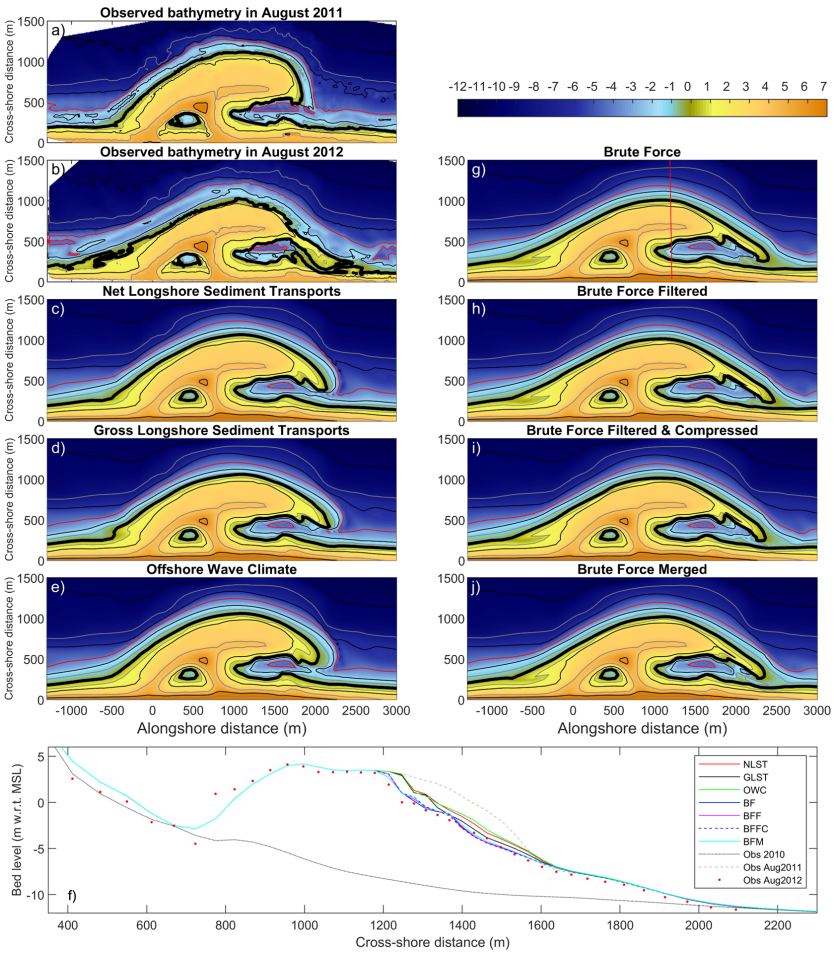

Figure 4.11: Observed and computed bed levels after one year: (**a**) observed bathymetry in August 2011, (**b**) observed bathymetry in August 2012, and the predicted bathymetries in August 2012 for (**c**) NLST, (**d**) GLST, (**e**) OWC, (**g**) BF, (**h**) BFF, (**i**) BFFC, (**j**) BFM. Cross-shore profiles for all observations and simulations are presented in (**f**) along the red transect shown in (**g**). The red line represents the -4 m MSL depth contour, while the thick black line shows the 0 m MSL depth contour.

Furthermore, compared to the wave schematization techniques, the brute force techniques predict a better cross-shore distribution of the deposited sand. For example, at the spit, a continuous alignment of the -4 m depth contour is predicted (see red contour line in Fig. 4.11), similar to the observations. The deviation between the wave schematization and brute force techniques in the first year highlights the better predictive capacity of the BF acceleration techniques at this time scale.

4.5.2 *Volume Changes 2011–2016*

The computed volume changes for the three control areas (see Fig. 4.7) show significant deviations between the different acceleration methods. The BFM simulation agrees best with the BF and observed temporal behavior of volume changes. The effect of the first storm season is captured well in the BF and BFM runs (see Fig. 4.12), resulting in a sediment loss of about 1.4 million m^3. The wave schematization techniques show much less erosion in the first year with peak differences of about 1 million m^3. The RMSE of the wave schematization cases ranges between 800,000 and 1 million m^3 for the first year. After about two years the net and gross transport techniques gradually move towards the BFM behavior. The wave energy technique shows the largest difference in erosion volume of the peninsula compared to the BF run; ∼700,000 m^3 after five years which is approximately 20%. The significant underprediction of the erosion volumes in the first two years demonstrates that the wave schematization techniques fail to reproduce the behavior in the first two years of the sandy intervention. The schematized techniques do not fully represent the range and variability in wave heights, directions and surge levels explaining the low performance at short time scales w.r.t. the observations. But over the five year time scale, the NLST and GLST techniques produce a similar end result (in terms of total eroded volumes) to that produced by the BF and BFM techniques. The GLST technique produces a lower RMSE after four years than the brute force techniques.

4.5.3 *Computational Times*

The selection of an acceleration technique to be applied in a coastal engineering study not only depends on its predictive capabilities but also on its computational requirement. The relative computational times for each of the acceleration techniques with respect to the BF simulation (benchmark) are presented here. All simulations were performed on the same quad core machine, although only the mormerge simulations benefit from multiple processors. The one-year BF simulation took 331 h (i.e., ∼2 weeks) to complete, while the BFF (BFFC) simulation took 53.3% (17.1%) of that (see Table 4.1). The BFM simulation required only 4.5% of the computational time of the BF simulation. The schematized techniques required even less computational times with values ranging between 1.0% and 1.6% of the computational time of the BF technique.

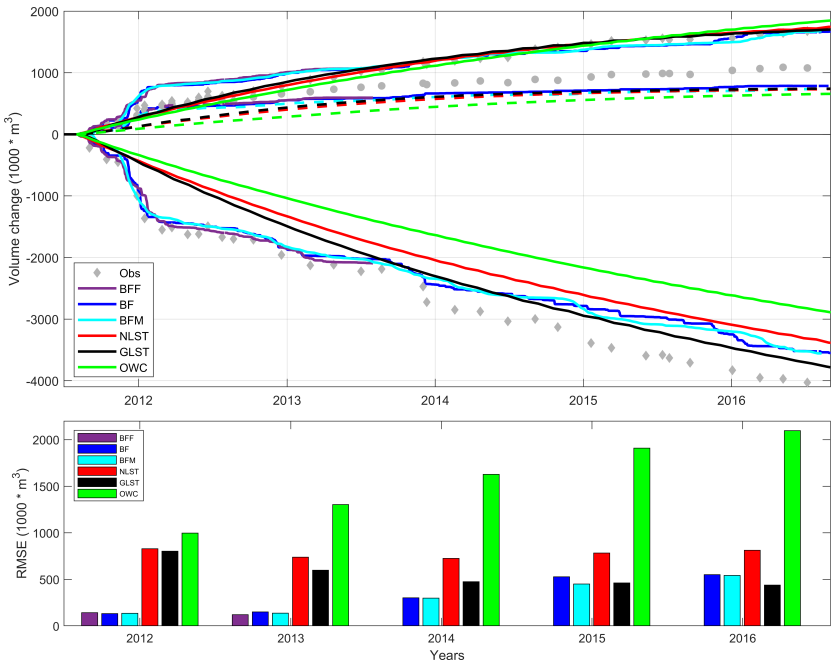

Figure 4.12: The upper panel presents the volume change in the period 2011–2016 for the three ZM control areas (see Fig. 4.7) for all considered acceleration techniques. The bottom panel presents the RMSE in each year for the four different acceleration techniques and the BF with respect to the observed erosion of the peninsula control areas. Due to long computational times the results of the BFF simulation are presented only for the first two years.

Table 4.1: Computational times for all considered acceleration techniques; computational times presented as hours run time to compute bed level changes after one year.

Abbr.	Acceleration Technique	Time (h)	Relative to BF (%)
BF	Brute Force	331.4	100.0
BFF	Brute Force Filtered	176.6	53.3
BFFC	Brute Force Filtered Compressed	56.5	17.1
BFM	Brute Force Merged	15.0	4.5
NLST	Net LST	3.9	1.2
GLST	Gross LST	3.2	1.0
OWC	Offshore Wave Climate	5.3	1.6

4.6 COMPARISON ACCELERATION TECHNIQUES FOR DECADAL FORECASTS

In the previous section the difference between the brute force and schematized techniques was discussed, where the brute force techniques show the best matches with the observations in the first two years. Also after five years the brute force simulations show the most accurate erosive behavior and accretion at the lagoon and spit when compared with the observations in that period. For the comparison at the decadal scale it is practically impossible to make predictions using the BF, BFF and BFFC techniques. A 30-year prediction using the BF technique would take more than 400 days of computational time, while the BFF (BFFC) simulation would take more than 220 (70) days; the BFM took only approximately 19 days. However, the BFM simulation shows very similar results to that of the BF simulation over the first five years (see Fig. 4.12). Considering its computational efficiency relative to the BF simulation, thus the BFM technique provides an optimal combination of phenomenological accuracy and computational efficiency over this time scale. Therefore, the BFM simulation is selected as the reference simulation in the evaluation at the decadal time scale. So, hereafter, results of four acceleration techniques will be presented: (a) BFM, (b) NLST, (c) GLST, and (d) OWC.

4.6.1 *Decadal Scale Evolution*

The bed levels for 2040 predicted by the four acceleration techniques show differences in the spit and channel characteristics and the surface area of the lagoon (see Fig. 4.13). The predicted spit formation in the NLST and GLST simulations remains narrow which resulted in a different surface area of the lagoon in 2040 compared to the BFM simulation; this results in different closure times of the lagoon. The predicted behavior of the area south of the peninsula is however quite similar in all techniques with the shoreline re-orienting towards the yearly-averaged incident wave angle. The accretive behavior in the area up to 3 km north of the peninsula differs significant among the simulations (see Fig. 4.15). The BFM simulation predicts that by 2030 a coastal stretch of just over 5 km would advance seaward due to the presence of the ZM, while the NLST and GLST predict a 6-km long seaward advancement of the coastline.

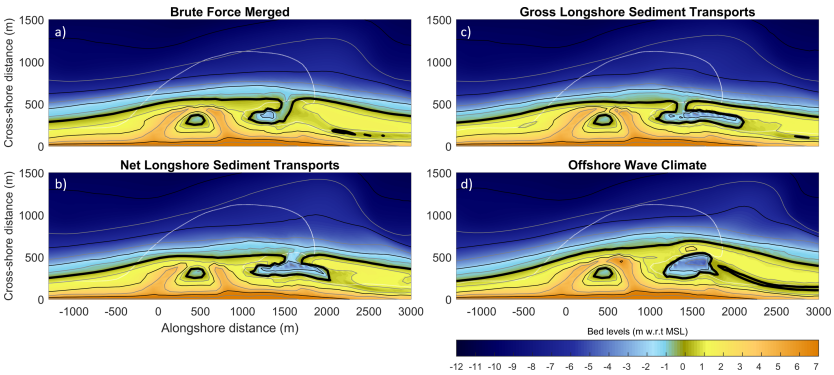

Figure 4.13: Computed bed levels in 2040 for the four considered acceleration techniques: (**a**) BFM, (**b**) NLST, (**c**) GLST, and (**d**) OWC. The white dotted line indicates the 2011 coastline just after ZM construction.

4.6.2 *Volume Changes 2011–2040*

By 2040 (i.e., ∼30 years after ZM construction) three out of four acceleration techniques predict very similar erosion volumes at the peninsula. The only deviation is in the results of the wave energy technique simulation which predicts an erosion volume that is approximately 1 million m^3 (∼13%) lower than that predicted by the other acceleration techniques at the end of the 30-year simulation period (see Fig. 4.14). While the sedimentation in the southern control area is equally predicted by all techniques, the accretion in the northern control area starts to differ among the simulations after 2020. The NLST prediction follows that of the BFM technique well, while the GLST technique predicts more dispersion and hence an accretion volume that is about 800,000 m^3 (∼30%) lower in 2040 in this control area.

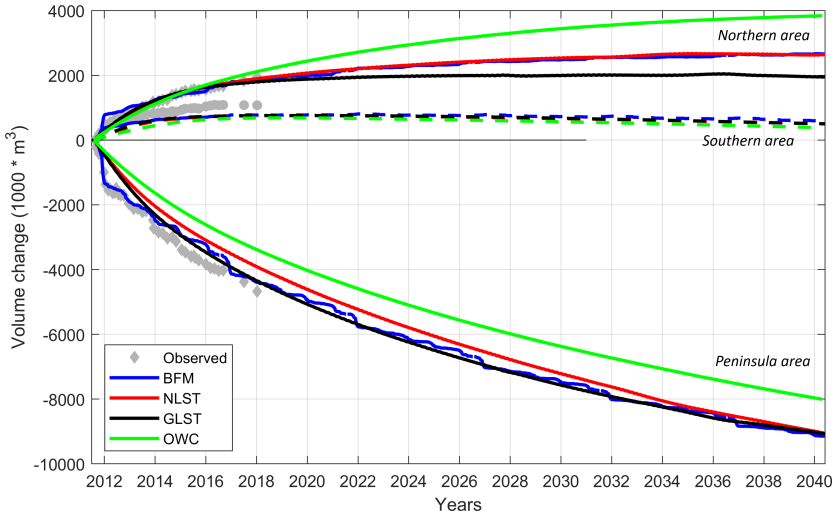

Figure 4.14: Volume changes in the period 2011–2040 for the four considered acceleration techniques for the three control areas (see Fig. 4.7).

The OWC technique underpredicts the erosion volume compared to the BFM technique and overpredicts the accretion in the northern control area by approximately 40%. Hence, this technique significantly underestimates the alongshore dispersion compared to the other techniques, indicating that the alongshore variation of the LST is not captured well in the OWC approach. This is probably because the alongshore distribution of the LST was not a target in this method. However, this result highlights the importance of using a input reduction method that is able to reproduce the alongshore distribution of LST realistically.

The long-term erosional behavior is captured well in all considered techniques with variations in volumes of about 1 million m^3 after three decades. The deviation between the brute force and the schematized techniques based on LST diminishes over time. This can be explained by the fact that the shoreline has largely retreated towards the situation prior to construction of the ZM. As the transport gradients around the ZM strongly reduce over time, the relative effect of gross transport diminishes, and the net transport technique becomes more valid again.

4.6.3 *Shoreline Positions in 2040*

The dispersion of sand along the coast entails that over time the LST distribution at a larger scale becomes increasingly relevant. As such, the presence of other coastal interventions may start to influence the dispersion and thus the coastal evolution. Here, the various acceleration techniques predict the coastal response and hence sediment transports

around the harbor moles of Scheveningen differently, which over time affects the updrift shoreline orientation (see Fig. 4.15). The selected conditions in the schematized forcing techniques are typically not representative for resolving the interaction with coastal structures such as sediment bypassing around the port. This led to an overprediction of the bypassing volumes at the Port of Scheveningen by approximately 0.8 million m^3 after 30 years (i.e., sediment loss from the coastal cell) for the LST-based techniques compared to the BFM technique. The brute force methods inherently represent the variations in wave directions and wave heights well, which results in a more realistic interaction with the coastal structures. This confirms that besides the benefits on the temporal scales, the relatively inexpensive BFM method also shows distinct advantages when predicting the morphodynamics at inter-dependent spatial scales.

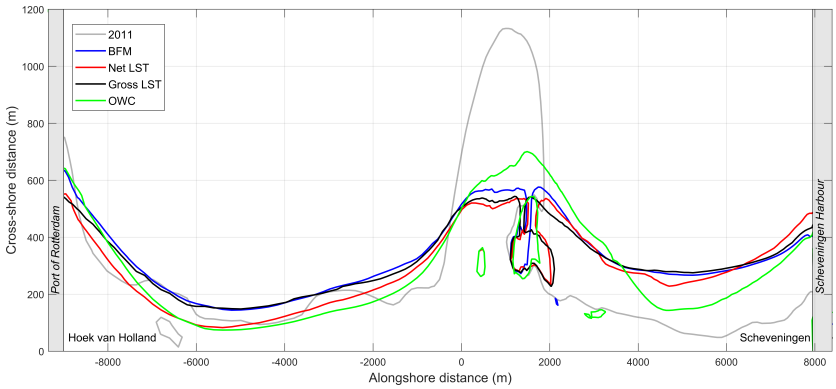

Figure 4.15: Predicted shoreline positions in 2040 for the four considered acceleration techniques showing the interscale impacts.

4.7 CONCLUSIONS

The design and acceptance of a sandy strategy as an erosion mitigating measure requires information on the predicted morphodynamics, both on the short and longer term. This study used the Sand Engine (ZM), located along the coast of the Netherlands, as a case study to evaluate the performance of different morphological acceleration techniques in predicting both short-medium term (1–5 years) and long-term (20–30 years) morphodynamic evolution. A Delft3D model of the ZM, calibrated with first year bathymetric measurements, is shown to be able to reproduce the observed morphological changes in the first five years. The observations and model predictions for the first five years after implementation of the ZM are used to evaluate six acceleration techniques: three based on brute force (real-time) time series and three based on representative (schematized) wave conditions.

Results show that acceleration techniques using representative (schematized) wave conditions are not capable of accurately reproducing the morphological response in the first two years. The optimal reproduction of the morphological behavior of the first five years is obtained by the brute force simulations. Seasonality in the wave climate, which is best reproduced by the brute force simulations, is relevant in the first two years. Applying input filtering and a compression factor provides similar accuracy yet with a factor five gain in computational cost. Applying wave input reduction (i.e., wave schematization techniques) on the magnitude and gradients in the longshore transports instead of the offshore wave climate results in better morphological behavior compared to the benchmark brute force simulation.

An attractive method for the medium to long time scales, which further reduces computational costs, is a method that uses representative wave conditions based on gross longshore transports, while showing similar results as the benchmark simulation. Erosional behavior is captured well in all considered techniques with variations in volumes of about 1 million m^3 after three decades. The predicted alongshore and cross-shore distribution of the morphological evolution as well as the spit development however have a strong dependency on the selected acceleration technique. The decadal predictions show a reduction of longshore sediment transport gradients over time and a distinct remaining signature of the Sand Engine after three decades.

The newly proposed 'brute force merged' technique, which incorporates the full variability of the wave directions and wave heights in the wave climate, provides an attractive and flexible method providing a combination of phenomenological accuracy and computational efficiency (factor 20 faster than the benchmark brute force technique) at both the short, medium and long time scales.

5

SEAMLESS MODELLING OF SANDY SOLUTIONS

Part of this chapter is based on: Arjen P. Luijendijk, Sierd de Vries, Thijs van het Hooft and Matthieu A. de Schipper. "Predicting dune growth at the Sand Engine by coupling the Delft3D Flexible Mesh and AeoLiS models". Coastal Sediments proceedings (2019).

The previous chapter has shown the importance of storms and seasonality followed by the recommendation to include aeolian transports as wind is able to transport large volumes of sand (300,000 - 500,000 m^3 per five years) from the intertidal area to the dry beach and dune areas at the Sand Engine. This chapter discusses the seamless coupling of Delft3D with AeoLiS, a morphodynamic model for the dry beach and dunes. The coupled model is applied to examine the added-value of a seamless modelling approach for sandy coastal interventions focusing on the interaction of processes in the subaqueous (wet) and subaerial (dry) domains.

5.1 INTRODUCTION

Beach-dune systems form a natural defense protecting the hinterland from flooding, while providing other functions such as recreation and nature development. Retreat of the shoreline can negatively impact the functions of these highly valued coastal areas. A typical measure for a coastal manager to mitigate erosion is the implementation of sand nourishments. Despite the limited lifetime of nourishments, sandy strategies are gaining in popularity for two reasons. Firstly, nourishments allow for adaptive management to changing conditions and unexpected circumstances. This flexibility means that costly maintenance can often be postponed, which can make sandy strategies more competitive than hard alternatives. Secondly, there is an increasing demand for solutions that integrate multiple functions (coastal safety, recreation and nature) at once, which a sandy solution can provide.

Up front, sound information on the expected sediment dynamics is required for the design and acceptance of a sandy solution. Without such information, the implemented solution may show unexpected, and possibly undesirable, behavior. For example, wind can blow large amounts of fine sand into the dunes (and inland villages) disturbing the dune ecology; or the sand placed at a concentrated nourishment may disperse too quickly, requiring new maintenance nourishments much sooner than anticipated.

Two large-scale sand nourishments in the Netherlands illustrate the need for information on multi-timescale (i.e. from storms to decades) and multi-domain (i.e. subaqueous and subaerial) information. First, the Sand Engine (hereafter referred to as ZM), a large-scale beach nourishment involving 21.5 million m^3, was constructed in 2011 (Stive et al., 2013; see left panel of Fig. 5.1). The natural forces of waves, wind and currents are expected to disperse the sand alongshore and into the dunes in the decades to come. Second, the Hondsbossche and Pettemer Zeewering no longer met current safety standards. Hence, the sea dike was reinforced in 2015 with a soft, natural barrier of 30 million m^3 of sand on the seaside of the dike, named Hondsbossche Dunes (Wittebrood et al., 2018; see right panel of Fig. 5.1).

Figure 5.1: Aerial photographs of two large-scale nourishments in the Netherlands: the Sand Engine (left) and the Hondsbossche Dunes (right)

The morphological impact assessments conducted in the EIA phase for both sandy interventions involved morphodynamic predictions at different time scales. Storm impact predictions were conducted with the XBeach model, while the long-term behavior was studied with different process-based area models. These morphological predictions were hence computed using a single morphological model for a specific temporal domain (here either storms or years-decades) and covering a specific spatial domain (here only subaqueous). These approaches involve several shortcomings in decadal predictions, such as; neglecting the effects of storm clusters and seasonality in wave energy when applying schematized forcing conditions; neglecting windblown transports that impact the cross-shore redistribution of sand and hence the dispersive behavior; neglecting the dune growth by sediment fluxes to the dunes and hence neglecting the growth of nature areas; and neglecting beach recovery. Without the aforementioned processes the dispersive behavior of the sandy intervention is potentially impacted as is the increasingly important dune ecosystem.

Recent model and technological developments are now allowing us to fully integrate models. Chapter 4 presents a novel technique that deals with a multi-timescale approach to incorporate storms and seasonality in decadal morphodynamic predictions.

A recent development in 1D profile mode is presented by Roelvink and Costas (2019), in which a new dune profile model, Duna, is developed and coupled with the XBeach model. Some additional improvements allow a much better behavior of the intertidal beach and the inclusion of chronic erosion or accretion through a longshore transport gradient. A recent development in 2DH is presented by Cohn et al. (2019) who discuss an application of a coupled model to explore marine and aeolian controls on coastal foredune growth.

The pioneering studies by Roelvink and Costas (2019) and Cohn et al. (2019) have shown the close connection between morphodynamic evolution in the subaqueous zone and the subaerial.

The shared sediment budget and feedback across the land-water interface require a frequent coupling between models to exchange information. Recently the Basic Model Interface (BMI; Peckham et al., 2013) has been presented as an coupling method between models, and applied with success for short timescales (days) in Cohn et al. (2019).

These recent advances in numerical model coupling, model descriptions and acceleration techniques provide the opportunity to evaluate the impact of complex interventions at timescales from days to decades.

This research examines the added value of a coupled modelling approach for sandy coastal interventions focusing on the interaction of processes across subaqueous and subaerial domains. The coupled approach involved a seamless integration of two morphodynamic models covering the subaqueous and subaerial (the intertidal and dry beach) areas. The Sand Engine (ZM) mega-nourishment is adopted as a first case study.

5.2 THE SEAMLESS MODELLING FRAMEWORK

Comprehensive monitoring of the ZM shows that the sediment transport towards the dunes is governed by the interaction between aeolian and hydro- and morphodynamic processes (see Chapter 3 and Hoonhout and Vries, 2019). A seamless modelling framework is developed that allows combining process-based models, which resolve the aeolian, hydro-, and morphodynamic processes, in a flexible and easy-to-use manner. Here, seamless coupling refers to a smooth, flexible and continuous exchange of model variables from various coupled models.

5.2.1 *Model components*

In this application three model components are combined. The first component is Delft3D Flexible Mesh (Kernkamp et al., 2011; hereafter referred to as FM) with the recently developed morphological module. The FM model calculates the hydrodynamics, sediment transport and bed level changes in the subaqueous area; see Appendix C for more details.

The advantage of the FM model over the Delft3D-v4 model setup is the compliance of FM with BMI (see next section), thus enabling a coupling with multiple models. The second component is the wave model SWAN (Booij et al., 1999), which is applied to compute the random, short-crested wind-generated waves. The third component is the aeolian morphodynamic model AeoLiS (Hoonhout and Vries, 2017). AeoLiS is used to compute the bed changes in the intertidal and dry beach area due to windblown transports.

5.2.2 *Basic Model Interface (BMI)*

Coupling between FM and AeoLiS is achieved via a component-based environment using the Basic Model Interface (BMI; Peckham et al., 2013) designed by the Community Surface Dynamics Modeling System. The BMI method allows interaction with models during simulation time. A model can be implemented as a library within a larger framework as the interface handles initialization, finalization and time stepping routines. The present implementation supports the specification of a callback function, which is called at the start of each time step and can be used to exchange data between all connected models.

The method allows for a parallel coupling of FM and AeoLiS, steered by a controller which uses hydrodynamic and wind time series as input. The exchange of information between FM and SWAN utilizes a well-established coupling interface (using a communication file) which is also steered by the controller.

5.2.3 *Exchange of variables*

All three models may use their specific grid configuration, boundary and initial conditions. Fig. 5.2 illustrates the exchange flow of variables between the models. First, the water levels are computed by FM and provided to AeoLiS and SWAN. Next, a stationary wave field is calculated by SWAN and provided to AeoLiS and FM. Then, AeoLiS calculates the bed level changes in the dry region using the most recent water levels from FM and waves from SWAN. Subsequently, FM calcu-

lates the bed level changes based on the waves from SWAN next to the tidal currents.

Next, the integrated model superpositions the calculated bed level changes by AeoLiS and FM and provides the combined updated bed level changes back to all three models. Finally, the model bathymetries are updated using these bed level changes, after which each component can compute the next time step. Below the three main variables are discussed in more detail.

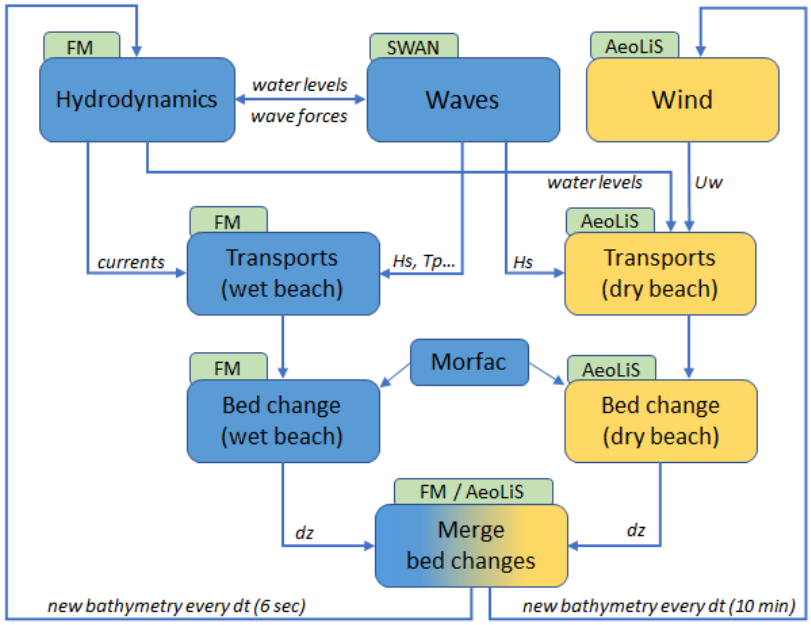

Figure 5.2: Schematization of the exchanged variables between FM, SWAN, and AeoLiS.

Water level

The interface between wet and dry areas in a tidal environment is an important, yet complex area to accurately model, mainly due to the continuous drying and flooding of grid cells. FM makes use of a water depth threshold to determine whether a cell is wet or dry. Water depth, the sum of water level and bed level, is one of the primary variables which is solved in the shallow water equations. As sediment transports and bed level changes are generally only calculated in wet cells, the instantaneous water depth also has an influence on bed changes at very shallow waters.

In AeoLiS, the water level, combined with the bed level, is also used for the distinction between wet and dry cells. Dry cells may erode due to wind forcing, while a high shear velocity threshold is defined at wet cells preventing local erosion. Furthermore, water level is also used

to calculate the moisture content of dry cells, which affects the shear velocity threshold and hence the saturated concentration of windblown sand.

Both AeoLiS and FM make use of a water depth threshold to determine whether a cell is wet or dry. As FM solves the water levels every time step during the computation, it is possible that an area temporarily becomes almost 'dry' during the lowering of the tide. If this is the case the water level will remain at the last computed value being just smaller than the threshold. To ensure a closed water balance, the water depth in that cell is not set to zero. Therefore, this can lead to an artificial thin film of water in dry cells. These values are exchanged to AeoLiS which could lead to an unrealistic decrease of aeolian sediment transport when this is not recognized as a fictitious water depth. It is therefore important to set the water level threshold of AeoLiS larger than or equal to the threshold in FM.

Wave height

The existing coupling between FM and SWAN is crucial for modelling the wave-driven currents (due to radiation stresses gradients) and wave-related transports (due to wave stirring by orbital velocities). Another important effect of waves is that they may rework sediments in the shallower waters. This sediment mixing is paramount for the sediment pickup, e.g. in the intertidal area, calculated by AeoLiS. Reworking of sediments up to a certain depth may break up an armored layer changing it into a well-mixed layer, which is able to erode during low tides. The wave height determines the mixing depth and is therefore provided to AeoLiS per cell.

Bed level

The simulated bed levels are the key output of the integrated model and are the result of different morphological processes in both FM and AeoLiS. The computation of bed level in AeoLiS is rather straightforward as the computed bed level changes directly originates from the sediment entrainment ('pickup' in AeoLiS literature). Due to wind forcing, sediment erodes from the areas where shear velocity threshold is exceeded (e.g. a dry area with a lot of fine sediment) and deposits where the shear velocity is lower than the threshold (e.g. at wet areas in the lagoon).

Where FM has the option to apply a morphological acceleration factor (*morfac*), AeoLiS does not provide such an option. Therefore, to synchronize the time scales and reduce the computational time of AeoLiS, a *morfac* concept is implemented in the controller script, similar to that in FM.

5.2.3.1 *Coupling in time and space*

The integrated model starts with FM to calculate the hydrodynamics. The instantaneous water depths are provided to SWAN for the wave calculation. SWAN recomputes the wave field frequently (typically every 20 min). AeoLiS uses a smaller time step (i.e. 10 min), while FM uses an even smaller (implicit) time step (here 6 sec). As the time step of AeoLiS is larger, FM performs several updates until the same time point as AeoLiS is reached. Then, when the update interval of SWAN is reached the stationary wave field is recomputed, starting from the previous wave state but using the most recent water levels and updated bed levels. This cycle is repeated until the end of the simulation time.

Fig. 5.3 shows the time line of the exchange of variables between the three model components.

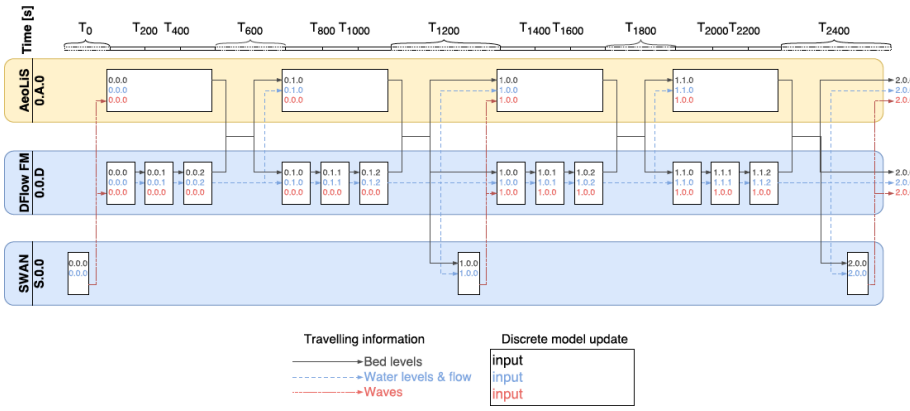

Figure 5.3: A graphical representation of the time line of data exchange between the model components in the integrated model framework. The arrows show moments of transfer of updated variables. The width of the white blocks correspond to the duration of one time step of each model component. Note the width of the FM time step is not to scale and the computed wave field by SWAN is applied for the full interval.

The spatial exchange of variables between the FM and AeoLiS grids is established by using a newly developed mass-conserving interpolation method specifically created for the rectilinear AeoLiS grid and the staggered grid used in FM (Velhorst, 2017).

5.3 THE INTEGRATED SAND ENGINE MODEL

To validate and quantify the benefits of the seamless coupling the Sand Engine is adopted as a case study because of the monthly surveys, covering the subaqueous and subaerial domains, and the large signal-to-noise ratio in bed level changes.

5.3.1 *Model setup*

AeoLiS uses a rectilinear grid of 25 m x 25 m grid cells. FM uses a curvilinear, yet unstructured, mesh with mesh sizes ranging from 240 m offshore to 30 m in the nearshore. In Fig. 5.4 the AeoLiS grid and FM mesh are shown; rotated by 48 degrees to provide a shore orthogonal view. The considered domain covers approximately eight km of coastline around the Sand Engine.

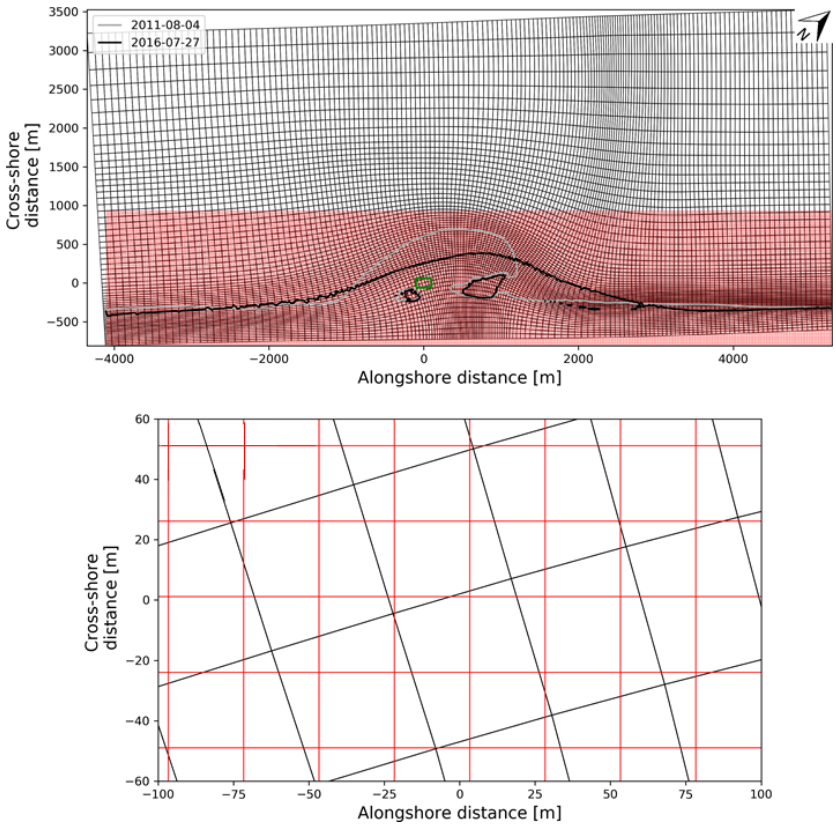

Figure 5.4: The computational mesh of FM (black) and grid of AeoLiS (red) as set up for the Sand Engine model (upper panel). The grey and black contours highlight the MSL-contour in the 2011 and 2016 resp. The bottom panel shows a detail in the green box, showing the overlap between AeoLiS and FM grid cells.

The FM model mesh and parameter settings are to a large extent similar to the Delft3D model setup presented in Chapter 3 and Luijendijk et al. (2017). As FM resolves the hydrodynamics differently, a few settings related to the hydrodynamic solver and drying and flooding have been altered. The sediment and morphological settings are identical to the parameter settings presented in Chapter 3.

The settings of the AeoLiS model are also adopted from Hoonhout and Vries (2019), except for settings related to the sediment grain size distribution, which are modified after a bugfix in a newer version of AeoLiS. For aeolian sediment transport, the grain size distribution is more important than the median grain size value (Hoonhout and Vries, 2017). Therefore, AeoLiS uses a (log normal) grain size distribution that is divided into 11 grain size fractions based on three soil samples

taken at the Sand Engine (see Fig. 5.5). The soil consists for 95% of sand varying between 0.1 - 2 mm and 5% of shells and roughness elements ranging between 2 - 32 mm.

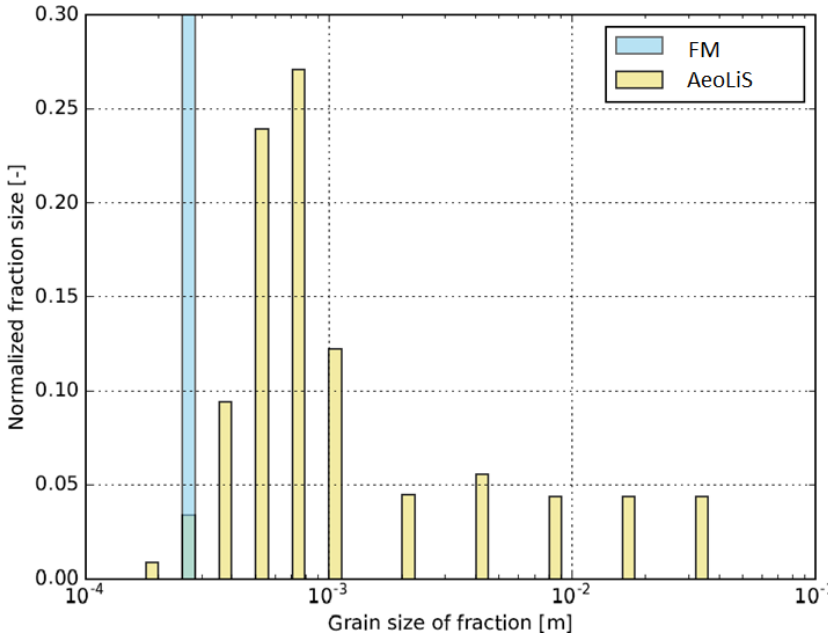

Figure 5.5: Grain size distributions in FM and AeoLiS.

A brute force (real-time) simulation was performed for the period August 2011 to July 2016, forced with measured surge, waves and wind time series. Here, a *morfac* of 3 is applied to accelerate the morphodynamics similar to the BFFC simulation[1] in Chapter 4. Hence, the forcing time series are compressed with a factor three.

1 Note that the BFM technique in combination with the coupling with AeoLiS over multiple processors was not yet operational at the time of writing.

5.4 MODEL DATA COMPARISON

Fig. 5.6 shows the observed and computed bed levels after five years simulated with the integrated model. The dispersion in the subaqueous domain of the ZM is reproduced well by the FM model and shows similar results as the Delft3D simulations in Chapter 4.

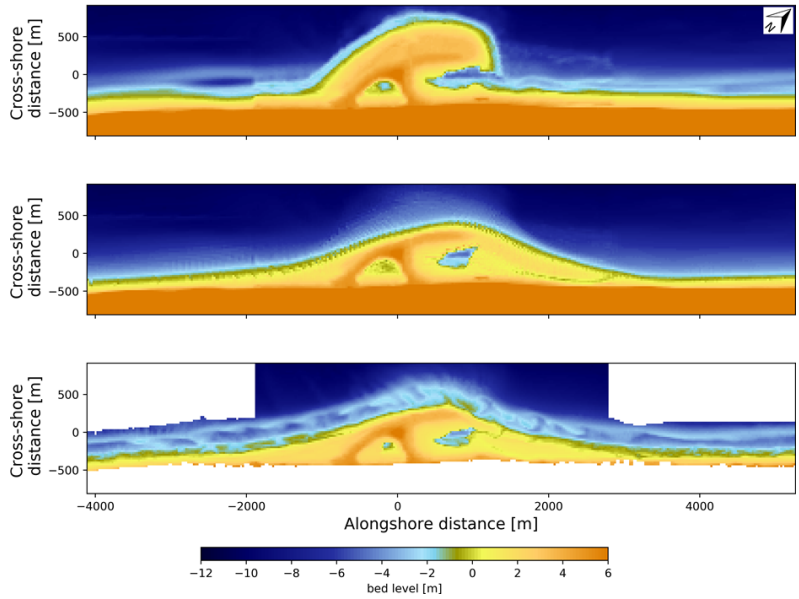

Figure 5.6: Measured bathymetry of August 2011 (upper panel) and July 2016 (lower panel), and the computed bathymetry for July 2016 (second panel).

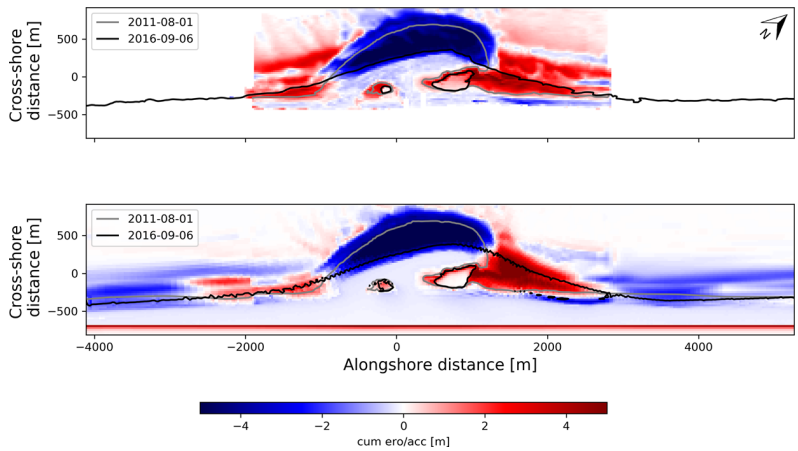

Figure 5.7: Bed level changes between August 2011 and September 2016 based on measurements (upper panel) and simulation of coupled marine and aeolian processes (lower panel).

The red patches at the dune lake and lagoon (see lower panel of Fig. 5.7) indicate the simulated deposition of wind-blown sand in these water bodies, which is also found in the measurements. Both observations and simulations show a gradual filling up of the dune lake with windblown sand, which significantly reduces the wet surface area of the lake. At the lagoon, computed deposition of windblown sand in the lagoon is more concentrated at the seaward edge while the observations show a more diffusive pattern. The observed deposition in deeper parts of the lagoon is partly related to the accumulation of fine sediments (silt and mud) as indicated by dual-frequency echo soundings (not shown). As the FM model does not include any cohesive sediments, this can not be reproduced by the model.

5.5 ADDED VALUE OF COUPLING IN SIMULATING DUNE GROWTH RATES

To quantify dune growth rates (in $m^3/m/yr$), the computed cross-shore sediment fluxes which are transported over the dune foot are integrated per year. The top panel in Fig. 5.8 shows the alongshore variation of the simulated annual dune growth rates computed by AeoLiS standalone. The colored lines show the simulated dune growth rates per year from August to August. The simulated dune growth rates in the first year are approx. five times larger than in subsequent years. The larger first-year dune growth rates are caused by the erosion of the unarmored dry beach area. After the first winter season armoring reduces the aeolian transports significantly resulting in much lower dune growth rates (Hoonhout and Vries, 2017).

The simulated mean dune growth rates of 5 $m^3/m/yr$ at the coastal sections adjacent to the ZM area are about three times smaller than the observed rates of 15 $m^3/m/yr$ in this area over the same period. Besides the underprediction in magnitude the increase in dune growth is restrained to the initial placement area of the ZM. This is because the dispersion of sand in the subaqueous zone is not resolved in the standalone AeoLiS model.

When incorporating the prediction of subaqueous morphodynamic changes by a seamless coupling of AeoLiS with FM, three additional processes are explicitly resolved: 1) the reworking of sand in the intertidal zone by waves breaking up the armored layer, 2) the erosion of dry beach by waves, surges and currents resulting in new beach areas exposed to aeolian transports, and 3) the widening of beaches adjacent to the ZM due to alongshore dispersion. These processes cause the difference between first year and subsequent years to be much smaller in the coupled simulation (see lower panel of Fig. 5.8).

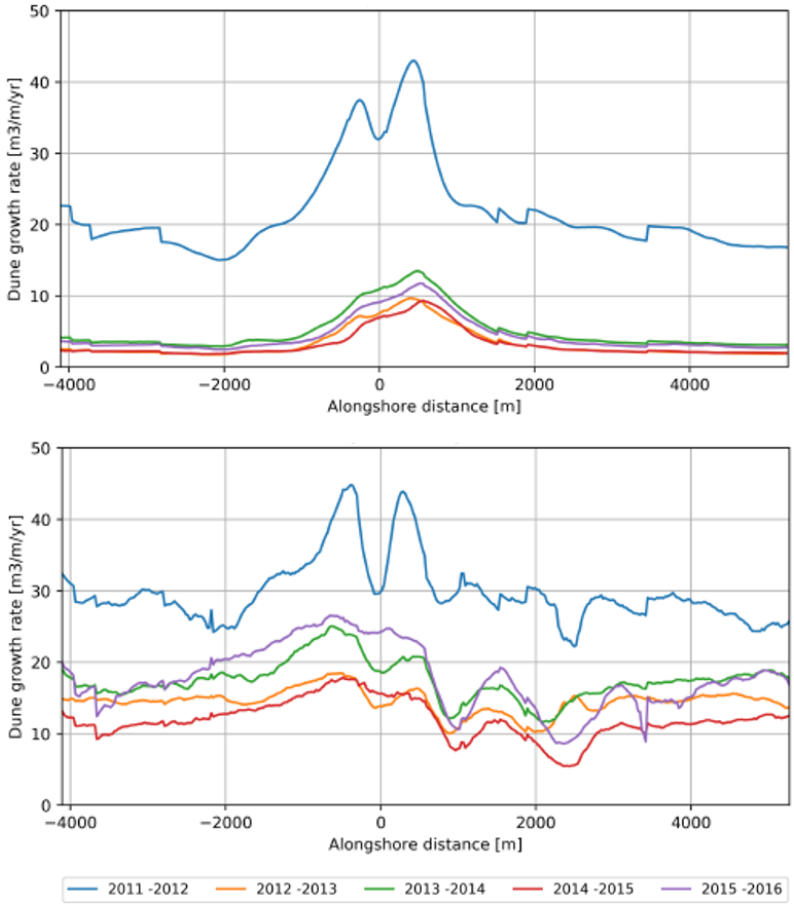

Figure 5.8: Alongshore variation of predicted annual dune growth rates at the Sand Engine. Top panel shows the results when applying AeoLiS standalone and the lower panel shows the results of simulation with the coupled model.

Moreover, the simulated mean dune growth rates of 18 $m^3/m/yr$ agree well with the observed mean dune growth values of 15 $m^3/m/yr$ for the period 2011 - 2016.

5.6 PREDICTING DUNE GROWTH RATES

The seamless model can be used to asses year to year variations in forcing and in dune growth. Hereto the predictions are extended by five more years (for the period 2016-2021). The forcing conditions in this period are replicated from the time series of waves, wind and surge levels in the first five years.

Fig. 5.9 presents the alongshore variation of the simulated dune growth rates for the years between 2011 and 2016. In the period 2011 - 2016 an average dune growth of 18 $m^3/m/yr$ is predicted, while a slightly lower average dune growth of 15 $m^3/m/yr$ is predicted for the period 2016 - 2021. This lowering could be attributed to the local reductions in dune growth north of the ZM (see Fig. 5.9, alongshore distance $\sim$4000 m).

The model results show larger dune growth in the sixth year (2016-2017; see Fig. 5.9 blue line), similar to the large rates predicted in the first year (2011-2012; see Fig. 5.8). These larger rates in the 1st of both five year prediction sets indicate that the large dune growth in the year 2011-2012 originate mostly from the favorable forcing conditions for dune growth, rather than changes in the subaqueous bed levels.

Therefore, besides the unarmored state of the beach in the first year, the forcing conditions also contribute to the larger dune growth of the first year. The average dune growth shows an increase directly south of the ZM center (alongshore distance of 0 m) and a decrease directly north of the ZM center. Furthermore, a northward migration of the local minimum in dune growth rates (around x=$\sim$1000 m) is found in the period 2016 - 2021, which was not apparent in the results for the period 2011 - 2016. It is hypothesized that this because of the gradual filling up of the dune lake from the south / southwest.

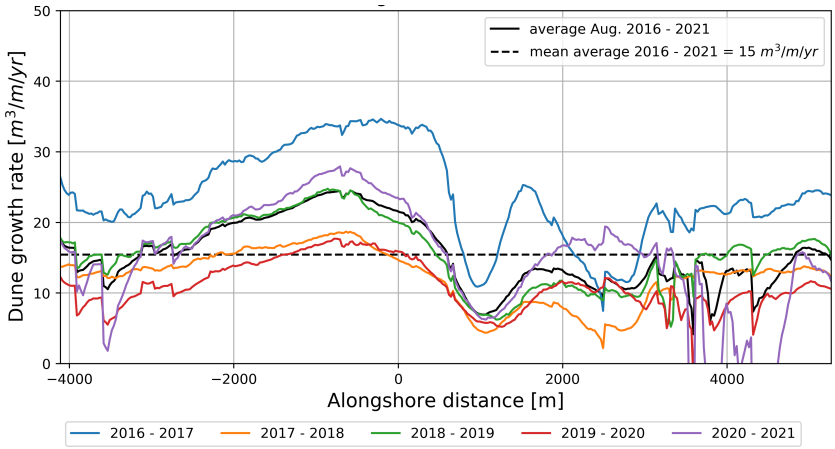

Figure 5.9: Five-year dune growth prediction of the integrated model at the ZM for the period 2016 to 2021.

5.7 CONCLUSIONS

Sandy interventions are often implemented with the objective to stimulate the natural growth of dunes. So far, the predicted growth of dune area is generally derived using empirical relations and not through process-based modelling.

Measurements at the ZM show a large difference (factor five) between the forecasted growth of the dune area. The empirical model in the EIA forecast predicted a steady growth of 25 ha in 20 yrs (i.e. 5 ha in 4 years), where the observations revealed less than 1 ha increase. This implies that a more advanced method is needed to predict dune growth in the vicinity of coastal nourishments.

Observations after five years show that a large volume of 400,000 m^3 of sand has been blown into the dunes, lake and lagoon, which confirms the relevance of the aeolian transports in the morphological behavior of the ZM. From a sediment budget analysis of the ZM it can be concluded that 58% of all sediments deposited in the dunes originate from the low lying beach zone that is regularly reworked by waves (Hoonhout and Vries, 2017). For these reasons a model is needed that takes the interaction between both the aeolian and hydrodynamic and morphodynamic processes into account.

A seamless integration of two morphodynamic models (being Delft3D Flexible Mesh (FM) and AeoLiS) has been developed and applied to the Sand Engine. The integrated morphodynamic simulation is well capable of reproducing the observed changes between 2011 and 2016 for both the subaqueous and subaerial domain.

Regarding dune growth, the simulated results of the integrated model compare well with the measured dune growth between 2012 - 2015; the measured yearly-averaged dune growth rates vary between 14 - 19 $m^3/m/yr$, while the simulated yearly-averaged dune growth rate is 18 $m^3/m/yr$.

The results for the ZM case show that the seamlessly coupled FM and AeoLiS can efficiently and realistically resolve the interactions between the subaqueous and dry beach morphodynamic evolution. Providing frequent point-based information on the waves, water levels and, in particular, the subaqueous bed levels to the AeoLiS simulation results in realistic dune growth rates; both in magnitude, spatial and interannual variations. Incorporating these processes is paramount not only for realistic predictions of coastal dune development but also for the longer term morphological behavior of the subaqueous domain.

Part III

SYNTHESIS

6 SYNTHESIS AND OUTLOOK

6.1 CONCLUSIONS

In a time of societal and environmental changes there is a growing demand for actions to protect and sustainably manage coastal ecosystems. In the last decade various nature-based solutions (NBS) have been implemented that combine the functions of safety, recreation and nature development. Such NBS however demand deep insight in the natural dynamics to arrive at optimal solutions. Coastal NBS require a comprehensive understanding of the system to better embed the solution in the natural ecosystem as they are typically designed to adapt to changing environmental conditions. There is a number of shortcomings in the understanding of sandy beach systems and predicting the development of (complex) sandy NBS that can be improved significantly. This work attempts to fill some of these gaps.

The main goal of this thesis is to cross borders in coastal morphodynamic models by augmenting the forecast horizon in temporal space by advanced morphodynamic acceleration techniques, and in spatial space by integrating subaerial and subaqueous morphodynamic processes. This study contributes to the predictive capabilities of process-based models applied to complex sandy coastal interventions. First, existing and novel morphodynamic acceleration techniques are assessed on their performance at multiple time scales. Second, performance of a novel integrated morphodynamic model is investigated that seamlessly fuses the subaqueous and subaerial coastal domain. The mega-nourishment Sand Engine is adopted as case study representing a complex sandy intervention. Yet, as a kickoff of this thesis, historic shoreline positions of all sandy beaches on our globe have been determined and analyzed using satellite imagery. This information forms an important and unprecedented source of information that can feed the understanding of the natural dynamics of sandy beaches.

Detailed conclusions of the four research objectives are given below.

1. Analyze the historical shoreline dynamics of sandy beaches at a planetary scale using satellite imagery

Coastal zones constitute one of the most heavily populated and developed land zones in the world. Despite utility and economic benefits that coasts provide, there is no reliable global-scale assessment of historical shoreline change trends. Here, via the use of freely available

optical satellite images captured since 1984, in conjunction with sophisticated image interrogation and analysis methods, a planetary-scale assessment of the occurrence of sandy beaches and rates of shoreline change therein is presented.

Applying pixel-based supervised classification, it is found that 31% of the world's ice-free shoreline are sandy. The application of an automated shoreline detection method to the identified sandy shorelines results in a global data set of shoreline change rates for the 33-year period 1984-2016. Analysis of the satellite derived shoreline data indicates that 24% of the world's sandy beaches are eroding at rates exceeding 0.5 m/yr, while 28% are accreting and 48% are stable. The majority of sandy shorelines in marine protected areas are eroding, raising cause for serious concern.

The developed methods provide a unique opportunity to retrieve historic information on shoreline dynamics at a decadal scale for any beach in the world.

2. Determine the natural processes driving the response of a large-scale sandy intervention

The anticipated increase in global nourishment volumes and size and the request for more complex nourishment shapes requires adequate predictions of the morphodynamic evolution of such sandy interventions. Yet, the primary drivers that control this evolution and the skill of current state-of-the-art models for such projects are not known. A process-based model has been used to successfully hindcast the initial response of the Sand Engine mega-nourishment in The Netherlands.

Analysis of the model results indicates that the erosional behaviour of the Sand Engine has a linear dependency on the cumulative wave energy of individual high-energy wave events, with the duration of a storm event being more dominant than the maximum wave height occurring during the storm. Wave directions during the events appear to be irrelevant for the aggregated erosional behavior of the nourishment. The integrated erosion volume due to the 12 events with the highest cumulative wave energy events sums up to approximately 60% of the total eroded volume of the peninsula after one year. The less energetic storm events, with a higher probability of occurrence, are hence equally important for the initial response of the Sand Engine.

The relative contributions of the different environmental forcings to the total erosional behavior of the nourishment are studied using the verified model. The model results show that wave forcing dominated the initial morphological response of the Sand Engine, accounting for approximately 75% of the total erosion volume after the first year. The vertical tide is the second most contributing factor accounting for

nearly 17% of the total erosion volume, with horizontal tide, surge and wind-driven currents playing only a very minor role.

3. *Evaluate the performance of morphodynamic acceleration techniques on the predicted evolution at multiple time scales*

The design and acceptance of a sandy strategy as an erosion mitigating measure requires information on the predicted morphodynamics, both on the short and longer term. This study used the Sand Engine as a case study to evaluate the performance of different morphological acceleration techniques in predicting both short-medium term (1-5 yrs) and long-term (20-30 yrs) morphodynamic evolution. A Delft3D model of the Sand Engine, calibrated with first year bathymetric measurements, is shown to be able to reproduce the observed morphological changes in the first five years. The observations and model predictions for the first five years after implementation of the Sand Engine are used to evaluate six acceleration techniques: three based on brute force (real-time) time series and three based on representative (schematized) wave conditions.

Results show that acceleration techniques using representative (schematized) wave conditions are not capable of accurately reproducing the morphological response in the first two years. The optimal reproduction of the morphological behavior of the first five years is obtained by the brute force simulations.

In the longer term, the importance of gross transports over net transports diminishes. Generally, the erosional behavior is captured well in all considered techniques with variations in volumes of about 1 million m^3 after three decades. However, the predicted details in alongshore and cross-shore distribution of the morphological evolution as well as the spit development have a strong dependency on the selected acceleration technique. The decadal predictions show a reduction of longshore sediment transport gradients over time and a distinct remaining signature of the Sand Engine after three decades.

A newly proposed 'brute force merged' technique, which incorporates the full variability of the wave directions and wave heights in the wave climate, provides an attractive and flexible method providing a combination of phenomenological accuracy and computational efficiency (factor 20 faster than the benchmark brute force technique) at both the short-medium and long time scales.

4. Develop and validate a seamlessly integrated morphodynamic model for the subaqueous and subaerial domains

Sandy interventions are often implemented with the objective to stimulate the natural growth of the dunes. So far, the predicted growth of dune area is generally derived using empirical relations and not through process-based modelling. Measurements at the Sand Engine after four years show a large difference (factor five) between the forecasted growth of the dune area (25 ha in 20 years) and the actual observed new dune area (1 ha in 4 years). This implies that a more advanced method is needed to predict dune growth in the vicinity of coastal nourishments.

Measurements after five years show that a large volume of 400,000 m^3 of sand has been blown into the dunes, lake and lagoon, which confirms the relevance of the aeolian transports in the morphological behavior of the Sand Engine. From a sediment budget analysis of the Sand Engine it can be concluded that 58% of all sediments deposited in the dunes originate from the low lying beach zone that is regularly reworked by waves. For these reasons a model is needed that takes the interaction between both the aeolian and hydrodynamic and morphodynamic processes into account.

A seamless integration of two morphodynamic models (being Delft3D Flexible Mesh (FM) and AeoLiS) has been developed and applied to the Sand Engine. The integrated morphodynamic simulation is well capable of reproducing the observed changes between 2011 and 2016 for both the subaqueous and subaerial domain; a BSS of 0.8 is obtained, which is judged as 'excellent' (according to Sutherland et al. (2004a)) and higher than the (non-coupled) Delft3D prediction.

Regarding dune growth, the simulated results of the integrated model compare well with the measured dune growth between 2012 - 2015; the measured yearly-averaged dune growth rates vary between 14 - 19 $m^3/m/yr$, while the simulated yearly-averaged dune growth rate is 18 $m^3/m/yr$.

The results for the Sand Engine case show that the seamlessly coupled FM and AeoLiS can efficiently and realistically resolve the interactions between the subaqueous and dry beach morphodynamic evolution. Providing frequent point-based information on the waves, water levels and, in particular, the subaqueous bed levels to the AeoLiS simulation results in realistic dune growth rates; both in magnitude, spatial and interannual variations. Incorporating these processes is paramount not only for realistic predictions of coastal dune development but also for the longer term morphological behavior of the subaqueous domain.

6.2 SYNTHESIS

Chapters 2 to 5 have discussed new advances in earth observation and coastal modelling that enable us to study the dynamics of sandy beaches in the past, present and future worldwide. Analyses of satellite-derived shorelines reveal that more than half of all sandy beaches are subject to chronic changes with rates exceeding 0.5 m per year. The remaining beaches, with limited long-term changes, still experience changes in a dynamic equilibrium at shorter time scales. This stresses the importance of obtaining insight in the dynamics of a certain coast before designing and implementing coastal interventions. The global database on shoreline changes[1] provides basic details for every beach in the world.

Process-based models are increasingly applied to predict the impact of coastal interventions on the adjacent coast. Resolving the detailed temporal responses of the beach to variations in forcing conditions is essential for realistic impact predictions. Numerical modelling applied to the Sand Engine case demonstrated that it is key to resolve the variations in wave energy, at time scales from storms to seasons to multi-year, in order to provide realistic answers at all desired time scales. Schematizing wave climates to reduce computational times often introduces sub-optimal model outcome. Here, a new morphodynamic acceleration technique is presented as a very attractive alternative. It can fully resolve the gross transport components in both longshore and cross-shore direction; the latter being important in representing the depth of closure and in areas influenced by surges. This technique can easily be extended by a real-time storm, accompanied by storm related model features, maximizing the multi-timescale potential of this technique.

The improvement in morphodynamic modelling since 2008 and notably this thesis have resulted in an increase in skill of the predictions (see Fig. 6.1). Original forecasts in 2008 (see Fig. 6.1, second row) show a dispersal of sand to both sides of the Sand Engine, while overestimating the development of a spit on the northern side of the peninsula.

First year calibration improved the model results for 2016 significantly (Stive et al., 2013). The brute force merged technique improved the results further both quantitative and qualitative (see Fig 6.1 fourth row). The dynamics and dimensions of the lagoon are better reproduced. Incorporating aeolian transports has significantly improved the skill of the dry beach, dunes, dune lake and lagoon. Incorporating these processes is paramount not only for realistic predictions of coastal dune development but also for the longer term morphological behavior of the subaqueous domain. An important, first step has been made in

1 shorelinemonitor.deltares.nl

developing a coastal landscaping model that is relevant for the research community as well as for applied research and consultancy.

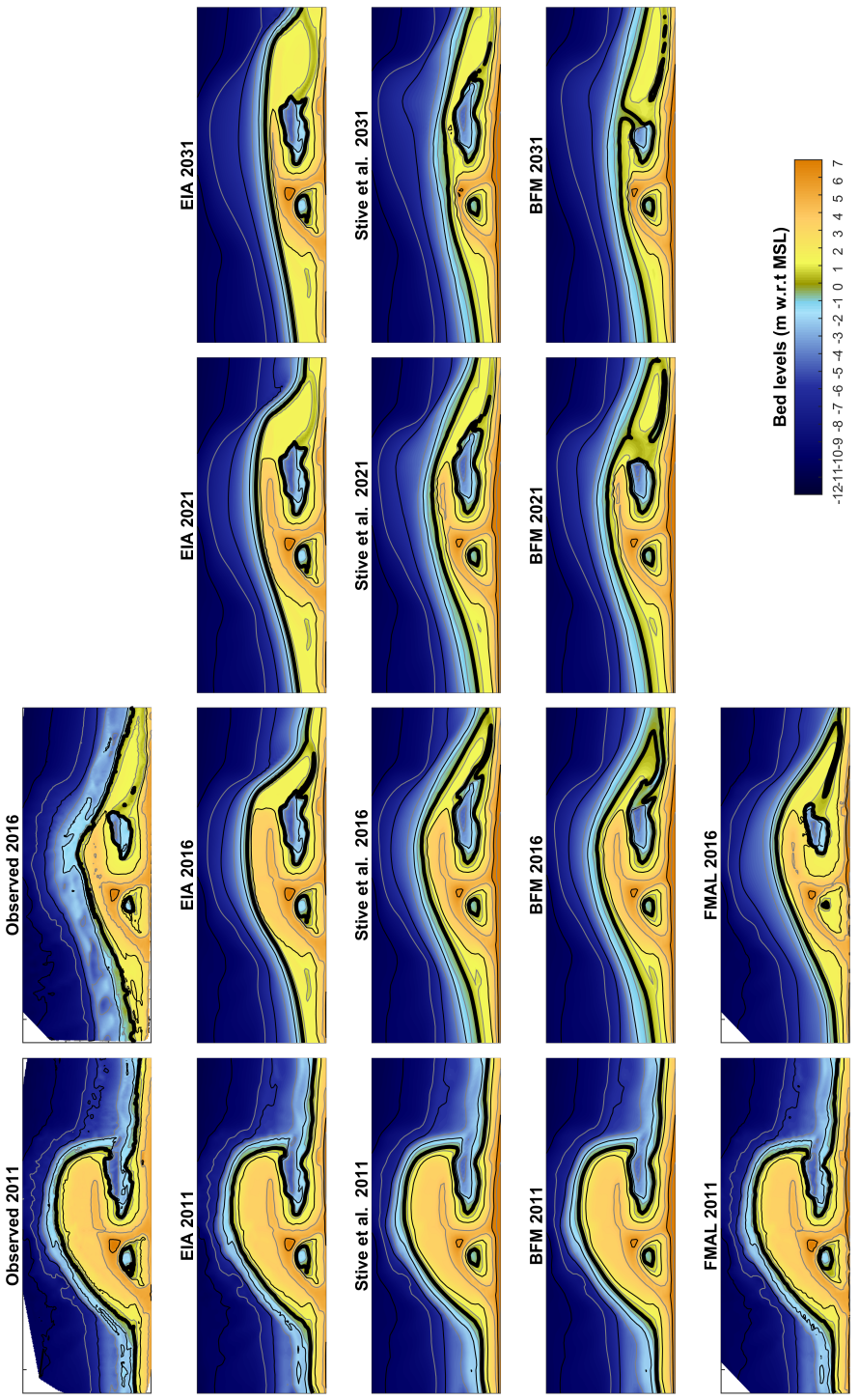

Figure 6.1: Advances in multi-scale morphodynamic predictions of the Sand Engine. The four columns represent the years 2011, 2016, 2021 and 2031. The first row shows the observed bed levels, while the subsequent rows show the predicted bed levels presented in EIA (Tonnon et al., 2009), Stive et al., 2013, BFM (Chapter 4), and the seamless model (Chapter 5), resp.

6.3 OUTLOOK

6.3.1 *Earth Observation*

In the near future, great potential for remote sensing techniques and big data analysis in operational monitoring of the world's coast and beaches is foreseen. The global sandy shoreline change analysis presented in this thesis is primarily based on Landsat imagery with 30 m resolution and a revisit time of 16 days.

In recent years new satellites (Sentinel-2a,b) have been launched, that will significantly enrich the satellite imagery data both in temporal (revisit time of a few days) and spatial resolution (<10 m). Furthermore, the development of small, low-cost earth observation satellites has resulted in the creation of constellations of satellites that can now capture the entire Earth's surface at a high frequency and resolution. At present, private institutions already provide satellite images at approx. 1 m resolution with a daily revisit and global coverage. Arrays of satellites can nowadays also provide short movies showing the dynamics on time scales of seconds and minutes at a coastal area; e.g. real-time waves propagating to shore. This exponential increase in resources will demand more emphasis on big data statistics in the near future to closely and better monitor how the planet is changing.

High-frequent and high-resolution satellite-derived shorelines require concurrent information on the water levels at the moment the image is captured from space to maximally exploit the images. This demands operational information on the total water levels, consisting of tides, surges and wave setup, across the globe. An operational global tide and surge model, like GLOSSIS, and an operational wave model, like WaveWatch III can provide the total water levels along the world's coastline. Using information from global models can truly utilize the Earth Observation data to its fullest potential.

6.3.2 *Seamless modelling*

Where Chapter 4 discussed the morphodynamic acceleration techniques, Chapter 5 presented the results of the seamlessly coupled morphodynamic model integrating the subaqueous and subaerial domains. A combination, in which the integrated model is forced with the 'brute force merged' approach, is a promising next step.

Consequently, extending the new 'brute force merged' technique by the incorporation storms becomes interesting. The storm condition may be resolved by Delft3D Flexible Mesh with unique model settings appropriate for extreme conditions, such as long wave effects, slumping of dry beach or dunes, etc. The storm condition may be forced with a realistic storm time series of wave heights, periods, direction and

surge levels. This condition is then computed on a separate node parallel to the other nodes computing the 'normal' conditions following the mormerge approach. Applying a time-varying morfac for each of the node simulations allows for a seamless simulation whereby the 'normal' wave time series are alternated with an episodic extreme storm condition. The above satisfies the increasing demand for studying the impact of an extreme storm on the decadal evolution of such sandy interventions.

The next step would be to extend the BFM technique, by including extreme events to the integrated model framework, to obtain a seamlessly coupled morphodynamic model covering time scales from storms to decades and both the subaqueous and subaerial domains.

The ultimate goal would be to make ensemble (e.g. Monte Carlo) predictions with the integrated model, forced with BFM including extreme events, for estimating the uncertainty in future evolution of (complex) sandy developments and NBS.

Part IV

APPENDIX

A

VALIDATION OF SAND DETECTION

To validate the sand detection method we followed the guidelines by Richards who recommends the use of 50 validation locations per class. These locations were selected independently from the training data set and were randomly spread over the world. Figures A.1 - A.6 show a subset of 39 sites at which validation was done via visual inspection. The yellow-colored areas on each satellite image are the 'sandy' pixels that the supervised classification method identified as 'sandy' areas.

For the 'sand' class, visual inspection of the 50 validation locations resulted in 96% accuracy. Only two sites were only partly identified as sand, although visually recognized as a fully sand beach: the white sandy Whitehaven Beach in Australia (see Fig. A.4d) and part of the sandy Ras Ghurab Island in Abu Dhabi (see Fig. A.3a).

Figure A.1: Satellite images for six selected sites in North-America and Caribbean: areas detected as 'sandy' are highlighted in yellow.

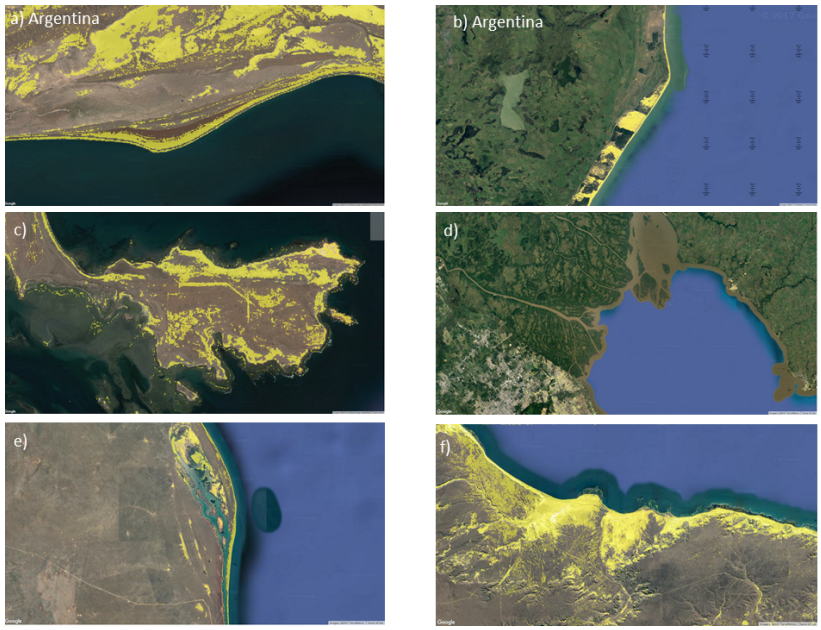

Figure A.2: Satellite images for six selected sites in South-America: areas detected as 'sandy' are highlighted in yellow.

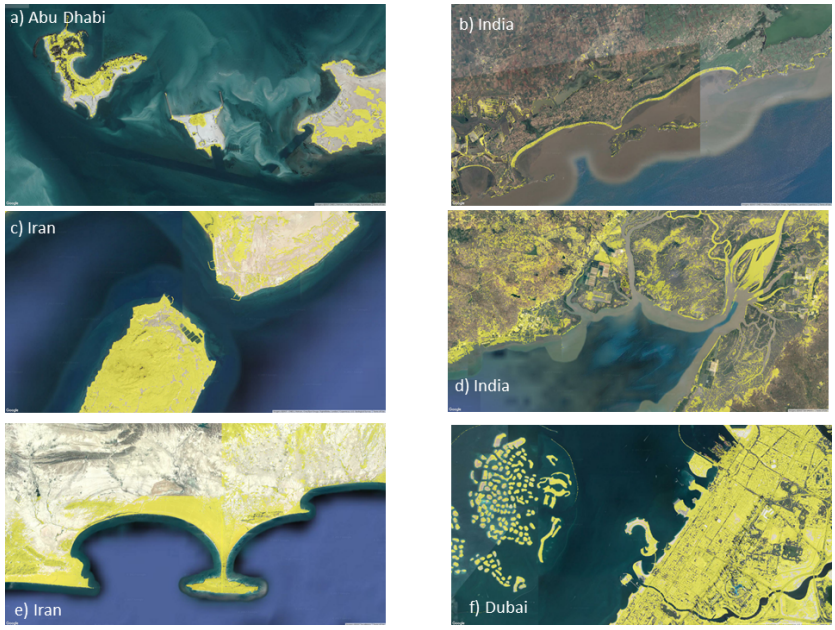

Figure A.3: Satellite images for six selected sites in the Middle East: areas detected as 'sandy' are highlighted in yellow.

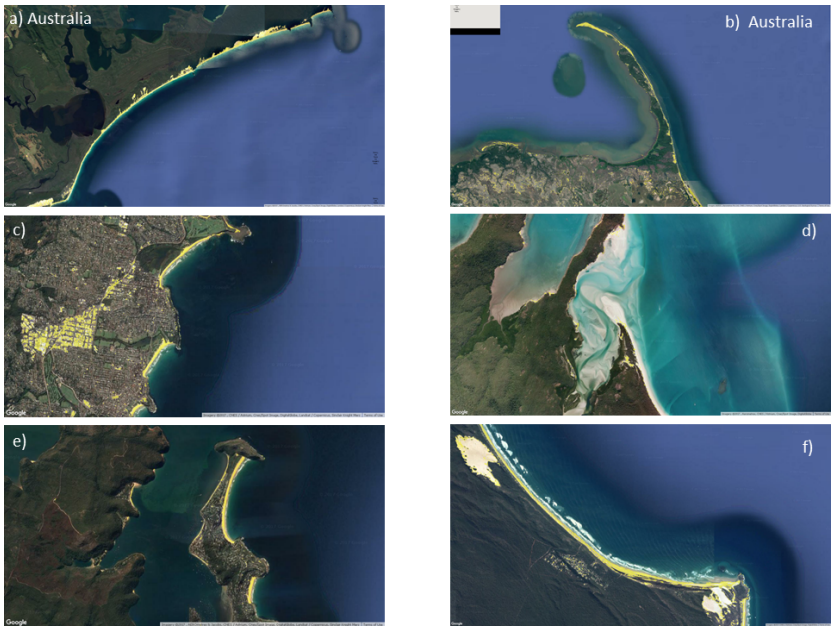

Figure A.4: Satellite images for six selected sites in Australia: areas detected as 'sandy' are highlighted in yellow.

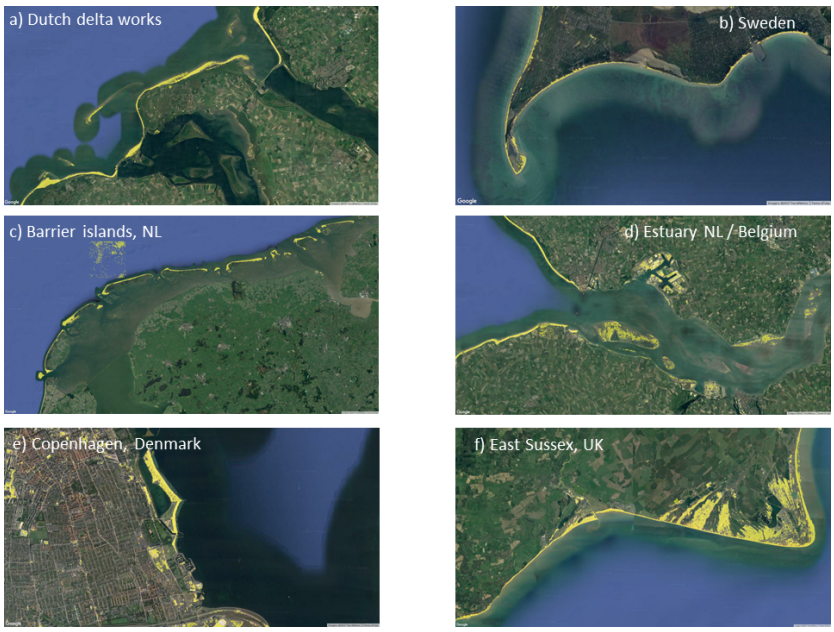

Figure A.5: Satellite images for six selected sites in Europe: areas detected as 'sandy' are highlighted in yellow.

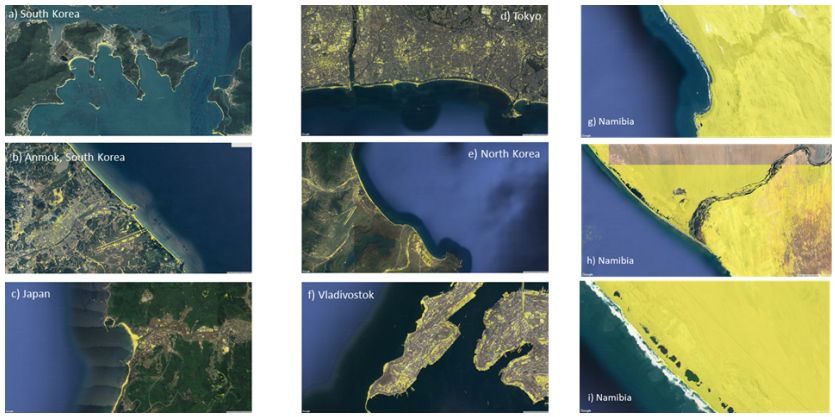

Figure A.6: Satellite images for nine selected sites in South-East Asia and Africa (Namibia): areas detected as 'sandy' are highlighted in yellow.

B

VALIDATION OF SHORELINE DETECTION

Four sites are used to validate and evaluate the shoreline detected method covering different tidal ranges and analysis periods (see Table B.1). For the Narrabeen (Australia) and Sand Engine (The Netherlands) sites, shoreline change analysis is conducted for five and 50 profiles, respectively. For Long Beach and Hatteras Island (both in the USA) we have also analysed the alongshore variability of the shoreline change trend rates covering periods of 18 and 13 years, respectively. In total, more than 3,600 surveyed shoreline positions are considered in the validation and positional accuracy quantification.

The positional accuracy at the four sites is quantified by directly comparing surveyed shoreline positions with the concurrent position of the satellite derived shorelines (SDS). For each site, the local coordinate system of survey transects were adopted. Fig. B.1 shows the resulting correlation between surveyed shorelines and SDS positions. The position of the SDS correlates well with surveyed shorelines as indicated by correlation coefficients ranging from 0.85 to 0.99 at the four sites (see Table B.1). The average of the offset values of three of four sites is 2.3 m and associated RMSE values range from half a pixel (0.5) to one pixel (1.1), which are comparable with findings of recent studies at micro tidal beaches (Hagenaars et al., 2017; Pardo-Pascual et al., 2012). Only in case of Long Beach, despite a high correlation (R2 of 0.98), a relatively large seaward mean offset was found (-35.2 m). This is attributed to the persistent presence of wave-induced foam due to breaking of swell waves along this highly energetic coastline as discussed in Section 2.3. Due to its persistency, the wave-induced foam effect on detected shorelines is however likely to be limited where long-term shoreline change rates at such sites are concerned. The relatively large RMSE value (50.5 m) is most probably related to the large tidal range; yet this needs to be further verified with additional in-situ surveyed shorelines. The high correlation (R2 of 0.98) found between surveyed shoreline and SDS positions at Long Beach, demonstrates that the shoreline data is still relevant to long-term shoreline change analysis.

Table B.1: Characteristics of validation data sets and error statistics.

Validation site	# of shoreline positions, # of transects, and spatial coverage	Analysis period (years)	Tidal range (m)	Mean offset (m)	RMSE (m)	R^2
1. Hatteras Island, USA	1234 shoreline positions 200 transects over ~60 km	13 (1989-2002)	1.7	-2.0	17.4	0.85
2. Narrabeen, Australia	1043 shoreline positions 5 transects over 3 km	29 (1986-2016)	1.9	1.1	13.7	0.88
3. Sand Engine, The Netherlands	485 shoreline positions 55 transects over ~10 km	4 (2011-2016)	2.0	-4.0	33.4	0.99
4. Long Beach, WA, USA	918 shoreline positions 17 transects over ~44 km	18 (1997-2015)	3.6	-35.2	50.5*	0.98

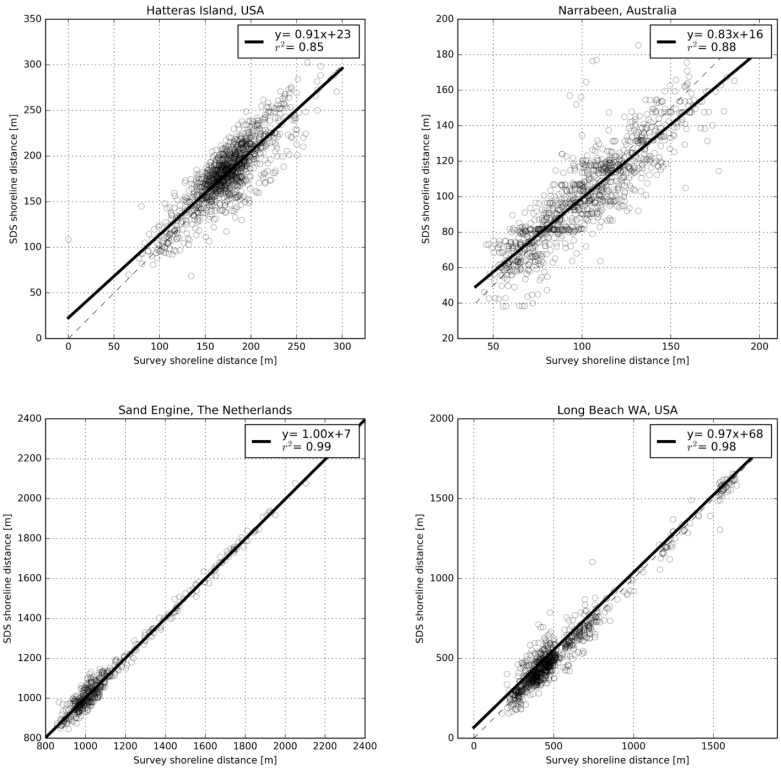

Figure B.1: Correlation between the surveyed shorelines and the SDS shorelines for the four validation sites. The linear regression fit is plotted in black, while the 1:1 line is plotted as a dashed grey line.

Below we present and describe time series of shoreline positions for three validation sites (Hatteras Island is already discussed in the manuscript).

B.1 VALIDATION CASE 2: NARRABEEN, AUSTRALIA

Beach profiles have been measured at approximately monthly intervals from 1976 to date at Narrabeen-Collaroy beach, Sydney, Australia (Turner et al., 2016). This is one of just a handful of sites worldwide where ongoing and uninterrupted beach monitoring now spans multiple decades. Monthly cross-shore beach profile surveys at five locations along the beach are here used as ground truth data to assess the accuracy of the shoreline detection method. For the period 1984 till 2016 we collated 397 cloud-free satellite images and determined the shoreline position at the PF1 profile. The variation in shoreline positions over the three decades is approx. 90 m; i.e. equivalent to three pixels. Yet, the SDS data shows remarkable resemblance with the in-situ measured variation in shoreline positions (see Fig. B.2), which is in line with the findings of **Liu2017**. The linear regression trend calculated from the SDS is identical to the observed shoreline change rates. This validation case highlights the capabilities in detecting shoreline changes at subpixel level.

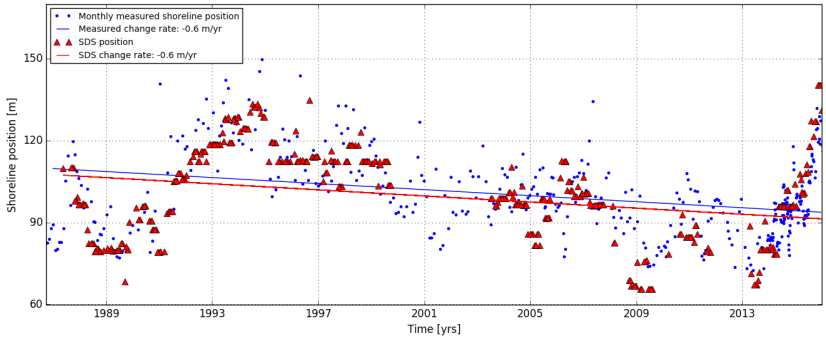

Figure B.2: In-situ measured and satellite-derived shoreline positions between 1987 and 2016 for profile PF1 (northern profile) at Narrabeen, Australia.

B.2 VALIDATION CASE 3: THE SAND ENGINE, THE NETHERLANDS

To assess the accuracy of the satellite derived shoreline from the satellite images the SDS should ideally be compared with a shoreline derived from in-situ measurements taken on the same day. This minimizes the effect of morphological changes on the coastline comparison. High-frequency bathymetric surveys available from a large-scale beach nourishment near The Hague, The Netherlands, enabled such a direct comparison of shorelines derived from in-situ measurements and a high-resolution SPOT satellite image on the same clear sky day (in July 2015). After tidal correction, the comparison revealed a highly accurate

SDS position with a spatial mean offset of 1.0 m (Hagenaars et al., 2017).

Monthly surveys are available after completion of the large-scale nourishment in 2011. Comparisons have been made for a series of transects of which two are presented below (see Fig. B.3). The behaviour of the shoreline changes is represented well by the SDS data, making it an attractive alternative for monitoring the shoreline evolution of such sandy interventions.

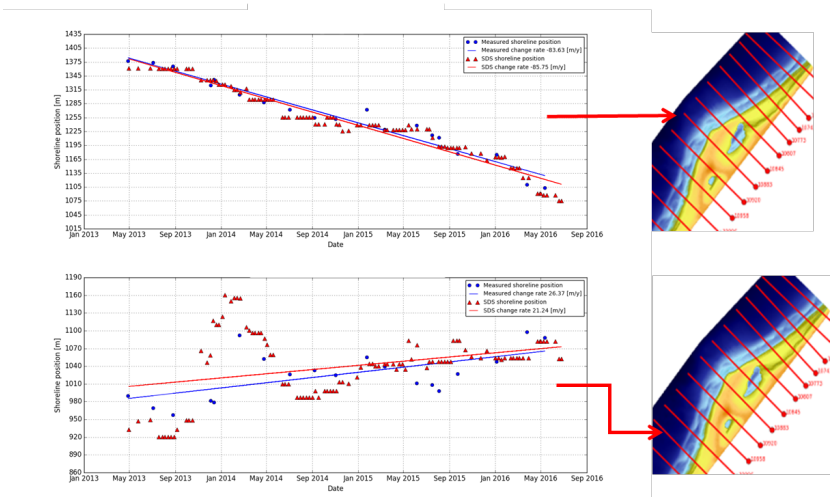

Figure B.3: In-situ measured and satellite-derived shoreline positions between 2013 and 2017 for two transects at the Sand Engine, The Netherlands.

B.3 VALIDATION CASE 4: LONG BEACH, WA, USA

The Long Beach sub-cell stretches 44 km between the north jetty of the Columbia River and Leadbetter Point at the tip of Long Beach Peninsula (see Fig. B.4). The initial shoreline response due to construction of the Columbia River North Jetty (1885–1913) was rapid and was confined to the development of a pocket beach between the jetty and North Head. Over the long term (1870s – 2002), the average shoreline change rate along Long Beach was 2.6 m/yr, with rates ranging from -12.1 to 10.3 m/yr (Ruggiero et al., 2013a). Seasonal profile measurements are available at various locations in the Long Beach sub-cell. These measurements are used to compare with the SDS positions between 1997 and 2016. The in-situ data indicates that the shoreline behaviour at two example locations shows significant temporal variation around a mean accretion trend. The SDS data also captures these temporal fluctuations.

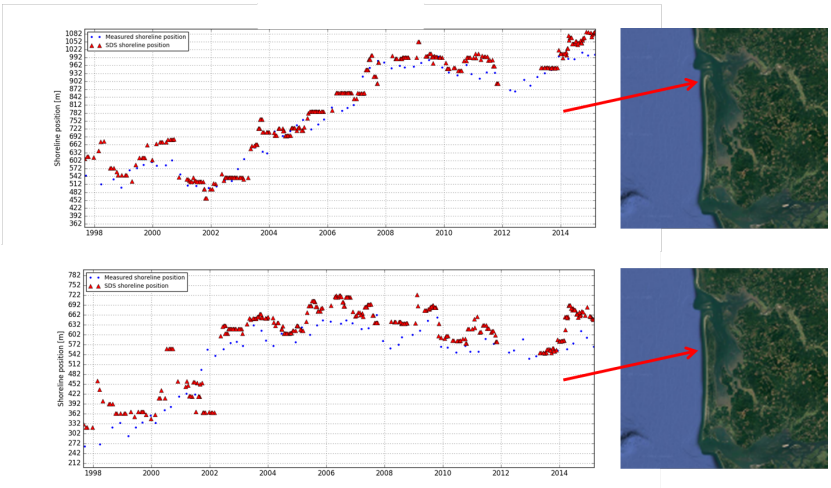

Figure B.4: In-situ measured and satellite-derived shoreline positions between 1997 and 2016 for two locations at Long Beach in Washington, USA.

Linear regression is performed on the SDS data between 1997 and 2016 for each transect in the sub-cell. A similar regression approach was applied by Ruggiero (Ruggiero et al., 2013b). The resulting trends of shoreline change rate at all transects are shown in alongshore direction in Fig. B.5 for both the in-situ measurements as well as the SDS data. The alongshore distribution based on the SDS is comparable with the alongshore graph reported by Ruggiero (Ruggiero et al., 2013a).

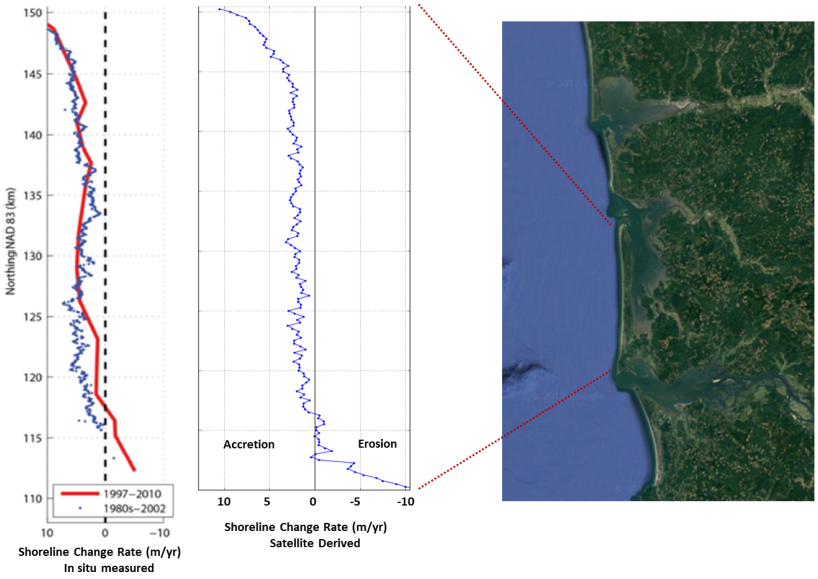

Figure B.5: Alongshore distribution of shoreline change rates along the Long Beach sub-cell in Washington, USA. Shoreline change rates are derived from in-situ measurements (panel at the left; from Ruggiero et al., 2013a) and SDS (panel in the middle) for the period 1997 - 2016.

C

DELFT3D FLEXIBLE MESH

Delft3D Flexible Mesh (FM) is used for the hydrodynamic processes. FM solves the two-dimensional shallow water equations for depth averaged velocities, hydrostatic pressures and an incompressible fluid that are derived from the Navier stokes equations. This results in the mass conservation (equation (C.1)), conservation of momentum in x direction (equation (C.2)) and conservation of momentum in y direction (equation (C.3)). The momentum equation of the vertical reduces to the hydrostatic pressure relation.

$$\frac{\partial h}{\partial t} + \frac{\partial Uh}{\partial x} + \frac{\partial Vh}{\partial y} = Q \tag{C.1}$$

$$\frac{\partial u}{\partial t} + u\frac{\partial u}{\partial x} + v\frac{\partial u}{\partial y} + w\frac{\partial u}{\partial z} - fv = -\frac{1}{\rho_0}\frac{\partial P}{\partial x} + F_x + \frac{\partial}{\partial z}\left(\nu_v \frac{\partial u}{\partial z}\right) + M_x \tag{C.2}$$

$$\frac{\partial v}{\partial t} + u\frac{\partial v}{\partial x} + v\frac{\partial v}{\partial y} + w\frac{\partial v}{\partial z} - fu = -\frac{1}{\rho_0}\frac{\partial P}{\partial y} + F_y + \frac{\partial}{\partial z}\left(\nu_v \frac{\partial v}{\partial z}\right) + M_y \tag{C.3}$$

where:

U	Depth averaged velocity in x direction
V	Depth averaged velocity in y direction
h	water depth
u	velocity in x direction
v	velocity in y direction
w	velocity in z direction
Q	Sink or source term (discharge or withdrawal of water, precipitation and evaporation)
fu, fv	Coriolis forces

F_x, F_y	horizontal Reynolds stresses
ν_v	Vertical eddy viscosity coefficient
M_x, M_y	Contributions due to external sources or sinks of momentum (external forces by hydraulic structures, discharge or withdrawal of water, wave stresses, etc.).
$\frac{\partial P}{\partial y}$, $\frac{\partial P}{\partial x}$	Pressure gradients

For simulating the morphodynamic changes the transport formulations of Van Rijn (1993) are used for calculating the suspended and bed load sediment transports. The numerical implementation is undertaken by means of the finite volume solver, where the continuity equation is solved implicitly in time and the advection term in the momentum equation explicitly in time. This results in an automatically chosen time step that complies with the CFL criteria. More detailed explanation of the implemented processes and numerical aspects can be found in the FM manual (Deltares, 2018). To summarise, the FM model takes the following processes into account:

- Free surface gradients
- The effect of the Earth rotation
- Tidal forcing at the open boundaries
- Space and time varying wind shear-stress at the water surface
- Space varying shear-stress at the bed
- Tide generating forces
- Influence of waves on the bed shear-stress
- Wave induced stresses (radiation stress) and mass fluxes
- Wind driven flows

Beta versions of FM are available that resolve the long wave phenomena, which will allow to simulate storm erosion in FM. Specific storm erosion features from XBeach have also been implemented in FM.

BIBLIOGRAPHY

Ali, E and I A El-Magd (2016). "Impact of human interventions and coastal processes along the Nile Delta coast, Egypt during the past twenty-five years." In: *The Egyptian Journal of Aquatic Research* 42.

Anthony, E. J. et al. (2015). "Linking rapid erosion of the Mekong River delta to human activities." In: *Sci. Rep* 5, p. 14745. DOI: 10.1038/srep14745.

Arriaga, J, J Rutten, F Ribas, A Falques, and G Ruessink (2017). "Modeling the long-term diffusion and feeding capability of a mega-nourishment." In: *Coastal Engineering* 121, pp. 1 –13. ISSN: 0378-3839. DOI: https://doi.org/10.1016/j.coastaleng.2016.11.011. URL: http://www.sciencedirect.com/science/article/pii/S0378383916303659.

Bascom, W. (1980). "Waves and beaches." In: *Anchor Press/Darbleday, New York* 366.

Battjes, J A and J P F M Janssen (1978). "Energy loss and set-up due to breaking of random waves." In: *16th International Conference on Coastal Engineering*. Vol. 1. 16. ASCE. Hamburg, Germany, pp. 570–587. URL: http://repository.tudelft.nl/view/ir/uuid:2fba43fe-f8bd-42ac-85ee-848312d2e27e/.

Bayram, B., U. Acar, D. Seker, and A. A Ari (2008). "Novel Algorithm for Coastline Fitting through a Case Study over the Bosphorus." In: *Journal of Coastal Research* 244, pp. 983–991. DOI: 10.2112/07-0825.1.

Belward, A S and J O Skøien (2015). "Who launched what, when and why; trends in global land-cover observation capacity from civilian earth observation satellites." In: *ISPRS Journal of Photogrammetry and Remote Sensing* 103. Global Land Cover Mapping and Monitoring, pp. 115 –128. ISSN: 0924-2716. DOI: https://doi.org/10.1016/j.isprsjprs.2014.03.009. URL: http://www.sciencedirect.com/science/article/pii/S0924271614000720.

Benedet, L., J.P.F. Dobrochinski, D.J.R. Walstra, A.H.F. Klein, and R. Ranasinghe (2016). "A morphological modeling study to compare different methods of wave climate schematization and evaluate strategies to reduce erosion losses from a beach nourishment project." In: *Coastal Engineering* 112, pp. 69 –86. ISSN: 0378-3839. DOI: https://doi.org/10.1016/j.coastaleng.2016.02.005. URL: http://www.sciencedirect.com/science/article/pii/S0378383916300205.

Berg, N Van den (2012). "Modelling the dynamics of large scale shoreline sand waves." PhD thesis. Barcelona, Spain: Universitat Politecnica de Catalunya.

Bird, E. C. F. (1985). *Coastline changes; A Global Review*. Chichester: Wiley.

Bird, E. C. F. (1996). *Beach management*. Chichester: John Wiley & Sons.

Bird, E. C. F. (2008). *Coastal geomorphology: an introduction*. Chichester: Wiley.

Booij, N, R C Ris, and L H Holthuijsen (1999). "A third-generation wave model for coastal regions 1. Model description and validation." In: *Journal Of Geophysical Research* 104.C4, p. 17.

Bosboom, J, A J H M Reniers, and A P Luijendijk (2014). "On the perception of morphodynamic model skill." In: *Coastal Engineering* 94.

Boyd, R., R. W. Dalrymple, and B. A. Zaitlin (1992). "Classification of clastic coastal depositional environments." In: *Sedimentary Geology* 80, pp. 139–150.

Brown, Andrew, Sean Milton, Mike Cullen, Brian Golding, John Mitchell, and Ann Shelly (2012). "Unified Modeling and Prediction of Weather and Climate: A 25-Year Journey." In: *Bulletin of the American Meteorological Society* 93.12, pp. 1865–1877. DOI: 10.1175/BAMS-D-12-00018.1. eprint: https://doi.org/10.1175/BAMS-D-12-00018.1. URL: https://doi.org/10.1175/BAMS-D-12-00018.1.

Brown, Jennifer M., Jack J.C. Phelps, Andrew Barkwith, Martin D. Hurst, Michael A. Ellis, and Andrew J. Plater (2016). "The effectiveness of beach mega-nourishment, assessed over three management epochs." In: *Journal of Environmental Management* 184, pp. 400 –408. ISSN: 0301-4797. DOI: https://doi.org/10.1016/j.jenvman.2016.09.090. URL: http://www.sciencedirect.com/science/article/pii/S0301479716307708.

Burke, L. et al. (2001). *Pilot analysis of global ecosystems: Coastal Ecosystems*. World Resources Institute.

CIA (2016). *World Factbook: Coastline*. United States Central Intelligence Agency. URL: https://www.cia.gov/library/publications/the-world-factbook/fields/2060.html.

Carraro, Francesco, Davide Vanzo, Valerio Caleffi, Alessandro Valiani, and Annunziato Siviglia (May 2018). "Mathematical study of linear morphodynamic acceleration and derivation of the MASSPEED approach." In: *Advances in Water Resources* 117. DOI: 10.1016/j.advwatres.2018.05.002.

Center, Heinz (2000). *Evaluation of erosion hazards*. Washington,D.C: The H. John Heinz III Center for Science Economics and the Environment.

Cohn, Nicholas, Bas M. Hoonhout, Evan B. Goldstein, Sierd De Vries, Laura J. Moore, Orencio Durán Vinent, and Peter Ruggiero (2019). "Exploring Marine and Aeolian Controls on Coastal Foredune Growth Using a Coupled Numerical Model." In: *Journal of Marine Science and Engineering* 7.1. ISSN: 2077-1312. DOI: 10.3390/jmse7010013. URL: http://www.mdpi.com/2077-1312/7/1/13.

Crowell, M., S. P. Leatherman, and M. K. Buckley (1993). "Shoreline Change Rate Analysis: Long Term Versus Short Term Data." In: *Shore and Beach*, pp. 13–20.

Davies, J. L. A (1964). "Morphogenic approach to world shorelines." In: *Zeitschrift for Geomorphologie* 8, pp. 1–42.

Davies, R. A. and M. O. Hayes (1984). "What is a wave dominated coast?" In: *Marine geology* 60, pp. 313–329.

De Schipper, M A, S de Vries, B G Ruessink, R C de Zeeuw, J Rutten, C van Gelder-Maas, and M J F Stive (2016). "Initial spreading of a mega feeder nourishment: observations of the Sand Engine pilot project." In: *Coastal Engineering*. submitted to Coastal Engineering in July 2015.

De Sonneville, B and A Van der Spek (2012). "Sediment- and morphodynamics of shoreface nourishments along the north-holland COAST." In: *Coastal Engineering Proceedings*.

De Vriend, H, M van Koningsveld, S G J Aarninkhof, M B de Vries, and M J Baptist (2015). "Sustainable hydraulic engineering through building with nature." In: *Journal of Hydro-environment Research* 9.2. Special Issue on Environmental Hydraulics, pp. 159 –171. ISSN: 1570-6443. DOI: https://doi.org/10.1016/j.jher.2014.06.004. URL: http://www.sciencedirect.com/science/article/pii/S1570644314000653.

De Vriend, HJ (2013). "Building with Nature: towards sustainable hydraulic engineering." In: *Proceedings 2013 IAHR World Congress, Chengdu, China*.

De Vries, S, H N Southgate, W Kanning, and R Ranasinghe (2012). "Dune behavior and aeolian transport on decadal timescales." In: *Coastal Engineering* 67, pp. 41–53. DOI: 10.1016/j.coastaleng.2012.04.002.

De Vries, S, S M Arens, M A de Schipper, and R Ranasinghe (2014). "Aeolian sediment transport on a beach with a varying sediment supply." In: *Aeolian Research* 15. DOI: 10.1016/j.aeolia.2014.08.001.

Dean, R G and R A Dalrymple (1991). *Water Wave Mechanics for Engineers and Scientists*. World Scientific Press: Singapore.

Deltares (2018). *D-Flow Flexible Mesh User Manual - DRAFT. Version: 1.2.1. Revision: 54829*.

Dhastgheib, A. (2012). "Long-term process-based morphological modelling of large tidal basins." PhD thesis. Delft, The Netherlands: IHE Delft.

Dissanayake, Pushpa, Jennifer Brown, Paul Wisse, and Harshinie Karunarathna (2015). "Comparison of storm cluster vs isolated event impacts on beach/dune morphodynamics." In: *Estuarine, Coastal and Shelf Science* 164, pp. 301 –312. ISSN: 0272-7714. DOI: https://doi.org/10.1016/j.

ecss.2015.07.040. URL: http://www.sciencedirect.com/science/article/pii/S0272771415300470.

Donchyts, G. et al. (2016). "Earth's surface water change over the past 30 years." In: *Nature Climate Change* 6, pp. 810–813.

Dyson, A., S. Victory, and T. Connor (2001). "Sand bypassing the Tweed River Entrance: an overview. Proc." In: *Coasts and Ports Conference* 2001, pp. 310–315.

Elias, E. P. L., A. J. F. van der Spek, Z. B. Wang, and J. G. de Ronde (2012). "Morphodynamic development and sediment budget of the Dutch Wadden Sea over the last century." In: *Netherlands Journal of Geosciences* 91.

Elias, E.P.L. (2006). "Morphodynamics of Texel Inlet." PhD thesis. Delft, The Netherlands: Delft University of Technology, Faculty of Civil Engineering and Geosciences.

Elko, N A and P Wang (2007). "Immediate profile and planform evolution of a beach nourishment project with hurricane influences." In: *Coastal Eng. 54*.

Elmoustapha, A.O., F. Levoy, O. Monfort, and V.G. Koutitonsky (2007). "A Numerical Forecast of Shoreline Evolution after Harbour Construction in Nouakchott, Mauritania." In: *Journal of Coastal Research* 23, p. 6.

Esteves, L. S. and C. W. Finkl (1998). "The problem of critically eroded areas (CEA): An evaluation of Florida beaches." In: *Journal of Coastal Research, SI* 26, pp. 11–18.

Eurosion (2004). *Living with Coastal Erosion in Europe: Sediment and Space for Sustainability. Part-1 Major Findings and Policy Recommendations of the EUROSION Project. Guidelines for implementing local information systems dedicated to coastal erosion management.* Tech. rep. Service contract B4-3301/2001/329175/MAR/B3 "Coastal erosion – Evaluation of the need for action". Directorate General Environment, European Commission.

Finkl, C. W. (2004). "Coastal classification: systematic approaches to consider in the development of a comprehensive scheme." In: *J. Coastal research* 20, p. 166.

French, J. et al. (2016). "Conceptualising and mapping coupled estuary, coast and inner shelf sediment systems." In: *Geomorphology*. DOI: 10.1016/j.geomorph.2015.10.006.

Friedman, G. M. (1961). "Distinction between dune beach and river sands from their textural characteristics." In: *Journal of Sedimentary Petrology* 31, pp. 514–520.

Galgano, F. A., S. P. Leatherman, and B. C. Inlets Dominate U. S. Douglas (2004). "Inlets Dominate U.S. East Coast Shoreline Change." In: *Coastal Research*.

Garcia-Rubio, G., D. Huntley, and P. Russell (2015). "Evaluating shoreline identification using optical satellite images." In: *Marine Geology* 359, pp. 96–105. DOI: 10.1016/j.margeo.2014.11.002.

Geleynse, N, J E A Storms, D J R Walstra, Z B Jagers H R A Wang, and M J F Stive (2011). "Controls on river delta formation; insights from numerical modelling." In: *Earth and Planetary Science Letters* 302.1-2, pp. 217–226. ISSN: 0012-821X. DOI: 10.1016/j.epsl.2010.12.013. URL: http://www.sciencedirect.com/science/article/B6V61-51V8Y5X-4/2/4b8144f70c5770a74a156637c6273637.

Giri, C. et al. (2011). "Status and distribution of mangrove forests of the world using earth observation satellite data." In: *Global Ecology and Biogeography* 20.1, pp. 154–159. DOI: 10.1111/j.1466-8238.2010.00584.x. URL: https://onlinelibrary.wiley.com/doi/abs/10.1111/j.1466-8238.2010.00584.x.

Gorelick, N. et al. (2017). "Google Earth Engine: Planetary-scale geospatial analysis for everyone." In: *Remote Sensing of Environment* 202.

Grunnet, Nicholas M and B G Ruessink (2005). "Morphodynamic response of nearshore bars to a shoreface nourishment." In: *Coastal Engineering* 52.2, pp. 119–137.

Grunnet, Nicholas, Dirk-Jan Walstra, and Gerben Ruessink (Sept. 2004). "Process-based modelling of a shoreface nourishment." In: *Coastal Engineering* 51, pp. 581–607. DOI: 10.1016/j.coastaleng.2004.07.016.

Hagenaars, G., S. de Vries, A. P. Luijendijk, W. P. de Boer, and A. J. H. M. Reniers (2017). "On the accuracy of automated shoreline detection derived from satellite imagery: A case study of the Sand Motor mega-scale nourishment." In: *Coastal Engineering* 133.

Hallegate, S., C. Green, R. J. Nicholls, and J. Corfee-Morlot (2013). "Future flood losses in major coastal cities." In: *Nature Climate Change* 3, pp. 802–6.

Hansen, M. C. et al. (2013). "High-Resolution Global Maps of 21st-Century Forest Cover Change." In: *Science* 342, pp. 850–853.

Hapke, C. J. and R. E. Henderson (2015). *Quantification of Shoreline Change Along Hatteras Island, North Carolina-Oregon Inlet to Cape Hatteras, 1978-2002, and Associated Vector Shoreline Data*. Tech. rep. USGS.

Hapke, Cheryl J, Owen Brenner, Rachel E Henderson, and B J Reynolds (2013). *Coastal change from Hurricane Sandy and the 2012-13 winter storm season: Fire Island, New York*. English. Tech. rep. Reston, VA, p. 43. URL: http://pubs.er.usgs.gov/publication/ofr20131231.

Hayes, M. O. (1967). "Relationship between coastal climate and bottom sediment type on the inner continental shelf." In: *Marine Geology* 5, pp. 111–132.

Hayes, M. O. (1979). "Barrier island morphology as a function of wave and tide regime." In: *Barrier islands from the Gulf of St. Lawrence to the Gulf of Mexico*. New York: Academic Press.

Hendriks, A (2011). "The impact of re-surfacing groins on hydrodynamics and sediment transport at the Delfland coast." MA thesis. Civil Engineering, TU Delft.

Hinkel, Jochen et al. (2013). "A global analysis of erosion of sandy beaches and sea-level rise: An application of DIVA." In: *Global and Planetary Change* 111, pp. 150 –158. ISSN: 0921-8181. DOI: https://doi.org/10.1016/j.gloplacha.2013.09.002. URL: http://www.sciencedirect.com/science/article/pii/S0921818113002026.

Hoonhout, B and S de Vries (May 2017). "Aeolian sediment supply at a mega nourishment." In: *Coastal Engineering* 123, pp. 11–20. DOI: 10.1016/j.coastaleng.2017.03.001.

Hoonhout, Bas and Sierd de Vries (2019). "Simulating spatiotemporal aeolian sediment supply at a mega nourishment." In: *Coastal Engineering* 145, pp. 21 –35. ISSN: 0378-3839. DOI: https://doi.org/10.1016/j.coastaleng.2018.12.007. URL: http://www.sciencedirect.com/science/article/pii/S0378383918301637.

Hopkins, Julia, Steve Elgar, and Britt Raubenheimer (2018). "Storm Impact on Morphological Evolution of a Sandy Inlet." In: *Journal of Geophysical Research: Oceans* 123.8, pp. 5751–5762. DOI: 10.1029/2017JC013708.

Hsu (2006). *Evaluation of Delft3D Performance in Nearshore Flows.* Tech. rep. Ocean dynamics and prediction branch Oceanography Division. Naval Research Laboratory.

Huisman, B J A, E E Sirks, L Van der Valk, and D J R Walstra (2014). "Time and Spatial Variability of Sediment Gradings in the Surfzone of a Large Scale Nourishment." In: *Journal of Coastal Research* Special Issue No. 70, pp. 127–132.

IUCN, UNEP-WCMC & (2016). *Protected Planet Report 2016*. Tech. rep. UNEP-WCMC, IUCN: Cambridge UK, and Gland, Switzerland.

Inman, D. L. and C. E. Nordstrom (1971). "On the Tectonic and Morphologic Classification of Coasts." In: *The Journal of Geology* 79, p. 1.

Johansen, K., S. Phinn, and M. Taylor (2015). "Mapping woody vegetation clearing in Queensland, Australia from Landsat imagery using the Google Earth Engine." In: *Remote Sensing Applications: Society and Environment* 1, pp. 36–49.

Kamphuis, J. W. (1991). "Alongshore sediment transport rate." In: *Journal of Waterways, Port, Coastal and Ocean Engineering, ASCE,* 117 (6), pp. 624–641.

Karunarathna, Harshinie, Jennifer Brown, Antonia Chatzirodou, Pushpa Dissanayake, and Paul Wisse (2018). "Multi-timescale morphological modelling of a dune-fronted sandy beach." In: *Coastal Engineering* 136, pp. 161 –171. ISSN: 0378-3839. DOI: https://doi.org/10.1016/j.coastaleng.2018.03.005. URL: http://www.sciencedirect.com/science/article/pii/S0378383917300200.

Kernkamp, H W J, A van Dam, G S Stelling, and E D de Goede (2011). "Efficient scheme for the shallow water equations on unstructured grids with application to the Continental Shelf." In: *Ocean Dynamics*. DOI: DOI:10.1007/s10236-011-0423-6.

Komar, P D (1987). "Selective grain entrainment by a current from a bed of mixed sizes: a reanalysis." In: *Journal of Sedimentary Petrology* 57 (2), pp. 203–211.

Kuleli, T., A. Guneroglu, F. Karsli, and M. Dihkan (2011). "Automatic detection of shoreline change on coastal Ramsar wetlands of Turkey." In: *Ocean Engineering* 38, pp. 1141–1149. DOI: 10.1016/j.oceaneng.2011.05.006.

Larson, M, H Hanson, and N C Kraus (1997). "Analytical Solutions of One-Line Model for Shoreline Change near Coastal Structures." In: *Journal of Waterway, Port, Coastal and Ocean Engineering* 123, pp. 180–191.

Le Cozannet, Gonéri et al. (Jan. 2019). "Quantifying uncertainties of sandy shoreline change projections as sea level rises." In: *Scientific Reports* 9.1, p. 42. ISSN: 2045-2322. URL: https://doi.org/10.1038/s41598-018-37017-4.

Leatherman, S. P. (1983). "Shoreline Mapping: A Comparison Techniques." In: *Shore and Beach* 51.

Lesser, G R, J A Roelvink, J A T M van Kester, and G S Stelling (Aug. 2004). "Development and validation of a three-dimensional morphological model." In: 51.8-9, pp. 883–915. DOI: 10.1016/j.coastaleng.2004.07.014.

Lesser, G.L. (2009). "An Approach to Medium-term Coastal Morphological Modelling." PhD thesis. Delft, The Netherlands: IHE Delft and Delft University of Technology.

Li, L., J.E.A. Storms, and D.J.R. Walstra (2018). "On the upscaling of process-based models in deltaic applications." In: *Geomorphology* 304, pp. 201 –213. ISSN: 0169-555X. DOI: https://doi.org/10.1016/j.geomorph.2017.10.015. URL: http://www.sciencedirect.com/science/article/pii/S0169555X16311850.

Liu, Q, J C Trinder, and I L Turner (2017). "Automatic super-resolution shoreline change monitoring using Landsat archival data: a case study at Narrabeen, Collaroy Beach, Australia." In: *Journal of Applied Remote Sensing* 11, pp. 11 –11 –17. DOI: 10.1117/1.JRS.11.016036. URL: https://doi.org/10.1117/1.JRS.11.016036.

Luijendijk, A P and A van Oudenhoven (2019). *The Sand Motor: a Nature-based Response to Climate Change*.

Luijendijk, A P, B.J.A. Huisman, and M.A. De Schipper (2015). "Impact of a storm on the first year evolution of the Sand Engine." In: *Proceedings of the Coastal Sediments 2015 conference*.

Luijendijk, A.P., G. Hagenaars, R. Ranasinghe, F. Baart, G. Donchyts, and S.G.J. Aarninkhof (2018). "The State of the World's Beaches."

In: *Scientific Reports* 8. https://doi.org/10.1038/s41598-018-24630-6, pp. 2045–2322.

Luijendijk, A.P., M.A. de Schipper, and R. Ranasinghe (2019). "Morphodynamic Acceleration Techniques for Multi-Timescale Predictions of Complex Sandy Interventions." In: *Journal of Marine Science and Engineering* 7.3. ISSN: 2077-1312. DOI: 10.3390/jmse7030078. URL: http://www.mdpi.com/2077-1312/7/3/78.

Luijendijk, Arjen P., Roshanka Ranasinghe, Matthieu A. de Schipper, Bas A. Huisman, Cilia M. Swinkels, Dirk J.R. Walstra, and Marcel J.F. Stive (2017). "The initial morphological response of the Sand Engine: A process-based modelling study." English. In: *Coastal Engineering* 119.Complete, pp. 1–14. DOI: 10.1016/j.coastaleng.2016.09.005.

Malenovský, Zbyněk, Helmut Rott, Josef Cihlar, Michael E. Schaepman, Glenda García-Santos, Richard Fernandes, and Michael Berger (2012). "Sentinels for science: Potential of Sentinel-1, -2, and -3 missions for scientific observations of ocean, cryosphere, and land." In: *Remote Sensing of Environment* 120. The Sentinel Missions - New Opportunities for Science, pp. 91 –101. ISSN: 0034-4257. DOI: https://doi.org/10.1016/j.rse.2011.09.026. URL: http://www.sciencedirect.com/science/article/pii/S0034425712000648.

Martínez, M.L., A. Intralawan, G. Vázquez, O. Pérez-Maqueo, P. Sutton, and R. Landgrave (2007). "The coasts of our world: Ecological, economic and social importance." In: *Ecological Economics* 63.2. Ecological Economics of Coastal Disasters, pp. 254 –272. ISSN: 0921-8009. DOI: https://doi.org/10.1016/j.ecolecon.2006.10.022. URL: http://www.sciencedirect.com/science/article/pii/S0921800906005465.

Mil-Homens, J, R Ranasinghe, J S M van Thiel de Vries, and M J F Stive (2013). "Re-evaluation and improvement of three commonly used bulk longshore sediment transport formulas." In: *Coastal Engineering*.

Miller, J K, T Sun, H Li, J Stewart, C Genty, D Li, and C Lyttle (2008). "Direct Modeling of Reservoirs through Forward Process-based Models: Can We Get There?" In: *International Petroleum Technology Conference*.

Mol, A. C. S. (2007). *Schematization of boundary conditions for morphological simulations.* Tech. rep. WL | Delft Hydraulics.

Moore, L. J. (2000). "Shoreline mapping techniques." In: *J. Coastal Res.* 16.

Mulder, J P M and P K Tonnon (2010). "Sand Engine : Background and Design of a Mega-Nourishment Pilot in the Netherlands." In: *Proceedings of the International Conference on Coastal Engineering* 32.

Nahon, Alphonse, X Bertin, André Fortunato, and Anabela Oliveira (Jan. 2012). "Process-based 2DH morphodynamic modeling of tidal inlets: A comparison with empirical classifications and theories." In: *Marine Geology* 291-294, pp. 1–11. DOI: 10.1016/j.margeo.2011.10.001.

Nicholls, R. J. et al. (2007). "Coastal systems and low-lying areas." In: *Climate Change 2007: Impacts, Adaptation and Vulnerability. Contribution of Working Group II to the Fourth Assessment Report of the Intergovernmental Panel on Climate Change, M.L. Parry, O.F. Canziani, J.P. Palutikof, P.J. van der Linden and C.E. Hanson*. Cambridge, UK: Cambridge University Press, pp. 315–356.

Nicholls, Robert J. and Anny Cazenave (2010). "Sea-level rise and its impact on coastal zones." eng. In: *Science* 328 (5985), pp. 1517–20.

OpenStreetMap (2015). "Planet dump retrieved from OpenStreetMap contributors." URL: https://planet.osm.org.

Otsu, N. A (1979). "Threshold Selection Method from Gray-Level Histograms." In: *IEEE Transactions on Systems, Man, and Cybernetics* 9, p. 1. DOI: 10.1109/TSMC.1979.4310076.

Pardo-Pascual, J. E., J. Almonacid-Caballer, and L. A. and Ruiz (2012). "Palomar-Vazquez." In: *Automatic extraction of shorelines from Landsat TM and ETM+ multi-temporal images with subpixel precision* 123, pp. 1–11. DOI: 10.1016/j.rse.2012.02.024.

Pawlowicz, R, B Beardsley, and S Lentz (2002). "Classical tidal harmonic analysis including error estimates in MATLAB using T-TIDE." In: *Computer and geosciences*.

Peckham, S D, E W H Hutton, and B Norris (2013). "A component-based approach to integrated modeling in the geosciences: The design of CSDMS." In: *Computers and Geosciences* 53. DOI: doi:10.1016/j.cageo.2012.04.002.

Pekel, J. F., A. Cottam, N. Gorelick, and A. S. Belward (2016). "High-resolution mapping of global surface water and its long-term changes." In: *Nature Letter*. DOI: 10.1038/nature20584.

Pelnard-Considère, R (1956). "Essai de théorie de l'évolution des formes de rivage en plages de sable et de galets." In: *4th Journées de l'Hydraulique, Les Énergies de la Mer, Question III* Rapport No. 1, 74–1–74–10.

Pontee, N. (2013). "Defining coastal squeeze: A discussion." In: *Ocean & Coastal Management* 84.

Pranzini, E. (2013). *Coastal Erosion and Protection in Europe*. Ed. by Enzo Pranzini. Allan Thomas Williams.

Ranasinghe, R. (2016). "Assessing climate change impacts on open sandy coasts: A review." In: *Earth-Science Reviews*.

Ranasinghe, R and M J F Stive (2009). "Rising seas and retreating coastlines." In: *Climatic Change* 97.

Ranasinghe, R, C M Swinkels, A P Luijendijk, J A Roelvink, J Bosboom, M J F Stive, and D J R Walstra (2011). "Morphodynamic upscaling with the MORFAC approach: Dependencies and sensitivities." In: *Coastal Engineering* 58.

Reniers, A J H M, J A Roelvink, and E B Thornton (2004). "Morphodynamic modeling of an embayed beach under wave group forc-

ing." In: *Journal of Geophysical Research* 109.C01030, pp. 1–22. DOI: 10.1029/2002JC001586.

Rest, P van de (2004). "Morphodynamica an hydrodynamica van de Hollandse kust." MA thesis. Delft University of Technology.

Rijn, L C van, D J R Walstra, B Grasmeijer, J Sutherland, S Pan, and J P Sierra (2003). "The predictability of cross-shore bed evolution of sandy beaches at the time scale of storms and seasons using process-based Profile models." In: *Coastal Engineering* 47.3, pp. 295–327.

Roelvink, J A (2006). "Coastal morphodynamic evolution techniques." In: *Coastal Engineering* 53, pp. 277–287.

Roelvink, J A and A J H M Reniers (2012). *A guide to modeling coastal morphology*. Ed. by Advances in Coastal and Ocean Engineering. World Scientific.

Roelvink, J A and D J R Walstra (2004). "Keeping it simple by using complex models." In: *The 6th Int. Conf. on Hydroscience and Engineering (ICHE-2004)*. Brisbane, Australia.

Roelvink, J A, T J G P Meijer, K Houwman, R Bakker, and R Spanhoff (1995). "Field validation and application of a coastal profile model." In: *Proc. Coastal Dynamics95 Conference*.

Roelvink, J.A. and S. Costas (2019). "Coupling nearshore and aeolian processes: XBeach and Duna process-based models." In: *Environmental Modelling & Software* 115. DOI: 10.1016/j.envsoft.2019.02.010.

Ronde, J. G. de, J. P. M. Mulder, and R. Spanhoff (2003). "Morphological developments and coastal zone management in the Netherlands." In: *International Conference on Estuaries and Coasts*.

Ruessink, B G, D J R Walstra, and H N Southgate (2003). "Calibration and verification of a parametric wave model on barred beaches." In: *Coastal Engineering* 48.3, pp. 139–149. ISSN: 0378-3839. DOI: 10.1016/S0378-3839(03)00023-1. URL: http://www.sciencedirect.com/science/article/B6VCX-487N1NP-1/2/8f3fca0d086f6c52c386baf3719ad54c.

Ruggiero, P, D J R Walstra, G Gelfenbaum, and M van Ormondt (2009). "Seasonal-scale nearshore morphological evolution: Field observations and numerical modeling." In: *Coastal Engineering* 56.11-12, pp. 1153–1172. ISSN: 0378-3839. DOI: 10.1016/j.coastaleng.2009.08.003. URL: http://www.sciencedirect.com/science/article/B6VCX-4X8BP8C-1/2/b97ba0e96f9d2fc80f3e57d841029a63.

Ruggiero, P, G M Kaminsky, and S Hacker (2013a). "Morphodynamics of prograding beaches." In: *Coastal Dynamics*.

Ruggiero, P, M G Kratzmann, E A Himmelstoss, D Reid, J Allan, and G Kaminsky (2013b). *National assessment of shoreline change—Historical shoreline change along the Pacific Northwest coast*. U.S. Geological Survey Open-File Report 2012–1007.

Scheveningen Harbour Authority (2018). *Maintenance dredging records Scheveningen Harbour 2010 - 2018*. Tech. rep. Scheveningen Harbour Authority.

Shepard, F. P. (1976). "Coastal classification and changing coastlines." In: *Geoscience and Man* 14, pp. 53–64.

Short, A. D. (1999). *Handbook of Beach and Shoreface Morphodynamics*. Chichester: John Wiley & Sons.

Slobbe, D C, M Verlaan, R Klees, and H Gerritsen (2013). "Obtaining instantaneous water levels relative to a geoid with a 2D storm surge model." In: *Continental Shelf Research* 52.

Small, C. and R. J. Nicholls (2003). "A Global Analysis of Human Settlement in Coastal Zones." In: *Journal of Coastal Research* 19.3, pp. 584–599. ISSN: 07490208, 15515036. URL: http://www.jstor.org/stable/4299200.

Soille, P., A. Burger, D. De Marchi, P. Kempeneers, D. Rodriguez, V. Syrris, and V. Vasilev (2018). "A versatile data-intensive computing platform for information retrieval from big geospatial data." In: *Future Generation Computer Systems* 81, pp. 30 –40. ISSN: 0167-739X. DOI: https://doi.org/10.1016/j.future.2017.11.007. URL: http://www.sciencedirect.com/science/article/pii/S0167739X1730078X.

Southgate, H N (2011). "Data-Based Yearly Forecasting of Beach Volumes along the Dutch North Sea Coast." In: *Coastal Engineering* 58.

Splinter, K D, J T Carley, A Golshani, and R Tomlinson (2014). "A relationship to describe the cumulative impact of storm clusters on beach erosion." In: *Coastal Engineering* 83.

Stive, M J F et al. (2002). "Variability of shore and shoreline evolution." In: *Coastal Engineering* 47.2, pp. 211–235.

Stive, M J F, L O Fresco, P Kabat, B W A H Parmet, and C P Veerman (2011). "How the Dutch plan to stay dry over the next century." In: *Proceedings of the Institution of Civil Engineers - Civil Engineering* 164.

Stive, M J F et al. (2013). "A New Alternative to Saving Our Beaches from Sea-Level Rise: The Sand Engine." In: *Journal of Coastal Research* 29 (5), pp. 1001 –1008. DOI: https://doi.org/10.2112/JCOASTRES-D-13-00070.1.

Sutherland, J, A H Peet, and R L Soulsby (2004a). "Evaluating the performance of morphological models." In: 51.8-9, pp. 917–939. ISSN: 0378-3839. DOI: 10.1016/j.coastaleng.2004.07.015.

Sutherland, J, D J R Walstra, T J Chesher, L C van Rijn, and H N Southgate (2004b). "Evaluation of coastal area modelling systems at an estuary mouth." In: *Coastal Engineering* 51.2, pp. 119–142. ISSN: 0378-3839. DOI: 10.1016/j.coastaleng.2003.12.003. URL: http://www.sciencedirect.com/science/article/B6VCX-4BV45KF-1/2/2529354b432a18ae4b775b6c64d2c818.

Taal, MD, M A M Löffler, C T M Vertegaal, J W M Wijsman, L Van der Valk, and P K Tonnon (2016). *Development of the Sand Motor; Concise report describing the first four years of the Monitoring and Evaluation Programme*. Report. Deltares.

Tonnon, P K, J van der Werf, and J P M Mulder (2009). *Morphological calculations for the EIA of the Sand Engine*. Tech. rep. Deltares.

Tran-Thanh, Tung, Jacobus Van De Kreeke, Marcel Stive, and Dirk-Jan Walstra (Sept. 2011). "Cross-sectional stability of tidal inlets: A comparison between numerical and empirical approaches." In: *Coastal Engineering* 60, pp. 21–29. DOI: 10.1016/j.coastaleng.2011.08.005.

Turner, Ian L., Mitchell D. Harley, Andrew D. Short, Joshua A. Simmons, Melissa A. Bracs, Matthew S. Phillips, and Kristen D. Splinter (Apr. 2016). "A multi-decade dataset of monthly beach profile surveys and inshore wave forcing at Narrabeen, Australia." In: *Scientific Data* 3, p. 160024. URL: https://doi.org/10.1038/sdata.2016.24.

Van Ormondt, M. (Feb. 2016). "Morphodynamic modelling of the Fire Island Wilderness Breach." In: *American Geophysical Union, Ocean Sciences Meeting 2016, abstract #MG14A-1918*.

Van Rijn, L C (1993). *Principles of sediment transport in rivers, estuaries and coastal seas*. Amsterdam : Aqua Publications. ISBN: ISBN 9080035629.

Van Rijn, L. C. (1995). "Sand Budget and coastline changes of the central coast of Holland between Den Helder and Hoek van Holland period 1964 - 2040; Project Kustgenese." In:

Van Rijn, L. C. (1997). "Sediment transport and budget of the central coastal zone of Holland." In: *Coastal Engineering* 32, pp. 61–90.

Van Rijn, L C (2007). "Unified view of sediment transport by currents and waves. II : Suspended transport." In: *Journal of Hydraulic Engineering* 133 (6), pp. 668–689.

Van Rijn, L.C. (1998). *Principles of coastal morphology*. Aqua publications.

Van Vessem, P and A Stolk (1990). "Sand budget of the Dutch coast." In: *Coastal Engineering Proceedings*. DOI: http://dx.doi.org/10.9753/icce.v22.%25p.

Vegt, H. van der, J.E.A. Storms, D.J.R. Walstra, and N.C. Howes (2016). "Can bed load transport drive varying depositional behaviour in river delta environments?" In: *Sedimentary Geology* 345, pp. 19 –32. ISSN: 0037-0738. DOI: https://doi.org/10.1016/j.sedgeo.2016.08.009. URL: http://www.sciencedirect.com/science/article/pii/S0037073816301336.

Velhorst, R (2017). "Towards a coupled morphodynamic model of the nearshore zone and the beach at the Sand Engine." MA thesis. TU Delft.

Vitousek, Sean, Patrick L. Barnard, Patrick Limber, Li Erikson, and Blake Cole (2017). "A model integrating longshore and cross-shore processes for predicting long-term shoreline response to climate change." In: *Journal of Geophysical Research: Earth Surface* 122.4, pp. 782–806. DOI: 10.1002/2016JF004065.

Vries, S de, S M Arens, M A de Schipper, and R Ranasinghe (2012). "Aeolian sediment transport in supply limited situations Part II; An analysis on field data." In: *Aeolian Research*.

Walstra, Dirk-Jan, R Hoekstra, P.K. Tonnon, and Gerben Ruessink (July 2013). "Input reduction for long-term morphodynamic simulations in wave-dominated coastal settings." In: *Coastal Engineering* 77, pp. 57–70. DOI: 10.1016/j.coastaleng.2013.02.001.

Warrick, Jonathan A et al. (2015). "Large-scale dam removal on the Elwha River, Washington, USA: Source-to-sink sediment budget and synthesis." In: *Geomorphology* 246, pp. 729 –750. ISSN: 0169-555X. DOI: https://doi.org/10.1016/j.geomorph.2015.01.010. URL: http://www.sciencedirect.com/science/article/pii/S0169555X15000227.

Wegen, M van der and J A Roelvink (2008). "Long-term morphodynamic evolution of a tidal embayment using a twodimensional, process-based model." In: *Journal of Geophysical Research* 113.C03016, pp. 1–23. DOI: 10.1029/2006JC003983.

Wijnberg, K M (2002). "Environmental controls on decadal morphologic behaviour of the Holland coast." In: *Marine Geology* 189.

Wijnberg, K M and J H J Terwindt (1995). "Extracting Decadal Morphological Behavior from High-Resolution, Long-Term Bathymetric Surveys Along the Holland Coast Using Eigenfunction Analysis." In: *Marine Geology* 126.1-4, pp. 301–330.

Wijsman, J.W.M. and E. Verduin (2011). "To Monitoring zandmotor Delftlandse kust: benthos ondiepe kustzone en natte strand." In: *Imares Wageningen UR*.

Wittebrood, M, S de Vries, P Goessen, and S Aarninkhof (2018). "Aeolian sediment transport at a man-made dune system; building with nature at the Hondsbossche dunes." In: *Coastal Engineering Proceedings*.

Wulder, Michael A., Jeffrey G. Masek, Warren B. Cohen, Thomas R. Loveland, and Curtis E. Woodcock (2012). "Opening the archive: How free data has enabled the science and monitoring promise of Landsat." In: *Remote Sensing of Environment* 122. Landsat Legacy Special Issue, pp. 2 –10. ISSN: 0034-4257. DOI: https://doi.org/10.1016/j.rse.2012.01.010. URL: http://www.sciencedirect.com/science/article/pii/S003442571200034X.

Zijl, F, M Verlaan, and H Gerritsen (2013). "Improved water-level forecasting for the Northwest European Shelf and North Sea through direct modelling of tide, surge and non-linear interaction." In: *Ocean Dynamics*.

ACKNOWLEDGMENTS

An intense, yet memorable, journey has come to an end. The ideation of this journey started, in hindsight, on the 30th floor of an office at La Défense in Paris. A high-level meeting with colleague and expert Han Winterwerp presenting our study findings to a client, made me realize how valuable a thorough understanding of (coastal) processes is in our advisory work. Shortly after, an interdisciplinary research project focusing on the Sand Engine was granted. The unprecedented pilot experiment, located in my backyard, put me on the spot: it was now or never. Together with Marcel Stive, and through support of NWO and generous support of Deltares, we created the unique opportunity to pursue a PhD research next to a 5-year postdoc position within NatureCoast and a part-time role at Deltares. Marcel, I am very grateful for having confidence in me and creating the possibility to conduct my PhD as a 'buitenpromovendus'. My grateful thanks are extended to Wiel Tilmans and Klaas Jan Bos, my unit manager and department head at the time, for supporting me in this venture, as well as to Peter van den Berg for making this financially possible.

The passion for coastal morphology started in the early days of my career at WL | Delft Hydraulics. I am indebted to Geoff. Toms for hiring me at Delft Hydraulics in 2002. Challenging projects with my colleagues Hans de Vroeg and Giles Lesser ignited the fascination for coasts and beaches and for simulating their dynamics using numerical models. The exposure to an inspiring group of morphologists, including Leo van Rijn, Dirk Jan Walstra and Dano Roelvink, really stirred up the fire. Thanks for sharing your experience, knowledge and ideas with me. The 'rose-colored glasses' that Dano can put up when looking at morphological model results was – and still is - fascinating and inspiring.

From the early days, Rosh Ranasinghe has been closely involved in my research, first through the TU and later through his part-time position at Deltares. Rosh, your knowledge, unstoppable drive and tendency to set the bar high have greatly contributed to my research and publications. Your reviews of my draft manuscripts were very systematic, sometimes red-penned, but you were (almost) always right. Thanks a million for an inspiring working relationship and all the reflections we had while drinking a beer at your table at Moodz.

Various people have contributed to this thesis in many ways. Bas Huisman, Matthieu de Schipper, Stefan Aarninkhof and Dirk-Jan Walstra; we share the same enthusiasm for the Sand Engine and the modelling of its evolution. Genna Donchyts, Josh Friedman, Fedor Baart

and Gerben Hagenaars; you made me realize that there is more than modelling in life! I never thought that, as a coastal engineer, I would enter the intriguing world of remote sensing. But you showed me the emerging potential of satellite imagery for the coastal engineering community. I am proud of the team effort we made in detecting the world's shorelines and that we dare-to-share the, already well-known, data set of the global historical shoreline changes.

My job satisfaction is largely determined by the interaction with colleagues. I very much appreciate the collaboration with my direct colleagues at the Harbour, Coasts and Offshore (HCO) and the Applied Morphology (AMO) departments of Deltares. The list of people is too long, therefore thank you all for your interest and collaboration in many ways over the last years. I would especially like to mention my room mates Jan-Joost Schouten at Deltares and Matthieu de Schipper and Sierd de Vries at TU for all the hours chatting about soccer and many other important things. Matthieu, I greatly appreciate your thorough review of my thesis and your valuable suggestions.

I have also much appreciated the inspiring collaboration with all 15 NatureCoast PhD students and postdocs. Thank you for teaching me about other disciplines than coastal morphology. A special thanks to Alexander van Oudenhoven, co-author of our book on the NatureCoast research outcomes. I look back at an intense, but very interesting process of editing a book together. It was a unique learning experience also with Baukje Kothuis.

I was fortunate to supervise more than 30 Master students of the TU Delft during my PhD period. Your inspiration, enthusiasm and eagerness fed my curiosity and supplied me with new energy. A special thanks to the Sand Engine related MSc students: Aline Kaji, Timon Pekkeriet, Lisa van der Molen, Pim van Steyn, Jeroen de Kort, Rufus Velhorst, Sophie van Zanten, Thijs van het Hooft, Daniel Caichac, Nan Wang, Paul Drenth, Laura Halbmeijer, Thomas Cowan, Ingrid Lambert, Joris Memelink and Etienne Kras.

Dear friends and family-in-law, thank you for your interests, the endless patience, and providing the necessary distraction from time to time, e.g. in the Vosges, Limburg and in De Kuip. To my high school friends, I know that you are as happy as I am that my 'afstudeer' period has finally come to an end.

Dear sisters, I'm grateful for your love, support and for the necessary distraction you provided during family outings over the last years. Marit and Stefan, thanks for offering your 'hut op de hei' to me when I needed focus for writing or for organizing my ideas. Annette and Nick, your mental support and interest is much appreciated and of course you deserve full credits for the cover design.

Dear pa and ma, these moments let me realize what great parents you are for me. You have raised us in a mix of confidence, love and adventure. Our years in Indonesia have greatly contributed to the ability to work together and empathize with people from other cultures (i.e. disciplines). Pa, your passion for water and for sharing your knowledge with others, whether they like it or not, impresses me over and over again.

Dear Cilia, thanks for the unconditional support, faith and freedom that you gave me over the past 6 years. It has been a roller coaster. Finding the balance between work, my PhD research, my role as father and, moreover, as partner was quite challenging. Especially caring and raising two little girls cost us a lot of energy and uncountable sleepless nights, and I am glad that these demanding years are now behind us. At the same time, our stay in Santa Cruz gave us unforgettable, sweet family memories and made us fall in love with California. Cilia, I greatly appreciate your valuable reflections, as a partner and as critical peer, and the time you spent on the English editing. Finally, my daughters Milou and Mare, thank you so much for the happy laughters you bring in our home.

Arjen Luijendijk
Scheveningen, October 2019

ABOUT THE AUTHOR

Arjen Luijendijk was born on May 20, 1976 in Rotterdam, The Netherlands. He grew up in Ridderkerk with a 3-year intermezzo in Jakarta and Bandung in Indonesia. He received secondary education at Guillaume Farel college, graduating in 1995. Driven by his interest in water and engineering – fed by his father Jan Luijendijk – he entered the Civil Engineering course at Delft University of Technology in 1995. Gradually, he obtained a passion for the fields of coastal engineering, boosted by an internship in Thailand studying beach erosion. Arjen graduated in October 2011 after spending almost a year at NIOZ, Texel. Here, he developed and calibrated a Delft3D model using ferry-mounted current measurements of the Marsdiep, Texel, under supervision of prof. Guus Stelling, prof. Marcel Stive, prof. Dano Roelvink and prof. Herman Ridderinkhof.

After travelling for 6 months in Latin America, Arjen joined WL | Delft Hydraulics in May 2002 as a junior coastal engineer at the Harbours and Offshore Technology group. Since the merger of Delft Hydraulics into Deltares in 2008, he works as a coastal morphology researcher and advisor at the Harbours, Coastal and Offshore department. Between 2010 and 2013, he joined the Coastal Engineering department of Delft University of Technology as a lecturer and researcher, followed by a post-doc position from 2013 to 2018 in the NatureCoast research program. He remained working at Deltares as a senior advisor and researcher. Early 2018, Arjen was a visiting scientist at the USGS office in Santa Cruz, California, for four months.

Since 2019, Arjen works as a specialist in coastal morphology and acts as morphology coordinator of the Harbours, Coastal and Offshore department at Deltares (0.7 fte). Next to this, he occupies a part-time position as researcher and lecturer at the Coastal Engineering department at TU Delft.

PERSONALIA

Arjen Pieter Luijendijk
20-05-1976, Rotterdam, The Netherlands

EDUCATION

1988 - 1995	Guillaume Farel (Farelcollege), Ridderkerk, VWO
1995 - 2001	Delft University of Technology, Civil Engineering

EMPLOYMENT

2001 - 2008	Delft Hydraulics
2008 - present	Deltares
2010 - 2013	TU Delft - Lecturer / researcher
2013 - 2018	TU Delft - Post-doc researcher in STW NatureCoast
2018 - 2018	USGS Santa Cruz - Visiting Scientist
2018 - present	TU Delft - Researcher

PUBLICATIONS

PEER-REVIEWED ARTICLES

Luijendijk, A.P., de Schipper, M.A., Ranasinghe, R. *Morphodynamic Acceleration Techniques for Multi-Timescale Predictions of Complex Sandy Interventions*, J. of Mar. Sci. Eng. **7(3)** (2019).

Luijendijk, A.P., Hagenaars, G., Ranasinghe, R., Baart, F., Donchyts, G., and Aarninkhof, S.G.J. *The State of the World's Beaches*, Nature Scientific Reports **8** (2018).

Luijendijk, A.P., Ranasinghe, R., de Schipper, M.A., Huisman, B.A., Swinkels, C.M., Walstra, D.J.R., and Stive, M.J.F. *The initial morphological response of the Sand Engine: A process-based modelling study*, Coastal Engineering **119** (2017).

Vousdoukas, M.I., Ranasinghe, R., Mentaschi, L., Plomaritis, T.A., Athanasiou, P., Luijendijk, A.P., Feyen, L. *Sandy coastlines under threat of erosion*, Nature Climate Change (2019)

Huizer, S., Luijendijk, A.P., Bierkens, M.F.P., Oude Essink, G.H.P. *Global potential for the growth of fresh groundwater resources with large beach nourishments*, Nature Scientific Reports 9 (2019)

Misra, A., Ramakrishnan, B., Vojinovic, Z., Luijendijk, A.P., and Ranasinghe, R. *Assessment of Complementary Medium-Resolution Satellite Imageries for Nearshore Bathymetry Estimation*, Journal of the Indian Society of Remote Sensing **47** (2019).

Duong T.M., Ranasinghe, R., Thatcher, M., Mahanama, S., Wang, Z.B., Dissanayake, P.K., Hemer, M., Luijendijk, A.P., Bamunawala, J., Roelvink, J.A., Walstra, D.J.W. *Assessing climate change impacts on the stability of small tidal inlets: Part 2 - Data rich environments*, Marine Geology **395** (2018).

Meirelles, S., Henriquez, M., Reniers, A.J.H.M., Luijendijk, A.P., Pietrzak, J., Horner-Devine, A.R., Souza, A.J., Stive, M.J.F. *Cross-shore stratified tidal flow seaward of a mega-nourishment*, Estuarine, Coastal and Shelf Science **200** (2018).

Misra, A., Vojinovic, Z., Ramakrishnan, B., Luijendijk, A.P., Ranasinghe, R. *Shallow water bathymetry mapping using Support Vector Machine (SVM) technique and multispectral imagery*, International Journal of Remote Sensing **39** (2018).

Huisman, B.J.A., Ruessink, B.G., de Schipper, M.A., Luijendijk, A.P., Stive, M.J.F. *Modelling of bed sediment composition changes at the lower shoreface of the Sand Motor*, Coastal Engineering **132** (2018).

Duong, T.M., Ranasinghe, R., Luijendijk, A.P., Walstra, D.J.W., Roelvink, J.A. *Assessing climate change impacts on the stability of small tidal inlets: Part 1 - Data poor environments*, Marine Geology **390** (2017).

Hagenaars, G., de Vries, S., Luijendijk, A.P., de Boer, W.P., and Reniers, A.J.H.M. *On the accuracy of automated shoreline detection derived from satellite imagery: A case study of the Sand Motor mega-scale nourishment*, Coastal Engineering **133** (2017).

Bosboom, J., Reniers, A.J.H.M., Luijendijk, A.P. *On the perception of morphodynamic model skill*, Coastal Engineering **94** (2014).

Stive, M.J.F., de Schipper, M.A.; Luijendijk, A.P.; Aarninkhof, S.G.J.; Van Gelder-Maas, C.; Van Thiel de Vries, J.S.M.; De Vries, S.; Henriquez, M.; Marx, S. and Ranasinghe, R. *A New Alternative to Saving Our Beaches from Sea-Level Rise: The Sand Engine*, Journal of Coastal Research **29(5)**, (2013).

CONFERENCES

Luijendijk, A.P., de Vries, S., van het Hooft, T., de Schipper, M.A. *Predicting dune growth at the Sand Engine by Coupling the Delft3D Flexible Mesh and Aeolis models* Coastal Sediments Proceedings, 2019.

Aarninkhof, S.G.A. et al. *ICON.NL: Coastline Observatory to Examine Coastal Dynamics in response to natural forcing and human interventions.* Coastal Sediments Proceedings, 2019.

Grasmeijer, B.T., van Rijn, L.C., van der Werf, J.J., Zijl, F., Huisman, B.J.A., Luijendijk, A.P., Wilmink, R.J.A., de Looff, A.P. *Method for Calculating Annual Sand Transports on the Dutch Lower Shoreface to Assess the Offshore Boundary of the Dutch Coastal Foundation.* Coastal Sediments Proceedings, 2019.

Donchyts, G., Verlaan, M., Luijendijk, A.P., Baart, F., Lodder, Q., Santinelli, G., Rogers, C. *Automated extraction and fusion of the intertidal and subtidal bathymetry from the Landsat and Sentinel satellite data.* Poster at EGU General Assembly, 2019.

Hoonhout, B., Luijendijk, A.P., de Vries, S. *How tides and waves enhance aeolian sediment transport at the Sand Engine mega nourishment.* Coastal Engineering Proceedings, 1(36), 2018.

Scheel, F., de Boer, W., Luijendijk, A.P., Stive, R., Bouw, R. *An integrated and interactive toolbox for the design of coastal infrastructure.* Coastal Engineering Proceedings, 1(36), 2018.

de Vries, S., de Schipper, M., Roest, B., Luijendijk, A.P., Aarninkhof, S. *Diffusion of a mega feeder nourishment - assessing 5 years of Sand Engine spreading.* Coastal Engineering Proceedings, 1(36), 2018.

Hoonhout, B., Luijendijk, A.P., Velhorst, R., de Vries, S., Roelvink, J.A. *How tides and waves enhance aeolian sediment transport at the sand motor mega-nourishment.* Proceedings of Coastal Dynamics 2017: Helsingør, Denmark (pp. 513-521)., 2017.

Hagenaars, G., Luijendijk, A.P., de Vries, S., de Boer, W.P. *Long term coastline monitoring derived from satellite imagery.* Proceedings of Coastal Dynamics 2017: Helsingør, Denmark, 2017.

Luijendijk, A.P., Velhorst, R., Hoonhout, B., de Vries, S., Ranasinghe, R. *Integrated modelling of the morphological evolution of the sand engine mega-nourishment.* Proceedings of Coastal Dynamics 2017: Helsingør, Denmark (pp. 1874-1885), 2017.

de Boer, W.P., Huisman, B., Yoo, J., McCall, R., Scheel, F., Swinkels, C. M., Luijendijk, A.P., Walstra, D. *Understanding coastal erosion processes at the Korean east coast.* Proceedings of Coastal Dynamics 2017: Helsingør, Denmark, 2017.

Donchyts, G., Baart, F., Luijendijk, A.P., Hagenaars, G. *The global coastline dataset: the observed relation between erosion and sea-level rise.* AGU Fall Meeting Abstracts, 2017.

Luijendijk, A.P., Hoonhout, B. *Multi-scale Modeling of the Evolution of a Large-Scale Nourishment* AGU Fall Meeting Abstracts, 2016.

Thiel de Vries, J. van, Eekelen, E. van, Luijendijk, A.P., Ouwerkerk, S., Steetzel, H. *Challenges in developing sustainable sandy strategies.* WODCON XXI proceedings, 2016.

Luijendijk, A. P., Huisman, B., De Schipper, M.A. *Impact of a storm on the first year evolution of the Sand Engine.* Proceedings of the Coastal Sediments conference, 2015.

Huisman, B., Van der Zwaag, J., Luijendijk, A.P., Ruessink, B. *Practical considerations on numerical modelling of sediment sorting at a large scale sand nourishment.* Proceedings of the Coastal Sediments conference, 2015.

Kaji, A., Luijendijk, A.P., van Thiel de Vries, J.S.M., de Schipper, M.A., Stive, M.J.F. *Effect of different forcing processes on the longshore sediment transport at the Sand Motor, the Netherlands.* Proceedings of 34th conference on coastal engineering (pp. 1-11)., 2014.

Scheel, F., de Boer, W.P., Brinkmann, R., Luijendijk, A.P., Ranasinghe, R. *On the generic utilization of probabilistic methods for quantification of uncertainty in process-based morphodynamic model applications.* Proceedings of 34th conference on coastal engineering (pp. 1-10)., 2014.

Stive, M.J.F., de Schipper, M.A., Luijendijk, A.P., Ranasinghe, R., van Thiel De Vries, J.S.M., Aarninkhof, S., Marx, S. *The sand engine: A solution for vulnerable deltas in the 21st century?* International conference on Coastal Dynamics (pp. 1537-1546), 2013.

Hasselaar, R.W., De Boer, W.P., Luijendijk, A.P. *Optimizing harbour maintenance strategies using Delft3D and D-Flow Flexible Mesh.* In Coasts and Ports 2013 (pp. 364-369), 2013.

Hoekstra, R., Scheel, F., De Boer, W.P., Luijendijk, A.P. *Development of a harbour design toolbox: Opportunities for multidisciplinary rapid assessment in harbour development.* In Coasts and Ports 2013 (pp. 388-393), 2013.

BOOKS

Luijendijk, A.P. and van Oudenhoven, A. *The Sand Motor: a Nature-based Response to Climate Change; Findings and reflections of the interdisciplinary research program NatureCoast* The Sand Motor: a Nature-based Response to Climate Change (2019).

Luijendijk, A.P., de Vries, S. *Global Beach Database*, Chapter in Sandy Beach Morphodynamics Eds. Derek Jackson and Andrew Short, (2019).

Borsje, B.W., de Vries, S., Janssen, S.K.H., Luijendijk, A.P., Vuik, V. *Building with Nature as Coastal Protection Strategy in the Netherlands.*, Chapter in Living Shorelines; The Science and Management of Nature-Based Coastal Protection (2017).

COLOPHON

Measurement data presented in this thesis is open-source and can be obtained through the 4TU.ResearchData initiative at:
https://data.4tu.nl/repository/collection:zandmotor

The Delft3D (Flexible Mesh) software used in this thesis is open-source and can be obtained through the Delft3D Open Source Community site at:
https://oss.deltares.nl/web/delft3dfm

The AeoLiS model presented in this thesis is open-source and can be obtained through the OpenEarth GitHub repository at:
https://github.com/openearth/aeolis-python/

This document was typeset using the typographical look-and-feel `classicthesis` developed by André Miede and Ivo Pletikosić.

Print: Ridderprint | www.ridderprint.nl

SEAMLESS MODELLING OF SANDY COASTAL INTERVENTIONS

Sand is the second-most used natural resource behind water and will be under increasingly high demand in coming decades. One of the reasons for this is that, worldwide, sand is more and more applied to counteract beach erosion. This thesis presents new techniques in remote sensing and numerical modelling to better understand beach erosion and predict the dynamics of our sandy coastlines. To this end, it explores the crossing of three types of borders.

First, international borders are crossed in a global assessment of historic beach dynamics using satellite imagery. Second, the boundaries between model time scales - from storms to decadal times - are dissolved by means of a new morphodynamic acceleration technique. Finally, the developed seamless modelling approach enables to cross the ever-changing boundary between water and land, where sand moves from the wet to the dry domain and vice versa.

This work results in a landscaping model that can better forecast the future behavior of sandy beaches in a changing climate.